DISSERTATION

VISCOELASTIC CHARACTERIZATION AND MODELING OF MUSCULOSKELETAL SOFT TISSUES

Submitted by

Kevin Levi Troyer

Department of Mechanical Engineering

In partial fulfillment of the requirements

For the Degree of Doctor of Philosophy

Colorado State University

Fort Collins, Colorado

Summer 2012

Doctoral Committee:

Advisor: Christian Puttlitz

Susan James
Paul Heyliger
Lakshmi Dasi

ABSTRACT

VISCOELASTIC CHARACTERIZATION AND MODELING OF MUSCULOSKELETAL SOFT TISSUES

Over the last decade there has been a dramatic rise in musculoskeletal soft tissue injuries in the general, athletic, and military populations. The etiology of this increase has been largely ascribed to dynamic loading events, including strenuous physical overuse and trauma. Additionally, instability arising from soft tissue pathology or trauma can induce and/or accelerate joint degeneration. Degenerative sequelae, such as post-traumatic osteoarthritis, can cause significant debility and an associated reduction in one's quality of life. Development of successful treatment modalities for joint instability and soft tissue compromise is highly dependent upon a thorough understanding of the affected tissue's mechanical (viscoelastic) behavior. However, current soft tissue viscoelastic characterization paradigms predominantly utilize quasi-linear viscoelastic (QLV) formulae despite substantial empirical evidence which has conclusively demonstrated that these tissues violate its fundamental assumption of elastic and viscous behavior separability. Furthermore, development of more applicable nonlinear viscoelastic formulations has been hindered by the inability of currently-available constitutive models and characterization methodologies to include relaxation manifested during dynamic loading events. As a result, implementation of nonlinear viscoelastic formulae in soft tissue computational models has not been widespread. To surmount these shortcomings, this work develops a novel, nonlinear viscoelastic constitutive formulation and a corresponding experimental characterization technique which can be included in current state-of-the-art computational algorithms. Specifically, the aims of this dissertation were: (1) Develop and validate a nonlinear viscoelastic characterization technique for musculoskeletal soft tissues that incorporates relaxation manifested during loading; (2) Characterize the nonlinear viscoelastic

behavior of various types of ligamentous tissues and tendon; (3) Integrate a fully nonlinear viscoelastic constitutive formulation into a finite element algorithm. Aims 1 and 2 were accomplished via development and application of a novel comprehensive viscoelastic characterization (CVC) technique and constitutive formulation to describe the nonlinear viscoelastic behavior of various human cervical spine ligaments (anterior and posterior longitudinal ligament and ligamentum flavum) and ovine Achilles tendon. Additionally, improvements in the predictive accuracy of the CVC fitted coefficients over previously accepted viscoelastic characterization techniques were quantified. Furthermore, a computationally tractable fully nonlinear viscoelastic formulation was developed and validated against an analytical solution (Aim 3). Implementation of the important nonlinear viscoelastic behavior into computational models will greatly accelerate our ability to understand the functional role of soft connective tissues in whole joint mechanics and facilitate future treatment options.

ACKNOWLEDGEMENTS

I will be the first to admit that I would not have made it this far, both academically and professionally, without the support and guidance of my advisor, Christian Puttlitz. For some strange reason, he had enough confidence in my abilities to allow me to freely pursue my interests in tissue viscoelasticity. He taught me how to be a credible researcher, how to write scientific manuscripts, and how to appreciate good beer. Very few people have such a profound impact on my life, and I will be forever indebted to Christian and his lab. From the bottom of my heart: thank you for everything.

Additionally, I would like to thank Drs. Lakshmi Dasi, Susan James, and Paul Heyliger for serving on my doctoral committee. I specifically selected each of you because I value your honest opinions. Thank you for your time and your constructive criticism.

I am grateful for the help of Dr. Donald Estep, who provided a very elegant mathematical proof (Appendix A) that was fundamental to the development of the constitutive formulae used herein. Additionally, I am indebted to Jim zumBrunnen for his help with statistics, and Mark Ringerud for his faithful upkeep of my computational resources.

I appreciate all of the help from the past and present OBRL crew, specifically: Dr. Brandon Santoni, Amy Lyons-Santoni, Dr. Kirk McGilvray, Dr. Ugur Ayturk, Dr. Snehal Shetye, Dr. Devin Leahy, Dr. Wes Womack, Cecily Broomfield, and future Drs. Ben Gadomski and Kevin Labus. All of you made working at the OBRL enjoyable and gave me a reason to get out of bed in the morning and go to work. Thank you for all of your help!

Finally, I would not be writing this today without the never-ending love and support from my family and friends. Thank you all for encouraging me to achieve my dreams.

DEDICATION

This work is dedicated to my big brother Jason, who is my definition of perseverance.

I happily reside in the shadow of his achievements.

TABLE OF CONTENTS

ABSTRACT ..... **ii**

ACKNOWLEDGEMENTS ..... **iv**

DEDICATION ..... **v**

1. Background **1**

1.1. Clinical Significance 1
1.2. Functional Anatomy of Ligamentous and Tendinous Tissues 2

1.2.1. Relevant tendon anatomy 2
1.2.2. Relevant ligament anatomy 4
1.2.3. Ligament and tendon biomechanics 5

1.3. Viscoelastic Theory 12

1.3.1. Linear viscoelasticity 13
1.3.2. Quasi-linear viscoelasticity 17
1.3.3. Fully nonlinear viscoelasticity 18

1.4. Specific Aims 19

2. Viscoelastic Effects During Loading Play an Integral Role in Soft Tissue Mechanics **22**

2.1. Introduction 22
2.2. Materials and Methods 23

2.2.1. Empirical data capture 24
2.2.2. Quasi-linear viscoelastic formulae 26
2.2.3. Fully nonlinear viscoelastic formulae 28
2.2.4. Comprehensive viscoelastic characterization method 29
2.2.5. Error quantification 31
2.2.6. Statistics 32

2.3. Results 32

2.3.1. QLV stress relaxation fits 32
2.3.2. QLV cyclic predictions 34
2.3.3. Fully nonlinear viscoelastic stress relaxation fits 37
2.3.4. Fully nonlinear viscoelastic cyclic predictions 41

2.4. Discussion 43
2.5. Conclusion 47

3. Nonlinear Viscoelasticty Plays an Essential Role in the Functional Behavior of Spinal Ligaments **48**

3.1. Introduction 48
3.2. Materials and Methods 49

3.2.1. Experimental methods 49
3.2.2. Constitutive formulation 50

3.3. Results 51

3.4. Discussion 59
3.5. Conclusion 62

4. Finite Element Implementation of Fully Nonlinear Viscoelasticity 63

4.1. Introduction 63
4.2. Materials and Methods 64

4.2.1. Experimental data acquisition 64
4.2.2. Nonlinear viscoelastic formulations 66
4.2.3. Finite element model 69

4.3. Results 70
4.4. Discussion 77
4.5. Conclusion 79

5. Overall Conclusions 80

6. Future Work 81

6.1. Anisotropic Nonlinear Viscoelastic Characterization 81
6.2. Interrogation of Various Nonlinear Viscoelastic Formulations 83

References 84

Appendix A: Uniqueness of a Prony Series with Fixed Time Constants 101

A.1. Proof of Uniqueness of a Prony Series With Fixed Time Constants 101

Appendix B: Interrogation of Inertial Artifacts 103

B.1. Introduction 103
B.2. Materials and Methods 104

B.2.1. Experimental data capture 104
B.2.2. Repeatability error quantification 105
B.2.3. Inertial artifact quantification 105

B.3. Results 105

B.3.1. Repeatability 105
B.3.2. Error between upper and lower load cells 106

B.4. Discussion 107
B.5. Conclusion 108

Appendix C: Pilot Experiments—Repeatability and Cross-Sectional Area Measurement 109

C.1. Repeatability 109

C.1.1. Materials and methods 109
C.1.2. Results and discussion 109
C.1.3. Conclusion 110

C.2. Cross-sectional Area Measurement 111

C.2.1. Materials and methods 111
C.2.2. Results and discussion 112
C.2.3. Conclusion 113

Appendix D: High Frequency (10 Hz) Cyclic Predictions 114

D.1. Introduction 114
D.2. Materials and Methods 114
D.3. Results 115
D.4. Discussion 115
D.5. Conclusion 118

Appendix E: Creep Predictions 119

E.1. Introduction 119

E.1.1. Relationship between creep and stress relaxation: linear viscoelasticity 119
E.1.2. Relationship between creep and stress relaxation: nonlinear viscoelasticity 120

E.2. Materials and Methods 121
E.3. Results 123

E.3.1. Sensitivity of creep coefficients to the initial guess 123
E.3.2. Average creep prediction: entire curve 124
E.3.3. Average creep prediction: creep period only 125

E.4. Discussion 126
E.5. Conclusion 127

Appendix F: Applied Integration Techniques 128

F.1. Introduction 128
F.2. Materials and Methods 128

F.2.1. Adaptive Gauss-Kronrod quadrature (QUADGK) technique 129
F.2.2. Convolution matrix technique 130
F.2.3. Computational efficiency 130

F.3. Results 131
F.4. Discussion 131
F.5. Conclusion 131

1. Background

1.1. Clinical Significance

Musculoskeletal soft tissue injuries resulting from strenuous or traumatic dynamic activities are becoming increasingly prevalent and costly. For example, automobile-related spinal ligamentous injuries such as whiplash[1-7] are common among the general population and carry corresponding annual costs of $4.5 billion in the United States[8,9]. Additionally, acute lower-limb and spinal soft tissue injuries are a frequent occurrence among athletes[10-14] and the military population due to physically rigorous training[15-18] and service[19-22] environments. In addition to the clinically debilitating nature and the societal costs of acute soft tissue injury alone, the resulting degenerative sequelae are equally burdensome. Compromise of peri-articular soft tissues significantly increases the risk of developing chronic post-traumatic osteoarthritis (PTOA) in the affected joint[7,23-26]. Long-term clinical follow-up studies have reported a 10-fold increase in the risk of developing knee osteoarthritis following a ligamentous or meniscal injury[27,28]. PTOA affects approximately 5.6 million individuals in the United States and carries a corresponding annual cost of $3 billion[28,29]. Alarmingly, current treatment methods have not been successful at eliminating or arresting PTOA progression[26,27]. Specifically, it has been reported that the post-treatment risk of developing PTOA following a significant joint injury is greater than 40%[28,30]. These data suggest that current repaired and reconstructed tissues do not restore the native, pre-injury mechanical environment of the tissue. Since the functional role of musculoskeletal soft tissues, such as ligament and tendon, is to facilitate, guide, and constrain joint motion under both physiologic and traumatic dynamic loading events, it is necessary to consider and characterize their temporal mechanical behavior. As a result, treatment modalities for musculoskeletal soft tissue injury may be significantly improved by accurately understanding

and characterizing the normal viscoelastic behavior of these tissues. This dissertation seeks to build upon current soft tissue viscoelastic characterization paradigms, specifically for tendon and ligament musculoskeletal soft tissues, in order to obtain accurate experimental data which will serve as the basis for development of future novel treatment modalities.

1.2. Functional Anatomy of Ligamentous and Tendinous Tissues

Ligament and tendon are dense fibrous connective tissues with similar, primarily mechanical, functional roles that provide locomotion and stabilize the skeleton. Tendinous tissues transmit muscular contractions to bone and limbs in order to invoke locomotion and provide active joint stability (via the musculature). Ligamentous tissues span across a joint (connecting adjacent bones) in order passively guide physiologic joint motion patterns and restrict potentially harmful movements. The gross (tissue-level) mechanical phenomena exhibited by these tissues are a result of their specific geometry and their biochemical and microstructural composition. The objective of this dissertation is to develop a general method and constitutive formulation to characterize and model the viscoelastic behavior of these musculoskeletal tissues. The following subsections outline the specific anatomy of ligamentous and tendinous tissues and relate these anatomical features to their functional mechanical role.

1.2.1. Relevant tendon anatomy

Tendon is a natural fibrous composite material with a hierarchical structure. It is composed of collagen fibers (predominately type I) embedded in a highly hydrated proteoglycan matrix (ground substance). Collagen fibers dominate the solid-phase microstructure, constituting more than 85% of the tissue's dry weight[31]. The collagen structure exhibits its own hierarchical organization, where tropocollagen molecules successively amalgamate to form three distinct structured bundles: (1) five tropocollagen molecules are linearly staggered at periodically repeating units spaced 67 nm apart[32] (called the D-period) to form microfibrils; (2)

microfibrils are grouped to form subfibril structures; (3) collagen fibrils are assembled from these subfibril structures (Figure 1)[33]. Each of these collagen substructures are tightly packed and exhibit a high degree of anatomical alignment parallel to the longitudinal axis of the tendon. Intermolecular and intramolecular crosslinks exist within the alpha-helix chains of the tropocollagen molecules and between adjacent tropocollagen molecules and the extracellular matrix, respectively, which allows these tissues to achieve high mechanical integrity (high tensile stiffness and strength)[34,35]. Additionally, the collagen fibrils exhibit a wavy crimp pattern that is thought to play an important role in the tissue's mechanical behavior (Figure 1)[36]. Fibrils are bound together via the ground substance and the associated proteoglycans (PGs) in order to form fascicle structures (Figure 1)[31,34,37]. Individual collagen fascicles are bound within a fascicular membrane sheath (endotenon), which is a loose connective tissue that supports blood vessels, nerve endings, and lymphatics[31,38]. Similarly, the external reticular membrane surrounds a group of fascicles to form the gross tendon structure (Figure 1).

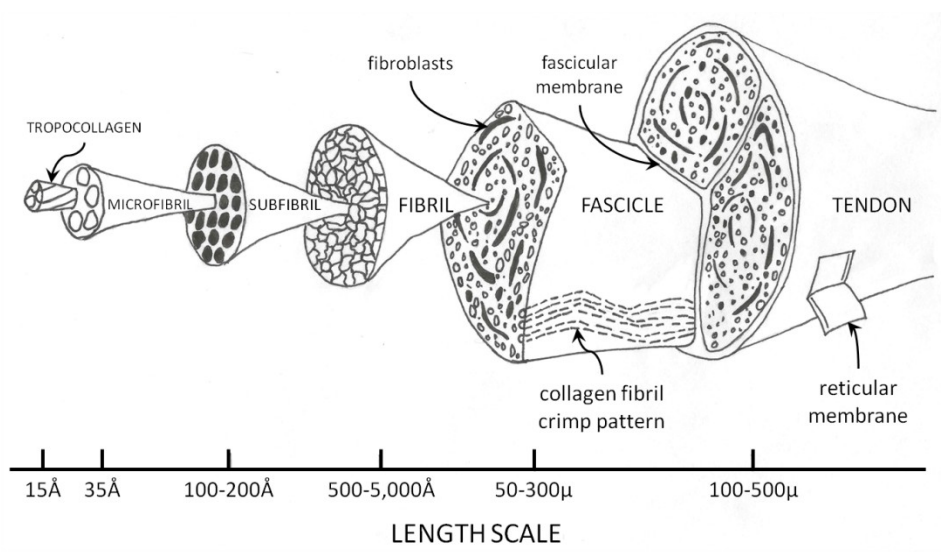

Figure 1: Structural hierarchy of the tendon. Adapted from Kastelic *et al.*[33].

Although PGs constitute a relatively small portion of the total solid phase tendinous microstructure (less than 2% of the total dry weight), these molecules are essential for maintaining tendon hydration (and therefore viscoelastic mechanical function) and collagen

fibrillogenesis[34,38]. Each PG contains a protein core with at least one glycosaminoglycan (GAG) side chain that determines its functional role. For example, PGs aggregated with the anionic hyaluronan GAG forms a hydrophilic molecule which imbibes water[34,39], thereby contributing to regulation of tissue hydration. Water constitutes more than half (approximately 60%) of the total wet weight of tendon[40]. Other GAG molecules, such as decorin, are important for maintaining proper collagen fiber diameters[41,42] and alignment[43,44] during fiber development.

Cellular components (predominately fibroblasts) are sparsely embedded within the fascicle ground substance and are aligned in the direction of the fibrils (Figure 1)[31]. These cells synthesize and secrete collagen fibers and extracellular matrix components[34,45,46]. Production of these extracellular components is regulated by mechanobiologic stimulation. For example, human tendon fibroblasts have been shown to modulate production of type I collagen when subjected to a dynamic loading environment[47]. Cellular nutrition is provided by diffusion or vascular supply[31,38].

1.2.2. Relevant ligament anatomy

Although ligaments are biologically and morphologically similar to tendons, these tissues contain distinct differences that reflect upon their unique physiologic role. For example, ligaments must exhibit greater extensibility than tendons in order to facilitate joint motion[40]. Morphologically, this reduced stiffness is achieved via a reduced collagen fiber content (70% of the total dry weight) and a reduced degree of parallel collagen fiber arrangement as compared to tendons[31,40,48-50]. The increase in collagen fiber dispersion is a result of the different *in vivo* loading conditions experienced by these two tissue types. Whereas tendons predominately experience consistent uniaxial (longitudinal) forces, ligaments may be subjected to multiaxial loading patterns[40] (depending on their anatomical location) that require specific mechanical properties in the off-axis directions. For example, the cruciate and collateral knee ligaments

exhibit a spatially varying collagen fiber arrangement in order to withstand multidirectional loads[51,52].

Additionally, ligaments typically contain greater amounts of the structural protein elastin (typically 1% to 2% of the total dry weight) as compared to tendons[40]. In some specialized ligaments, such as the spinal ligamenta flava, elastin is the predominate fibrous component[53]. This greater elastin content gives the ligamenta flava unique mechanical properties that allow it to undergo a greater amount of elastic deformation as compared to the other, predominately collagenous, spinal ligaments[14,54,55].

In addition to the primary mechanical function of the ligament, recent studies have suggested that these tissues contain innervations that may play a secondary role in joint stability and proprioception. It has been demonstrated that mechanoreceptors within ligamentous tissue become activated under deformation, which may trigger the peri-articular musculature to actively stabilize the joint[56]. Therefore, joint instabilities resulting from ligament compromise may not only be a result of a disruption to the ligament's normal mechanical behavior, but also a loss in proprioception[57] via damage to these mechanoreceptors.

1.2.3. Ligament and tendon biomechanics

The following subsections provide a background of the empirical elastic (quasi-static or time-independent) and viscoelastic (time-dependent) behavior of ligament and tendon, and relate this behavior to the tissue's anatomy described above.

Elastic behavior

The quasi-static elastic behavior of ligament and tendon has been extensively studied. These tissues experience nonlinear, finite deformations *in vivo* which cannot be described by the infinitesimal strain theory (Hooke's law) of typical engineering materials[58]. When these tissues are tensioned at a constant strain rate, they exhibit the nonlinear, hyperelastic force-

displacement (or stress-strain, σ-ε) relationship shown in Figure 2[59]. The concave-up region from 0 to A is commonly referred to as the "toe region" of the curve. This nonlinear region typically encompasses the physiologic range of the tissue; the relatively linear region from A to B typically lies outside of this range[59]. The increased stiffness (slope or $d\sigma/d\varepsilon$) in the A-B region serves as a protective mechanism for the tissue and its associated joint by increasing the tissue's energy-absorbing capacity and restricting non-physiologic joint motions. Following this linear region, a nonlinear sub-failure region (from B to C) is proceeded by ultimate tissue failure at C.

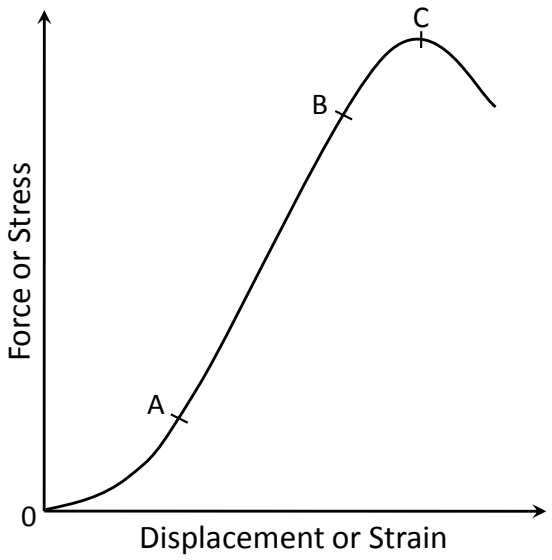

Figure 2: A typical force-displacement (or stress-strain) curve for dense connective tissue.

Tendons and ligaments have unique load-deformation profiles that are specific to their *in vivo* mechanical function. Tendons typically have a smaller toe region and a greater stiffness and ultimate strength than ligaments. These properties maximize the efficiency with which muscular contractions are transmitted to the bone and protect the tissue when subjected to large musculoskeletal forces[31,40]. The high mechanical integrity (stiffness and strength) of the tendon is derived from its relatively high proportion of longitudinally-aligned collagen fibers[31]. Conversely, ligaments exhibit a longer toe region (i.e., they undergo a greater amount of deformation at a reduced stiffness), in order to facilitate joint movement[40]. This increased

extensibility decreases the amount of muscular expenditure required to move the joint throughout physiologic motions[55].

The shape of the nonlinear loading curve is related to the tissue's microstructure, specifically collagen fiber recruitment and orientation. In the zero-force configuration, the collagen fibrils are crimped (Figure 1) and offer negligible resistance to deformation. As a tensile load is applied to the tissue, these fibrils become successively straightened and recruited[60], resulting in the toe region of the loading curve. The linear region of the loading curve arises as more fibrils are recruited and become load-bearing[60]. By direct measurement of the collagen fiber spread of spinal ligaments during deformation (via X-ray diffraction techniques), Kirby *et al*.[50] and Hukins *et al*.[49] demonstrated an increase in fibril alignment towards the loading axis. As the fibers became more oriented with the loading axis, apparent stiffness of the tissue also increased.

Viscoelastic behavior

While the elastic properties offer some insight into the functional mechanical role of tendons and ligaments, application of these static properties is severely restricted since these hydrated tissues are subjected to transient and dynamic deformations *in vivo*. As a result, these tissues exhibit a significant amount of viscoelastic, or time-dependent, behavior, such as: creep, stress relaxation, hysteresis, and strain-rate dependent stiffness. Creep describes the continued increase in tissue strain over time when subjected to a constant stress (Figure 3). Stress relaxation describes the temporal stress decay within the tissue when it is subjected to a constant strain (Figure 4). The viscoelastic effects of hysteresis and strain-rate dependent stiffness arise during tissue loading and unloading. Hysteresis is defined as the energy lost during cyclic loading, and is evidenced by energy dissipation (depicted as different loading and unloading profiles) on a stress-strain plot of a loading cycle [Figure 5(a)]. Finally, the effective

stiffness of a viscoelastic material is dependent upon the rate which the tissue is extended [Figure 5(b)]. A primary objective of this dissertation is to develop a robust method to characterize the transient experimental stress relaxation behavior of musculoskeletal soft tissues which incorporates the viscoelastic effects present during the experimental loading period.

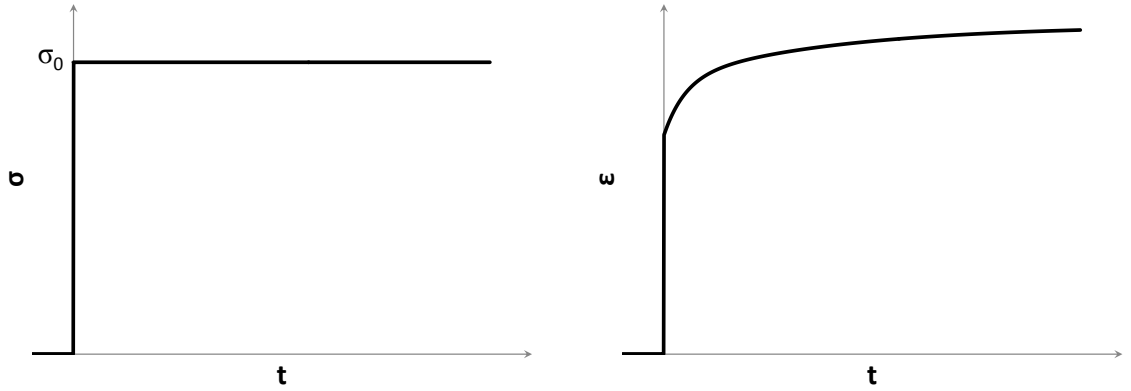

Figure 3: Creep behavior. If a constant stress of σ_0 is instantaneously applied to a viscoelastic material (left), the resulting strain will increase (or creep) over time (right).

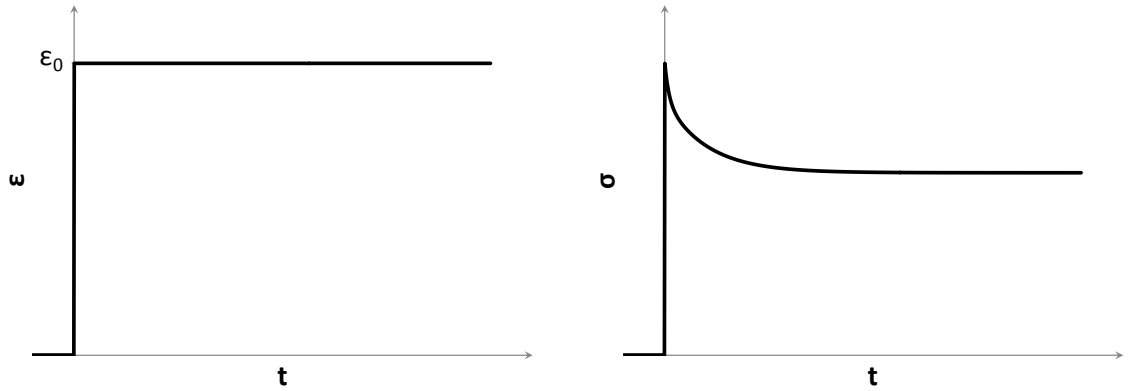

Figure 4: Stress relaxation behavior. If a constant strain of ε_0 is instantaneously applied to a viscoelastic material (left), the resulting stress will decrease (or relax) over time (right).

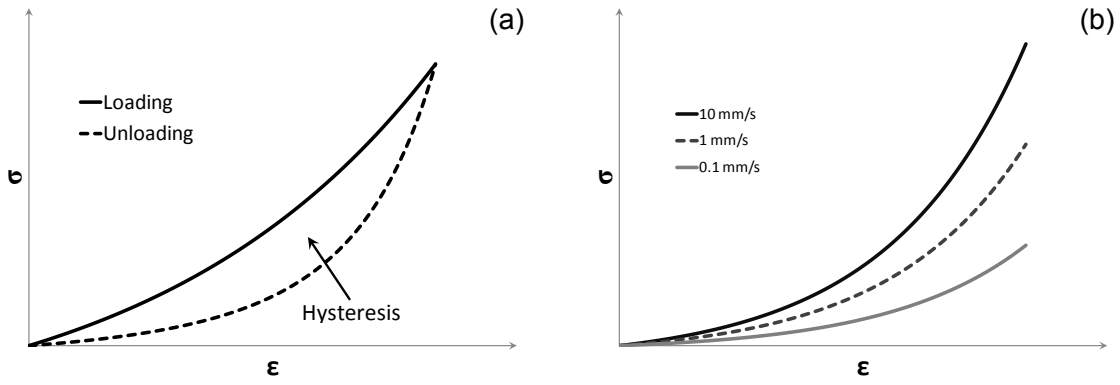

Figure 5: Viscoelastic effects during loading and unloading. (a) Hysteresis is the energy dissipated during cyclic loading. (b) The stiffness of a viscoelastic material ($d\sigma/d\varepsilon$) is dependent upon the loading rate.

While it is widely accepted that the phenomenological viscoelastic behavior of soft connective tissues arises from its morphology, the specific microstructural mechanisms for this behavior are a subject of ongoing debate. Current theories speculate that the origin of tendon and ligament viscoelasticity arises from mechanisms acting on different length scales, including: intermolecular viscoelasticity of the collagen fibrils, interactions between the solid-phase (collagen and PG) constituents, and/or movement of fluid through the tissue. Intermolecular viscoelastic effects within the collagen fibrils themselves have been reported via observation of changes in the D-period spacing between tropocollagen molecules in tendon subjected to creep experiments[61]. Additionally, development of theoretical constitutive models has led some to hypothesize that interactions between the GAG and fibril constituents contribute to tissue-level viscoelasticity[62,63]. However, recent experimental work has demonstrated that GAG-fibril interactions do not significantly affect the viscoelastic behavior of the tissue[39]. Instead, the GAG constituents may contribute to tissue-level viscoelasticity by regulating fluid flow through the tissue. Similar to cartilage, the GAG constituents in ligament affect its transverse permeability in compression[64]. This compressive behavior may affect fluid flow through the matrix (inducing tissue-level viscoelasticity) during axial tensile loading because of the relatively large Poisson's ratio (lateral contraction) observed by these tissues[64-67]. Collectively, these previous

experimental studies of molecular-level viscoelasticity and fiber-level fluid flow suggest that several mechanisms, at different length scales, are responsible for the gross viscoelastic behavior of the tissue.

As with the elastic mechanical behavior describe above, the viscoelastic properties of tendon and ligament have important contributions to normal physiologic function by facilitating joint motion, minimizing muscular expenditure, and protecting the joint (and the tissue itself) during traumatic events. Both tendon and ligament exhibit strain-rate dependent stiffness[31]; displaying a reduced stiffness at slow (physiologic) strain rates, and a high stiffness at fast (traumatic) strain rates [Figure 5(b)]. For ligaments, a reduced stiffness decreases the amount of muscular energy required to produce physiologic joint motions. At traumatic strain rates, the increased stiffness and ultimate load indicates an increased energy-absorbing capacity, improving the tissue's resistance to abnormal motions and mitigating ligamentous and/or joint injury. Similar strain-rate dependent behavior has been reported for muscle-tendon units[68] protecting these tissues from injury during fast loading rates. Additionally, tendon creep (lengthening under constant load) minimizes the rate of muscle fatigue during isometric contractions by allowing the muscle to shorten[31].

Historically, mathematical models used to describe connective tissue viscoelasticty have treated the elastic and time-dependent mechanical properties as separate entities (refer to section 1.3.2 below). Recent work has shown that separability of these behaviors cannot provide a comprehensive representation of the experimental tissue behavior[69-74]. The outcome of this dissertation will significantly contribute to the development of these non-separable viscoelastic models by developing a more robust and comprehensive mathematical model to describe connective tissue mechanics.

Effect of injury, healing, and current surgical treatment techniques on ligament and tendon mechanical properties

Ligament and tendon injury can occur as a result of an single overstretch event (sprain), where the elastic limit (Figure 2, region between B and C) of the tissue is exceeded, or by repetitive cyclical loading (overuse)[75]. Sprains are clinically characterized by three grades: Grade I is minimal overstretch without tissue disruption; Grade II is moderate overstretch with gross tears and hemorrhages; Grade III is complete tissue disruption[31]. Sub-failure injuries (sprain Grades I and II and cyclical overuse) can greatly affect the mechanical performance of the native tissue immediately following the injury (i.e., if no healing is allowed to occur). Alterations in elastic properties include a rightward shift in the toe region on the stress-strain curve, a reduced stiffness in the linear region, and/or a decreased strength[76-80]. Viscoelastic alterations include a greater amount of creep and altered stress relaxation behavior, which suggests that injured tissues dissipate energy abnormally[48,79,81].

In addition to the effects of injury, there have been several studies which have interrogated the effects of healing and treatment on the mechanical properties of these tissues. Many of these previous studies utilized the knee medial collateral ligament (MCL) model because this tissue is known to exhibit spontaneous healing[82]. For healing times ranging from seven days to two years, improvements in the mechanical integrity of the injured MCL have been reported; however, the mechanical properties (elastic and viscoelastic) remain inferior to the normal state[80-90]. Additionally, treatment of injured anterior cruciate ligament (ACL), which does not exhibit spontaneous healing[31,91], is typically performed via bone-patellar tendon-bone or hamstring tendon grafts[82]. Biomechanical evaluation of human cadaveric knees determined that these grafts restore physiologic anterior tibial translation motion, but not rotary motion[92]. This may be a result of the difference inherent mechanical properties of the graft compared to

the native ACL, the graft placement, and/or a reduction of the initial graft tension following insertion (because of graft relaxation)[31,82,92]. Furthermore, surgical treatment of tendon via sutures is complicated by the inherent viscoelasticity of the tissue as well as the viscoelastic behavior of the suture material, which can affect the gap distance between the ruptured ends of the tendon[31].

Together, the inferior mechanical behavior of healing and/or treated ligament and tendon may cause significant joint laxity and instability, altered joint kinematics and loading patterns, altered muscular contraction characteristics, and a higher incidence of tissue failure. It is thought that these alterations following injury or treatment are the mechanism of the abovementioned high incidence of PTOA. Effective treatment practices of these injuries would restore the normal mechanical function of these tissues. Therefore, this dissertation seeks to develop a robust and accurate mechanical characterization method and a mathematical formulation that elucidates the normal mechanical behavior of tendon and ligament tissues, thereby establishing a basis wherein novel treatment modalities can be established.

1.3. Viscoelastic Theory

Visceolastic theory describes the time-dependent relationship between stress and strain for a solid material. Consequently, the current mechanical state of the material depends on previous loading events; that is, the mechanical behavior is dependent upon the loading history (history-dependent behavior). All biological tissues, especially soft tissues such as ligament and tendon, exhibit viscoelastic behavior. In the previous section, it was demonstrated that this time-dependent behavior is necessary to perform the important functional roles of the tissue. This section develops the mathematical formulae typically used to model viscoelastic phenomena in biological tissues.

1.3.1. Linear viscoelasticity

Transient behavior

For typical engineering materials (e.g., steel, aluminum, titanium) at room temperature subjected to small strains, the one-dimensional stress response (σ) to an instantaneous application of strain (ε_0) is described by Hooke's law:

$$\sigma = E\varepsilon_0 \tag{1}$$

where E is the Young's modulus of the material that characterizes its resistance to deformation (stiffness). Similarly, the material's compliance (J) in response to an instantaneous stress application of σ_0 can be described by the inverse of equation (1): $J = 1/E = \varepsilon/\sigma_0$. For a viscoelastic material, the intrinsic parameter relating stress and strain (analogous to E for elastic materials) depends on time, t. Thus, the time-dependent stress response to an instantaneous (transient) strain application of ε_0 is given by:

$$\sigma(t) = E(t) \cdot \varepsilon_0 \tag{2}$$

where $E(t)$ is the *relaxation modulus* (or *relaxation function*) of the material that characterizes its stress decay (stress relaxation) over time. An analogous form of equation (2) can be developed to describe the time-dependent strain in response to an instantaneous stress application of σ_0: $\varepsilon(t) = J(t) \cdot \sigma_0$, where $J(t)$ is the *creep compliance* of the material that characterizes its creep behavior. The mathematical form of the relaxation function is not arbitrary; thermodynamic restrictions require it to be a monotonically decreasing function[93,94]. A linear viscoelastic relaxation function that has been used among the biomechanics community is derived from the standard linear solid model[59]:

$$E(t) = E_\infty + E_0 e^{-t/\tau_r} \tag{3}$$

where E_∞ represents the (steady-state) elastic component of the mechanical behavior (as $t \to \infty$) and E_0 represents the strength of the viscous (time-dependent) relaxation component corresponding to the time constant τ_r.

Cyclical behavior

If a linear viscoelastic material is subjected to harmonic oscillations, the strain will "lag" the stress due to internal material damping (Figure 6); a consequence of the viscous component of the material[94]. Thus, for a sinusoidal stress applied to a material at a specific frequency (ν, expressed in units of Hz):

$$\sigma(t) = \sigma_0 \sin(2\pi\nu t) \tag{4}$$

the resulting out-of-phase strain is:

$$\varepsilon(t) = \varepsilon_0 \sin(2\pi\nu t - \delta) \tag{5}$$

where δ represents the phase lag between stress and strain (Figure 6). The tangent of the phase lag, $\tan(\delta)$, is called the *loss tangent* and is a measure of a material's internal damping[94]. As a consequence of the phase lag between stress and strain, the dynamic stiffness (E^*) of a material can be expressed as a complex number[94]:

$$\frac{\sigma}{\varepsilon_0} = E^* = E' + iE'' \tag{6}$$

which has a magnitude of:

$$|E^*| = \sqrt{(E')^2 + (E'')^2} \tag{7}$$

The storage modulus (E') and the loss modulus (E'') in equations (6) and (7) are defined as:

$$E' = |E^*|\cos(\delta) \tag{8}$$

$$E'' = |E^*|\sin(\delta) \tag{9}$$

where E' represents the energy stored within the material and E'' represents the energy dissipated per cycle[95].

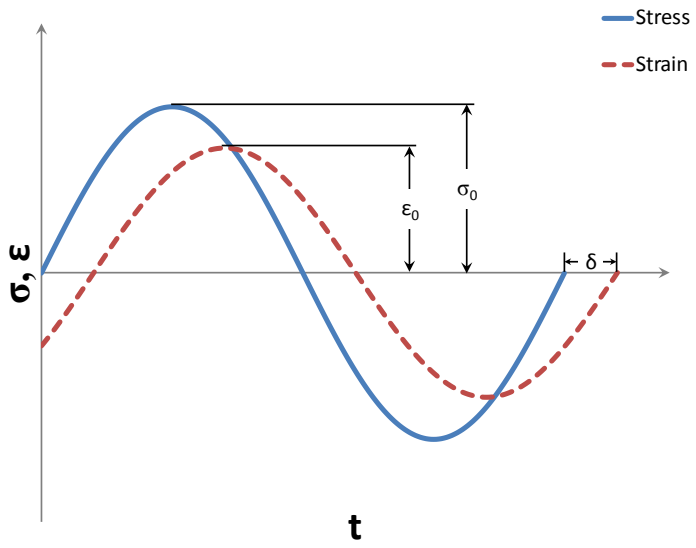

Figure 6: Cyclic behavior of a viscoelastic material. The strain lags the stress by a phase shift, δ.

Constitutive (general) behavior

The equations developed above apply to very specific (transient and cyclical) loading histories. Since biological tissues are subjected to complex, arbitrary load applications *in vivo*, it is desirable to obtain general constitutive formulae to describe linear viscoelastic behavior. Such a mathematical form can be developed using the Boltzman superposition principle, which postulates that the effect of a compound cause is a sum of the individual causes[94]. Utilizing a more rigorous mathematical approach[96], recall from above that for a single instantaneous input of strain:

$$\varepsilon(t) = \varepsilon_0 H(t) \tag{10}$$

where ε_0 is the input strain magnitude and $H(t)$ is the Heaviside step function defined as:

$$H(t) = \begin{cases} 0 & \text{for} \quad t < 0 \\ \frac{1}{2} & \text{for} \quad t = 0 \\ 1 & \text{for} \quad t > 0 \end{cases} \tag{11}$$

the resulting stress output is: $\sigma(t) = \varepsilon_0 E(t)$ for $t > 0$. A series of such step increases in strain can be used to describe any arbitrary strain input profile. Hence, for r discrete step increases in strain, equation (10) can be recast as:

$$\varepsilon(t) = \sum_{i=1}^{r} \Delta\varepsilon_i \, H(t - \tau_i) \tag{12}$$

where $\Delta\varepsilon_i$ is the change in strain magnitude for the i^{th} step occurring at time τ_i, and t is the current time. Utilizing the Boltzmann superposition principle, the resulting stress output [from equation (2)] is:

$$\sigma(t) = \sum_{i=1}^{r} \Delta\varepsilon_i \, E(t - \tau_i) H(t - \tau_i). \tag{13}$$

As the number of strain steps increases to infinity, equation (13) converges to the hereditary integral:

$$\sigma(t) = \int_0^t E(t - \tau) H(t - \tau) \, d\varepsilon(\tau). \tag{14}$$

where τ is a continuous time variable of integration representing the history effect[94,96]. In equation (14), the term $H(t - \tau) = 1$ since $\tau > 0$ is imposed and falls within the bounds of integration[96]. Therefore, for a differentiable strain history, the final form of the constitutive relationship for a linear viscoelastic material can be cast as:

$$\sigma(t) = \int_0^t E(t - \tau) \, \frac{d\varepsilon(\tau)}{d\tau} \, d\tau \tag{15}$$

It can be shown that for a single instantaneous strain history of $\varepsilon(\tau) = \varepsilon_0 H(\tau)$, the transient stress response given by equation (2) is recovered from equation (15). Additionally, if a harmonic strain history $\varepsilon(\tau)$ is imposed, the stress given by equation (15) can be represented as a complex number in the form of equation (6)[94]. If the relaxation function given by equation (3) is assumed and input into equation (15), the complex moduli are determined by[94]:

$$E'(\omega) = E_\infty + E_0 \frac{\omega^2 \tau_r^2}{1 + \omega^2 \tau_r^2} \tag{16}$$

$$E''(\omega) = E_0 \frac{\omega \tau_r}{1 + \omega \tau_r} \tag{17}$$

where $\omega = 2\pi\nu$ (ν is the loading frequency as defined above).

Linear viscoelasticity assumes that both the elastic and the viscous components of the mechanical behavior are linear. Specifically, a material modeled utilizing linear viscoelasticity must satisfy two assumptions: (1) the relationship between stress and strain during stress relaxation experiments performed at different strain magnitudes (taken at isochrones) is linear (linear elastic behavior assumption), and (2) the relaxation modulus is independent of the applied strain level (linear viscous behavior assumption)[94]. Soft connective tissues which undergo finite deformations violate the assumptions of linear viscoelasticity. Therefore, more general, quasi-linear and fully nonlinear formulations have been developed to describe the nonlinear viscoelastic behavior of soft tissues.

It is important to note that the one-dimensional (i.e., uniaxial) nonlinear formulae in the following sections (1.3.2 and 1.3.3) are presented in terms of infinitesimal engineering strains in order to simplify their interpretation as a generalization of the linear viscoelastic formulation [equation (15)]. These nonlinear formulae are applicable to one-dimensional finite deformations because rotations are not present in uniaxial tensile tests and these infinitesimal strain values can be readily converted to finite deformation strain measures (e.g., Green-Lagrangian strain)[34].

1.3.2. Quasi-linear viscoelasticity

The quasi-linear viscoelastic (QLV) theory proposed by Fung[97] has been widely-accepted as the gold-standard to describe the time-dependent behavior of soft connective tissues[21,84,98-105]. This formulation incorporates the known nonlinear, hyperelastic behavior exhibited by soft connective tissues by generalizing the linear elastic behavior assumption of linear viscoelastic theory. Specifically, the strain- and time-dependent stress in response to an instantaneous (Heaviside) strain application is modeled as the separable convolution ($*$) of the hyperelastic $\sigma^e(\varepsilon)$ and viscous $G(t)$ components of the mechanical behavior:

$$\sigma(t,\varepsilon) = G(t) * \sigma^e(\varepsilon) \tag{18}$$

A restriction is imposed on the relaxation function $G(t)$ such that $G(0) = 1$. This normalized function is called the *reduced relaxation function*. For general strain histories, the QLV equation takes the form[59]:

$$\sigma(t,\varepsilon) = \int_0^t G(t-\tau)\frac{\partial\sigma^e(\varepsilon)}{\partial\varepsilon}\frac{\partial\varepsilon(\tau)}{\partial\tau}d\tau \tag{19}$$

Since $G(t)$ is independent of the applied strain magnitude, a fundamental assumption of QLV theory is linear viscous behavior.

1.3.3. Fully nonlinear viscoelasticity

Recent studies have conclusively demonstrated both that tendon[69] and ligament[70-74] exhibit fully nonlinear viscoelastic behavior (nonlinearity in both the elastic and the viscous aspects of the tissue's mechanical behavior) at strain magnitudes associated with physiologic joint motion. This nonlinear behavior cannot be accurately captured by equation (19). Fully nonlinear viscoelastic formulations allow relaxation to occur as a function of the applied strain via a non-separable formulation[94]:

$$\sigma[t,\varepsilon(t)] = \int_0^t E[\varepsilon(\tau), t-\tau]\frac{d\varepsilon(\tau)}{d\tau}d\tau \tag{20}$$

where $E(\varepsilon,t)$ is the strain- and time-dependent relaxation modulus. The non-separability condition in equation (20) necessarily imposes the condition that $E(\varepsilon,t)$ simultaneously describe both elastic and viscous nonlinearities. Several techniques for direct integration of equations (15) and (20) are presented in Appendix F. Under a Heaviside strain application of ε_0, equation (20) reduces to:

$$\sigma[t,\varepsilon(t)] = E(\varepsilon,t)\cdot\varepsilon_0 \tag{21}$$

An objective of this dissertation is to interrogate the errors associated with the predicative accuracy of the QLV model. Additionally, in order to shift the current FE modeling

paradigm to include fully nonlinear viscoelastic effects and accurately model physically-important dynamic loading events, a fully nonlinear viscoelastic formulation and characterization methodology will be developed and implemented into a FE algorithm.

1.4. Specific Aims

As described above, there is a significant need to characterize and model the normal, nonlinear viscoelastic behavior of connective tissues. Therefore, the overall objectives of this dissertation are to develop a robust viscoelastic characterization technique to model the nonlinear viscoelastic behavior of soft biological tissues, and to implement this model into current FE software. In order to achieve this objective, three specific aims are designated for this dissertation:

Specific Aim 1: Develop and validate a nonlinear viscoelastic characterization technique for musculoskeletal soft tissues that incorporates relaxation manifested during loading.

Viscoelastic relaxation during tensioning is an intrinsic protective mechanism of musculoskeletal soft tissues. However, current viscoelastic characterization methodologies for these tissues either negate this important behavior or attempt to incorporate this behavior using methods that are restricted to a specific viscoelastic formulation and/or assume an *a priori* (linear) strain ramp history. In order to address these shortcomings, chapter 2 presents the development and validation of a novel finite ramp time correction method for stress relaxation experiments that is transferrable between various viscoelastic formulations and can accommodate an arbitrary strain ramp history. Additionally, the errors associated with currently accepted characterization methodologies which utilize specific QLV and fully nonlinear viscoelastic formulations are elucidated. The data presented in this chapter: (1) indicate that this novel correction method significantly reduces the errors associated with previous characterization techniques, and (2) demonstrate the necessity for the use of a fully nonlinear

viscoelastic formulation, which incorporates relaxation manifested during loading, to model the viscoelastic behavior of biological soft tissues.

Specific Aim 2: Characterize the nonlinear viscoelastic behavior of various types of ligamentous tissues and tendon.

Since ligamentous tissues exhibit large variability in morphology and biochemistry[40], specific ligaments exhibit substantially different viscoelastic characteristics[72]. In addition, tendinous tissues may exhibit different nonlinear viscoelastic behavior than ligament[69]. Therefore, in order to gain a measure of the robustness and the applicability of the characterization methodology and constitutive formulae developed in chapter 2 to describe general musculoskeletal soft tissue viscoelasticity, this method and formulae are used to fit and predict the viscoelastic behavior of various spinal ligaments and tendinous tissue.

Chapter 3 applies the characterization method developed in chapter 2 to three human spinal ligaments which display unique mechanical properties. The nonlinear viscoelastic behavior of the human anterior longitudinal ligament (ALL), posterior longitudinal ligament (PLL) and ligamentum flavum (LF) were elucidated across the temporal spectrum associated with physiologic spinal motion patterns. It was observed that the strain-dependent viscoelastic behavior of the longitudinal ligaments (ALL and PLL) was dominated by both the short-term (0.1 s) and the steady-state (>> 100 s) behavior. Conversely, the LF exhibited consistent relaxation behavior across the temporal spectrum. From these data, it can be concluded that the unique strain-dependent temporal behavior of these spinal ligaments may be a functional adaptation that minimizes muscular expenditure during quasi-static postures while maximizing structural stability during transient loading events.

Chapter 4 interrogates the applicability of the characterization method and the constitutive formulae developed in chapter 2 to describe tendinous nonlinear viscoelasticity.

The nonlinear stress relaxation behavior of ovine Achilles tendon was characterized using the methodology developed in chapter 2, and the ability of the fitted coefficients to predict physiologic dynamic behavior was elucidated and quantified. The results indicated successful application of the developed characterization method to describe tendinous nonlinear viscoelasticity by maintaining a high degree of predictive accuracy.

Specific Aim 3: Integrate a fully nonlinear viscoelastic constitutive formulation into a finite element algorithm.

The widespread use of QLV theory as a model for soft tissue viscoelasticity in computational models stems from the relative ease in which the material parameters can be input into various software packages. Therefore, in order to shift the current computational modeling paradigm from these over-simplified QLV formulations towards incorporation of fully nonlinear viscoelastic behavior, chapter 4 provides the derivation and validation of a novel, nonlinear viscoelastic formulation [based on equation (20)] that can be directly input into FE algorithms. This formulation and an accompanying experimental characterization technique (chapter 2) is compared to a previously accepted characterization method and validated against an independent analytical model. The results demonstrated that the FE approximations are in good agreement with the analytical solution. Additionally, the predictive accuracy of these approximations was highly dependent upon the experimental characterization technique.

Completion of these specific aims will represent a significant advancement in our capability to characterize and model the complex nonlinear viscoelastic behavior of musculoskeletal soft tissues. Development of the constitutive formulae that can be implemented in computational models will greatly accelerate our ability to understand the functional role that these tissues play in whole joint mechanics and facilitate future treatment options.

2. Viscoelastic Effects During Loading Play an Integral Role in Soft Tissue Mechanics

The data presented in chapter 2 has been published in the literature (Troyer KL, Estep DJ, Puttlitz CM. Viscoelastic effects during loading play an integral role in soft tissue mechanics. *Acta Biomaterialia*. 2012; 8(1):234–243).

2.1. Introduction

Relaxation during loading may play a vital role in soft tissue mechanics. For example, the spinal anterior longitudinal ligament (ALL) exhibits a greater stiffness, ultimate load, and peak energy at faster loading rates than at slower ones[14,106,107]. This rate-dependent behavior facilitates and guides normal spinal motion patterns at slow loading rates, but prevents excessive joint motion and tissue damage by absorbing additional energy during (fast loading rate) traumatic situations[108]. Unfortunately, this intrinsic relaxation mechanism during loading complicates the experimental viscoelastic characterization of these soft tissues.

From a modeling perspective, soft tissue viscoelasticity can be characterized via stress relaxation experiments to define the tissue's relaxation modulus. Theoretically, the relaxation modulus completely characterizes the temporal stress behavior of the tissue in response to an instantaneous (Heaviside or step) strain application. However, inertial limitations of physical testing devices prevent instantaneous strain applications, and very fast ramp times are intractable due to issues such as overshoot, vibration, and poorly approximated strain histories[84,98,109-112]. Empirical deviations from a true step strain application can cause significant errors in the determination of the tissue's relaxation modulus because of the intrinsic relaxation that occurred during the ramping (loading) period of the experiment.

Several methods have been developed to either correct for the finite ramp time of stress relaxation experiments, or to reduce the error associated with fast ramp times[69-

[71,94,99,109,110,113-116]. However, these methods either negate relaxation manifested during the short-term loading period, or are restricted to very specific (linear) strain applications and/or viscoelastic formulations. To the best of the author's knowledge, no formal study has been performed to interrogate the errors associated with negating the important short-term relaxation behavior. Additionally, for fast ramp times, which accurately represent *in vivo* loading conditions during the activities of daily living[110], the inertial effects of the testing device result in poor linear ramp approximations. Thus, a finite ramp time correction method that is restricted to a linear ramp assumption may introduce errors if physiologic loading rates are used for the experiment. Furthermore, multiple QLV[21,59,98,100,109] and fully nonlinear viscoelastic[69-71,110,117] formulations have been proposed to describe soft tissue viscoelasticity. Current finite ramp time correction methods are not transferrable between these various formulations. Therefore, there exists a significant need to develop a general method to characterize the viscoelastic behavior of these tissues which incorporates relaxation manifested during loading. The aims of this chapter were: (1) to develop and validate a finite ramp time correction method for stress relaxation experiments that is independent of the shape of the applied ramp history and the specific viscoelastic formulation, and (2) to interrogate the errors associated with (a) using a linear ramp history assumption applied to fast-ramp stress relaxation experiments and (b) negating the short-term relaxation behavior.

2.2. Materials and Methods

In order to demonstrate the transferability of the finite ramp time correction method [hereafter referred to as the *comprehensive viscoelastic characterization* (CVC) method] between various viscoelastic formulations, this method was used to fit a QLV and a fully nonlinear viscoelastic formulation to an empirical stress relaxation data set. Since our laboratory is specifically interested in spinal tissues, this method was developed using the human cervical

spine ALL as the model for soft tissue viscoelasticty. Structurally, the ALL is a narrow fibrous band (with predominant fiber alignment parallel to the spinal axis) connecting the anterior aspects of adjacent vertebrae[108]. Functionally, this ligament stabilizes the spinal column during flexion-extension motions and maintains intradiscal pressures by resisting disc bulge[108,118,119]. Although the ALL is known to exhibit fully nonlinear viscoelastic behavior[72], experimental data were also fitted to the QLV formulation in order to demonstrate the transferability of the CVC method between viscoelastic formulations commonly used to describe soft tissue mechanics. The parameters obtained from the stress relaxation fits were used to predict an independent cyclic data set. All stress relaxation fits and cyclic predictions were performed in MATLAB (version 7.11; TheMathWorks, Inc.; Natick, MA).

2.2.1. Empirical data capture

The ALL experimental data utilized in this chapter represents a subset of a larger study which also interrogated the viscoelastic behavior of the posterior longitudinal ligament (PLL) and the ligamentum flavum (LF)[72]. The following briefly describes the dissection procedure used to isolate all three ligaments (ALL, PLL, and LF). Data regarding the PLL and LF nonlinear viscoelastic behavior are presented in chapter 3 along with the interpretation of the behavior for all three ligaments with regard to functional spinal biomechanics. The experimental data in the current chapter utilizes the ALL data as a tissue model strictly to develop and validate the CVC methodology.

Briefly, the C5-C6 motion segment of eight human cadaveric spines (mean age: 59 ± 9.2; 2 females, 6 males) was isolated and all non-osteoligamentous tissues were carefully removed. In order to separate the longitudinal ligaments from the LF, a cranial-to-caudal cut was made at the pedicles to isolate the anterior column from the posterior elements. The ALL (n=8) and PLL (n=8) were isolated into bone-ligament-bone (BLB) preparations by transecting the anterior

column in its mid-coronal plane and carefully removing the disc tissues. The LF (n=6) BLB preparations were isolated by transecting the facet capsular ligaments and the interspinous and supraspinous ligaments of the posterior elements. Two LF preparations were damaged during dissection and were excluded from study. The vertebral elements of the BLB preparations were potted in polymethylmethacrylate for attachment to the testing device. Hydration was maintained throughout the dissection and potting procedures via periodic saline spray. Each potted BLB preparation was placed in an environmental chamber (isotonic saline maintained at 37°C), which was affixed to a servohydraulic mechanical testing device (858 Mini Bionix II; MTS; Eden Prairie, MN) with a load cell (500 N capacity; model 661.11B-02; MTS; Eden Prairie, MN) placed in the load train, and allowed to equilibrate for 1 hour in its zero-force configuration. Inertial artifacts caused by the load cell placement (connecting the testing device actuator to the specimen) were determined to be minimal (Appendix B).

Following hydrothermal equilibration, each ligament was tensioned to 5 N[110,123,128] and allowed to relax for 600 s. The resulting displacement was used as the reference configuration. Each ligament was then subjected to a cyclic (haversine) frequency sweep (0.001 Hz, 0.01 Hz, 0.1 Hz, and 1 Hz) at 10% and 15% peak-to-peak strain amplitudes. The slowest frequency (0.001 Hz) was performed as a preconditioning procedure. The remaining frequencies were chosen to observe the model's predictive accuracy with regard to varying physiologic loading rates, from quasi-static (0.01 Hz) to dynamic (1 Hz). Following this cyclic protocol, the reference configuration was re-defined under 5 N of pretension, and the specimen was preconditioned (10% peak-to-peak strain amplitude, 1 Hz, 120 cycles) and subjected to stress relaxation experiments (ramp time: < 0.3 s, hold: 600 s, recover: 600 s[123,128]) at 4%, 6%, 8%, 10%, 14%, 16%, 18%, 20%, and 25% engineering strain magnitudes. These strain magnitudes are well below the failure strains reported for these ligaments[22] and fall within the physiologic bounds predicted by

computational and mathematical models[14,120]. The cross-sectional area of each ligament was measured using *post hoc* digital image capture[72].

2.2.2. Quasi-linear viscoelastic formulae

For this chapter, the QLV formulation was cast as:

$$\sigma(\varepsilon,t)=\int_0^t G(t-\tau)\frac{\partial\sigma^e(\varepsilon)}{\partial\varepsilon}\frac{\partial\varepsilon(\tau)}{\partial\tau}d\tau+\sigma_0 \tag{22}$$

where σ_0 represents the initial tissue pretension in the reference configuration. The reduced relaxation function was approximated by the Prony series[21,72,121]:

$$G(t)=G_\infty+\sum_{i=1}^{4}G_i e^{-t/\tau_i} \tag{23}$$

subjected to the constraint:

$$G_\infty+G_1+G_2+G_3+G_4=1 \tag{24}$$

where G_∞ is the steady-state relaxation coefficient [$G_\infty=\lim_{t\to\infty}G(t)$], and the G_i coefficients represent the relaxation strength corresponding to the τ_i time constants. This relaxation function was selected such that it was similar in form to the fully nonlinear relaxation modulus described in detail in the following section (2.2.3). The Prony series representation (with fitted parameters G_∞, G_i, and τ_i) is known to yield non-unique solutions[59]. However, a unique solution can be achieved by fixing the τ_i time constants (Appendix A). Additionally, our previous work[72] has demonstrated that this Prony series representation is insensitive to initial guesses spanning five decades (0.001 to 10). Therefore, the shortest fixed time constant, τ_1 = 0.1 s, was chosen to temporally coincide with the experimental ramp time (< 0.3 s). Succeeding time constants were incrementally increased by decade values[21,72], ending at the decade value which corresponded with the length of the experiment: τ_2 = 1 s, τ_3 = 10 s, τ_4 = 100 s. The instantaneous elastic stress, and its derivative, was represented by the nonlinear equations:

$$\sigma^e(\varepsilon) = A(e^{B\varepsilon} - 1) \tag{25}$$

$$\frac{\partial \sigma^e(\varepsilon)}{\partial \varepsilon} = ABe^{B\varepsilon} \tag{26}$$

where A and B are the instantaneous elastic parameters[21,72,121].

If the applied strain ramp history is complex (not a pure linear ramp and constant hold), differentiation of the applied strain history $\varepsilon(\tau)$ complicates direct numerical integration of equation (22). Therefore, in order to simplify the integration of equation (22), the differential operator was removed from the input strain history via integration by parts:

$$\begin{aligned}\sigma(\varepsilon, t) &= ABe^{B\varepsilon}\left[-\int_0^t \frac{dG(t-\tau)}{d\tau}\varepsilon(\tau)d\tau + G(t-t)\varepsilon(t) - G(t-0)\varepsilon(0)\right] + \sigma_0 \\ &= ABe^{B\varepsilon}\left[-\int_0^t \frac{dG(t-\tau)}{d\tau}\varepsilon(\tau)d\tau + G(0)\varepsilon(t)\right] + \sigma_0\end{aligned} \tag{27}$$

Several finite ramp time correction methods have been developed for QLV formulations[99,109,114,115]. For this study, our method is compared to that developed by Abramowitch and Woo[109], which has been implemented in many recent studies[72,82,84,122-125]. The methods used for obtaining the data for these comparisons is outlined in our previous manuscript[72]. Limitations of the Abramowitch and Woo method include the assumption of QLV tissue behavior (linear viscous behavior) and the assumption of a pure linear strain ramp application, which require very long (non-physiologic) ramp times. In order to elucidate errors associated with a pure linear strain assumption applied to an actual (nonlinear, fast-ramp) strain history, the fitted parameters obtained using the methodology of Abramowitch and Woo were used to predict the full (ramp-relax) stress relaxation experiment, and the cyclic experiments, by numerically integrating equation (27) with the actual strain history used as input. Since the QLV theory assumes that $G(t)$ is independent of strain magnitude, only stress relaxation data at the 10% strain magnitude were fitted for this study.

2.2.3. Fully nonlinear viscoelastic formulae

For the current chapter, the fully nonlinear viscoelastic formulation was cast as:

$$\sigma[\varepsilon(t), t] = \int_0^t E[\varepsilon(\tau), t-\tau] \frac{d\varepsilon(\tau)}{d\tau} d\tau + \sigma_0 \tag{28}$$

The nonlinear (strain- and time-dependent) relaxation modulus was approximated by the Prony series[126]:

$$E(\varepsilon, t) = E_\infty(\varepsilon) + \sum_{i=1}^{4} E_i(\varepsilon) e^{-t/\tau_i} \tag{29}$$

where $E_\infty(\varepsilon)$ represents the strain-dependent steady-state modulus [$E_\infty(\varepsilon) = \lim_{t\to\infty} E(\varepsilon, t)$], and the $E_i(\varepsilon)$ represent the strain-dependent moduli corresponding to the τ_i time constants. Analogous to equation (27), equation (28) was integrated by parts to simplify the numerical integration:

$$\begin{aligned} \sigma[\varepsilon(t), t] &= -\int_0^t \frac{dE[\varepsilon(\tau), t-\tau]}{d\tau} \varepsilon(\tau)\, d\tau + E[\varepsilon(t), t-t]\varepsilon(t) - E[\varepsilon(0), t-0]\varepsilon(0) \\ &= -\int_0^t \frac{dE[\varepsilon(\tau), t-\tau]}{d\tau} \varepsilon(\tau)\, d\tau + E[\varepsilon(t), 0]\varepsilon(t) + \sigma_0 \end{aligned} \tag{30}$$

To the best of the author's knowledge, there are relatively few finite ramp time correction methods for fully nonlinear viscoelastic materials[113,116]. However, these previous attempts were developed specifically for the Schapery nonlinear viscoelastic material model, rather than the single integral formulation of the modified superposition method [i.e., equation (28)][94,96] which has been recommended for modeling ligament viscoelasticity[117]. Instead of directly correcting for the finite ramp time, equation (28) has traditionally been used with fast ramp times that approximate a true (Heaviside) step function, which has the form:

$$\sigma[t, \varepsilon(t)] = E(\varepsilon, t) \cdot \varepsilon_0 + \sigma_0 \tag{31}$$

Data from the relaxation period of the experiment are then considered only after a specified amount of time in order to reduce the transient errors of the testing device. Multiples of the

ramp time (t_0), such as $10t_0$[70,71,94] and $2.5t_0$[69,94,110], have been used or recommended for connective tissues. These methods negate important short-term relaxation information and may not be appropriate if the relative degree of short-term relaxation is substantial[111]. Since the short-term relaxation behavior plays an important role in the mechanical performance of soft tissues, the errors associated with the $10t_0$ and the $2.5t_0$ fitting methods are elucidated in this chapter by quantifying the ability of their fitted parameters to predict the full (ramp-relax) stress relaxation experiment and the cyclic experiments (via numerical integration of equation (30) using the actual strain history). For the fully nonlinear viscoelastic formulation the stress relaxation curves from all strain magnitudes were fitted using the $10t_0$ method, the $2.5t_0$ method, and the CVC method.

2.2.4. Comprehensive viscoelastic characterization method

Thermodynamic limitations require the relaxation modulus to be a monotonically decreasing function[93,94]. Therefore, the CVC method was designed to fit only the decreasing (relaxation) period of the full experimental curve so that the fitted parameters are unconstrained. The relaxation manifested during loading is then incorporated by utilizing the following iterative algorithm:

(a) **Fit the relaxation period of the experimental data, assuming a Heaviside strain application**. For the QLV formulation, an instantaneous strain application can be considered by assuming separability of the functions $\sigma^e(\varepsilon)$ and $G(t)$ [100,109]. Thus, equation (25) was fitted to the ramping period ($0 < t < t_0$, where t_0 is defined by the maximum stress), and equation (23), subjected to the constraint in equation (24), was fitted to the normalized $[\sigma(t_0) = 1]$ relaxation period ($t \geq t_0$)[100,109]. For the fully nonlinear formulation, a Heaviside step was assumed, and data in the relaxation period were fitted to equation (31).

(b) Predict the full (ramp-relax) experiment by inputting the Heaviside assumption parameters obtained from step (a) into the integral form of the constitutive equation (Figure 7). The integral formulations [equation (27) for the QLV formulation, equation (30) for the fully nonlinear formulation] were numerically integrated (*quadgk* MATLAB function). The actual experimental strain history was included in this integration by use of a fitted cubic spline (*csaps* MATLAB function) to functionally describe $\varepsilon(\tau)$.

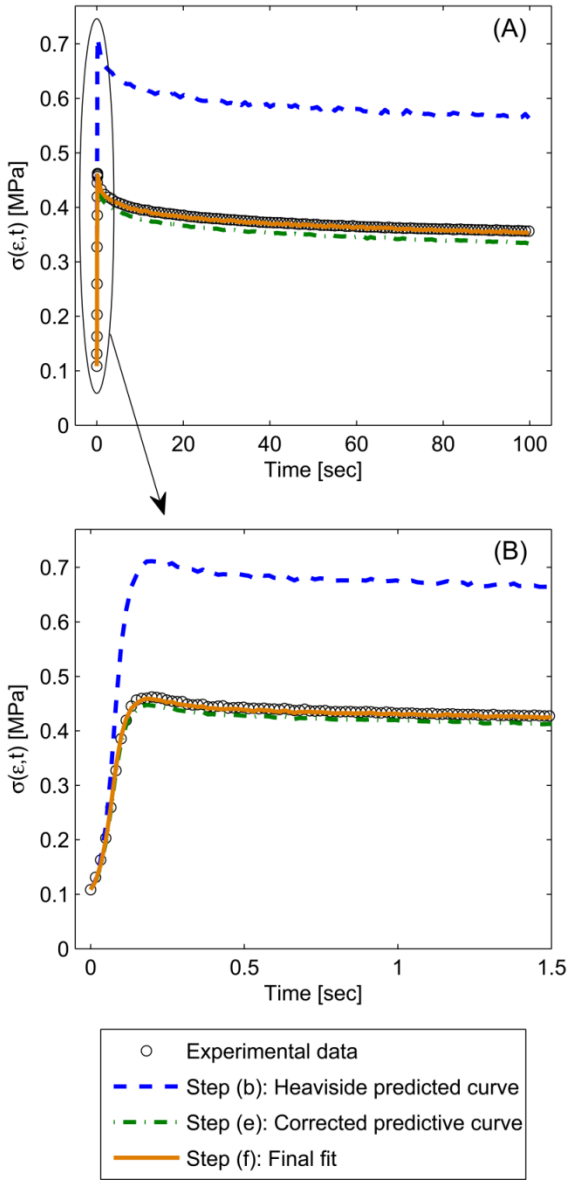

Figure 7: Depiction of the CVC method for a typical specimen for both (A) the long-term behavior, and (B) the short-term behavior.

(c) Fit the relaxation period of the predicted curve obtained from step (b), assuming an instantaneous strain application [see step (a) for the analogous fitting procedure].

(d) **Calculate the difference $\{\delta\}$ between the fitted parameters for the experiment and the current prediction as**:

$$\{\delta\} = \{\Theta\}_{\text{exp}} - \{\Theta\}_{\text{pred}} \tag{32}$$

where $\{\Theta\}_{\text{exp}}$ is a vector containing the fitted parameters from step (a), and $\{\Theta\}_{\text{pred}}$ is a vector containing the fitted parameters determined form step (c). For the QLV fits: $\{\Theta\} = \{\text{A}, \text{B}, \text{G}_\infty, \text{G}_1, \text{G}_2, \text{G}_3, \text{G}_4\}$; for the fully nonlinear fits: $\{\Theta\} = \{\text{E}_\infty, \text{E}_1, \text{E}_2, \text{E}_3, \text{E}_4\}$.

(e) **Define a new set of parameters $\{\boldsymbol{\Theta}\}_{\text{new}}$ as input into the integral form of the constitutive equation and integrate to obtain a new predicted curve (Figure 7)**:

$$\{\Theta\}_{\text{new}} = \{\Theta\}_{\text{exp}} + \{\delta\} \tag{33}$$

(f) **Iterate steps (c) through (e) until the following criterion (tolerance, $\boldsymbol{TOL}$) is satisfied**:

$$|\max\{\delta\}| \leq TOL \tag{34}$$

For the present study, TOL = 10^{-6} (Figure 7). By utilizing initial guesses within the range described above, and forcing the shape of the predicted curve to match the experimental curve [step (d)], the prescribed (relatively low) tolerance necessitates that the best set of (unique) coefficients has been obtained.

2.2.5. Error quantification

Since the coefficient of determination (r^2 value) is a poor measure of goodness-of-fit for stress relaxation experiments due to the disproportionately large amount of datum points in the long-term behavior[72], a weighted root mean-squared error ($RMSE$)[111,127] was calculated in order to determine the probable error of the fitted stress relaxation curves:

$$RMSE = \sqrt{\frac{\sum_{k=1}^{n}\left\{w(t_k)\cdot\left[\left(\sigma_{\text{exp}}\right)_k - \left(\sigma_{\text{model}}\right)_k\right]\right\}^2}{n}} \tag{35}$$

where n is the number of datum points. The weighting function, $w(t_k)$, was defined as:

$$w(t_k) = \frac{e^{-t_k/\tau_1} + e^{-t_k/\tau_2} + e^{-t_k/\tau_3} + e^{-t_k/\tau_4}}{4} \tag{36}$$

where t_k is the k^{th} time datum point, and $\left(\sigma_{\text{exp}}\right)_k$ and $\left(\sigma_{\text{model}}\right)_k$ are the k^{th} experimental and model stress datum points, respectively. The $RMSE$ was also calculated without the weighting function to quantify the error associated with the cyclic predictions. Additionally, the percent error between the k^{th} datum points for the cyclic predictions were calculated as:

$$\%\ error = \left|\frac{\left(\sigma_{\text{model}}\right)_k - \left(\sigma_{\text{exp}}\right)_k}{\left(\sigma_{\text{exp}}\right)_k}\right| \cdot 100\% \tag{37}$$

2.2.6. Statistics

All statistical analyses were performed using SAS statistical software (SAS Institute, Inc.; Cary, NC). Due to the large number of separate statistical analyses, each statistical test in this chapter is outlined in the corresponding figure or table caption for clarity. Unless otherwise stated, $p<0.05$ was used to define statistical significance.

2.3. Results

2.3.1. QLV stress relaxation fits

Figure 8 depicts a typical QLV stress relaxation curve fit using the Abramowitch and Woo method and the CVC method. Although there was not a statistical difference between the $RMSE$ calculated for both methods ($p=0.547$; Table 1), there was a statistically significant difference between several of the fitted reduced relaxation function coefficients (Table 2). With the actual strain history used as input for equation (27), the Abramowitch and Woo parameters poorly predicted the stress relaxation experiment (Figure 8), as indicated by statistically

significant increases (one order of magnitude) in $RMSE$ (p=0.008 for both comparisons; Table 1).

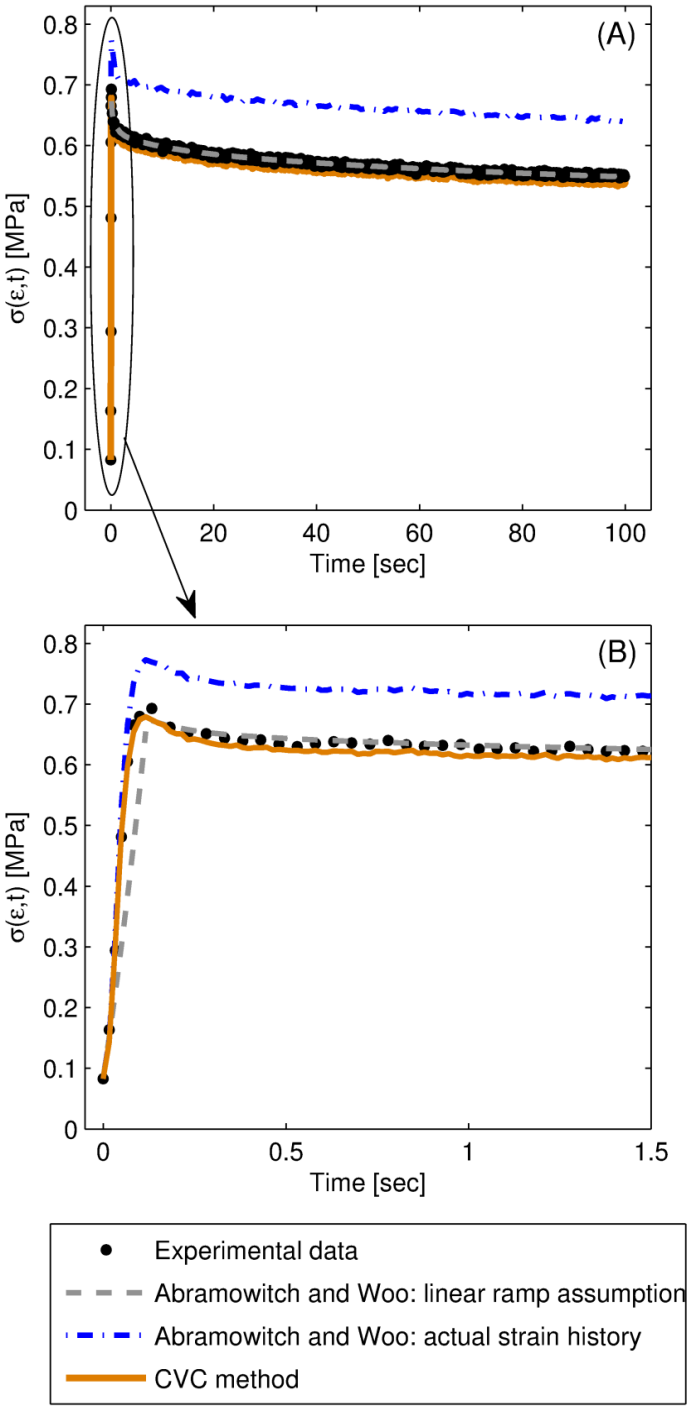

Figure 8: A typical QLV stress relaxation curve fit from a representative specimen for both (A) the long-term and (B) the short-term behavior.

Table 1: Median $RMSE$ values (95% lower confidence limit, 95% upper confidence limit) for the two QLV curve fitting methods compared to the stress relaxation curves predicted by inputting the Abramowitch and Woo (linear ramp assumption) fitted parameters into

Method	$RMSE$ [kPa]
Abramowitch and Woo: linear ramp assumption	1.89 (1.10, 4.79)[a]
Abramowitch and Woo: actual strain history	49.98 (23.01, 67.66)[b]
CVC method	1.81 (0.65, 3.14)[a]

Superscript letters indicate statistical groupings; different letters indicate p<0.017

Table 2: Comparison of the median fitted parameters (95% lower confidence limit, 95% upper confidence limit) for the two QLV fitting methods. The Abramowitch and Woo fitted parameters (with a linear ramp assumption) significantly under-predicted the amount of relaxation that actually occurred during the experiment, as indicated by the reduced G_1, G_3, and G_4 coefficients. These under-predictions were manifested as an increase in the G_∞ coefficient. Statistical analyses were performed by using a Wilcoxon signed-rank test.

Parameter	Abramowitch and Woo		CVC method		p-value
A	0.262	(0.219, 1.173)	0.203	(0.094, 1.31)	0.148
B	8.908	(4.031, 11.111)	8.380	(7.359, 13.716)	0.742
$\boldsymbol{G_\infty}$	**0.725**	**(0.704, 0.833)**	**0.601**	**(0.567, 0.695)**	**0.008**
$\boldsymbol{G_1}$	**0.036**	**(2.318E-4, 0.066)**	**0.112**	**(0.082, 0.178)**	**0.008**
G_2	0.076	(0.056, 0.109)	0.059	(0.048, 0.092)	0.195
$\boldsymbol{G_3}$	**0.065**	**(0.040, 0.097)**	**0.097**	**(0.063, 0.125)**	**0.008**
$\boldsymbol{G_4}$	**0.098**	**(0.062, 0.175)**	**0.117**	**(0.075, 0.195)**	**0.008**

2.3.2. QLV cyclic predictions

A significant amount of error was observed for the cyclic predictions within each frequency and amplitude for both QLV fitting methods (Figure 9). However, the CVC method cyclic prediction had a significant reduction in error when compared to the curve predicted using the Abramowitch and Woo method (Table 3). The cyclic predictions from each of the QLV fitting methods, except for the 10% strain amplitude, 1 Hz frequency, had a greater $RMSE$ and a statistically larger percent error than the experimental error (Table 3), indicating that these predictions were outside the bounds of experimental variability.

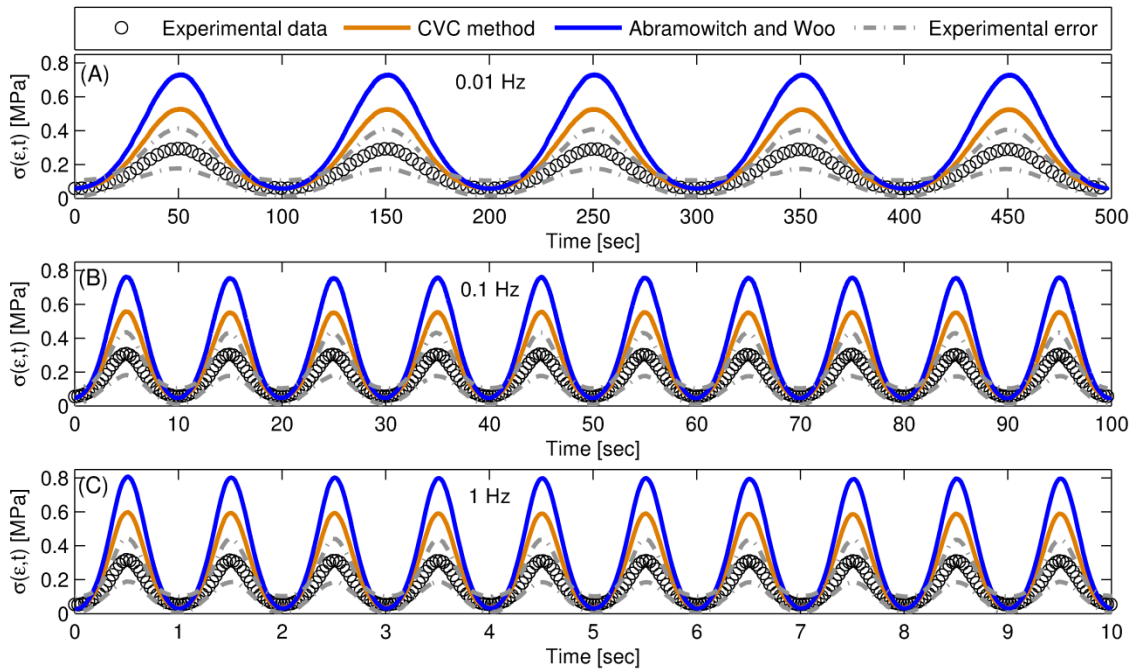

Figure 9: Comparison of the 10% cyclic strain amplitude predictions for both QLV fitting methods at the (A) 0.01 Hz, (B) 0.1 Hz, and (C) 1 Hz loading frequencies. Although both fitting methods produced good stress relaxation fits, each method poorly predicted the average cyclic experimental data across all frequencies. The cyclic predictions for the 15% strain amplitude were similar. Experimental error was defined as one standard deviation from the experimental mean.

Table 3: Summary of the error calculations for the QLV cyclic predictions for both fitting methods at (A) the 10% and (B) the 15% strain amplitudes. The median percent error (95% lower confidence limit, 95% upper confidence limit) and $RMSE$ for the predictions from both fitting methods were outside the bounds of experimental error (defined as one standard deviation from the experimental mean). Statistical analyses were performed on the percent error by using a Kruskal-Wallis test within each strain amplitude and frequency grouping. *Post hoc* pairwise comparisons were performed by a Wilcoxon rank-sum test with Bonferroni adjustment (statistical significance defined as p<0.017).

	Percent error [%]						$RMSE$ [MPa]		
	0.01 Hz		0.1 Hz		1 Hz		0.01 Hz	0.1 Hz	1 Hz
(A) 10% strain amplitude									
CVC method	53.79	(53.07, 54.45)[a]	53.41	(51.66, 55.05)[a]	56.52	(48.97, 63.22)[a]	0.126	0.132	0.146
Experimental error	40.17	(40.14, 40.20)[b]	42.30	(42.22, 42.41)[b]	40.36	(40.03, 40.77)[a]	0.071	0.076	0.074
Abramowich and Woo	107.21	(106.00, 108.47)[c]	106.64	(103.87, 109.55)[c]	111.16	(99.32, 121.08)[b]	0.239	0.245	0.261
(B) 15% strain amplitude									
CVC method	76.65	(75.50, 77.96)[a]	80.27	(79.40, 81.1)[a]	96.07	(90.89, 99.98)[a]	0.306	0.333	0.348
Experimental error	44.93	(44.87, 44.98)[b]	43.96	(43.83, 44.09)[b]	44.34	(44.07, 44.58)[b]	0.121	0.125	0.126
Abramowich and Woo	151.40	(149.44, 152.89)[c]	151.15	(146.33, 155.29)[c]	152.66	(135.91, 167.06)[c]	0.532	0.562	0.575

Superscript letters indicate statistical groupings within each strain amplitude and frequency; different letters indicate p<0.017

2.3.3. Fully nonlinear viscoelastic stress relaxation fits

Both the $10t_0$ and the $2.5t_0$ methods fit the relaxation period of the data equally well, producing relatively small $RMSE$ values that were not statistically different (p=0.262; Table 4). Although these small $RMSE$ values indicated that the $10t_0$ and the $2.5t_0$ methods produced a good fit of the relaxation period of the experiment, a significant amount of error was observed when their resulting fitted parameters were input into equation (30) with the actual (ramp-relax) strain history (Figure 10; Table 5). Statistical analyses demonstrated larger $RMSE$ values for the predictions from the $10t_0$ and the $2.5t_0$ methods when compared to the CVC method (p<0.001 for both comparisons).

The fully nonlinear viscoelastic strain-dependent moduli [equation (29)] were also dependent upon the fitting method (p<0.001; Figure 11). Statistical differences based on the fitting method were observed for the $E_1(\varepsilon)$, $E_2(\varepsilon)$, and $E_\infty(\varepsilon)$ moduli, and no differences were observed for the $E_3(\varepsilon)$ and $E_4(\varepsilon)$ moduli (Figure 11).

Table 4: Median $RMSE$ values (95% lower confidence limit, 95% upper confidence limit) for the $2.5t_0$ and the $10t_0$ fitting methods (which fit only the *relaxation* period of the data) at each strain magnitude. Statistical analyses were performed using an Analysis of Covariance model (in the SAS PROC MIXED procedure) in order to account for strain magnitude, with a logarithmic transformation used to normalize the variance of the $RMSE$ values.

Strain [%]	$2.5t_0$ $RMSE$ [kPa]		$10t_0$ $RMSE$ [kPa]	
4	0.193	(0.141, 0.911)	0.131	(0.104, 0.922)
6	0.269	(0.193, 0.950)	0.178	(0.129, 0.970)
8	0.317	(0.203, 0.969)	0.217	(0.141, 0.988)
10	0.296	(0.189, 0.912)	0.195	(0.125, 0.919)
12	0.338	(0.242, 0.968)	0.292	(0.154, 0.955)
14	0.441	(0.399, 0.965)	0.322	(0.278, 0.939)
16	0.475	(0.307, 0.961)	0.342	(0.189, 0.978)
18	0.665	(0.379, 1.064)	0.497	(0.297, 1.014)
20	0.603	(0.395, 1.122)	0.433	(0.285, 1.046)
25	0.855	(0.469, 1.247)	0.535	(0.426, 1.033)

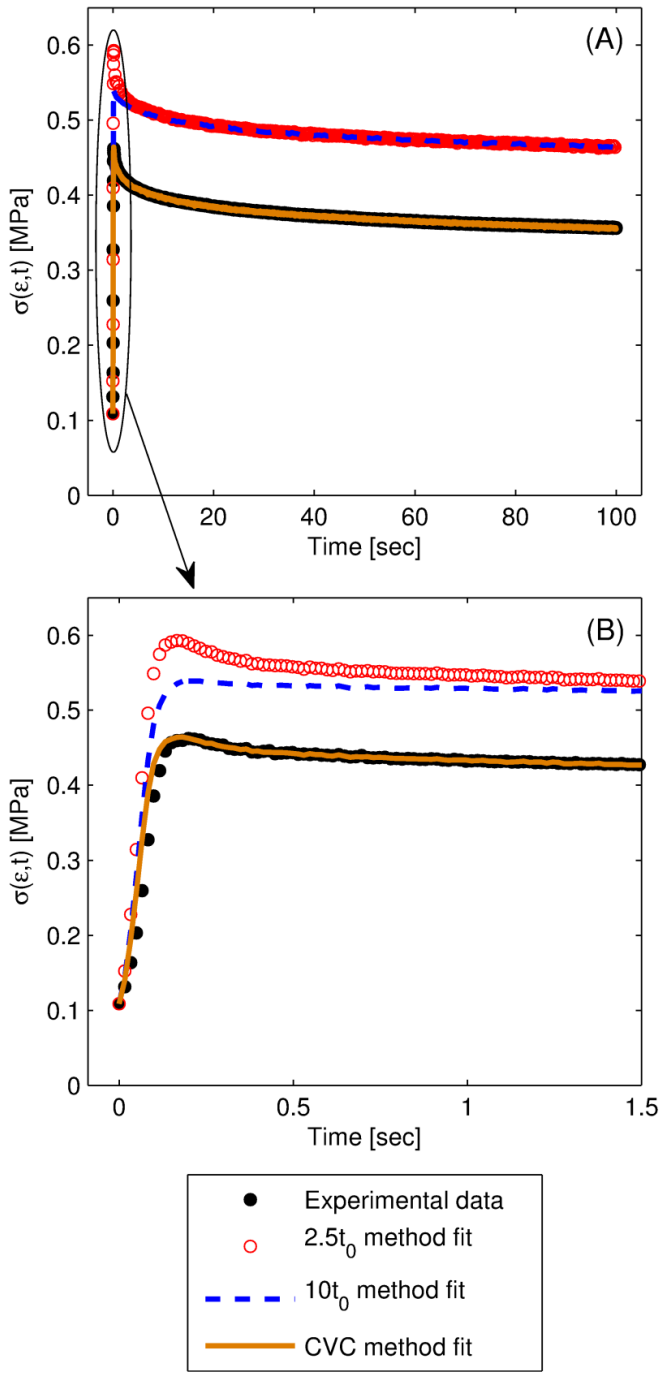

Figure 10: Typical fully nonlinear viscoelastic stress relaxation curve fits from a representative specimen for (A) the long-term and (B) the short-term behavior. Both the $10t_0$ and $2.5t_0$ fitting methods over-predicted the experimental stress relaxation curve because these methods neglect important short-term relaxation behavior which was manifested before 10 and 2.5 times the ramp time, respectively.

Table 5: Median $RMSE$ values (95% lower confidence limit, 95% upper confidence limit) for the fully nonlinear viscoelastic CVC method fits, as well as the $2.5t_0$ and the $10t_0$ predictions. The $RMSE$ values were different for all comparisons within this table (p≤0.03). The CVC method produced the best representation of the data (smallest $RMSE$ values) for these three methods. On average, the median $RMSE$ values for the $2.5t_0$ and the $10t_0$ predictions were more than 1,500% larger than the $RMSE$ values for the CVC method fits. Statistical analyses were performed using an Analysis of Covariance model (in the SAS PROC MIXED procedure) in order to account for strain magnitude. A logarithmic transformation was used to normalize the variance of the $RMSE$ values.

Strain [%]	CVC method $RMSE$ [kPa]		$2.5t_0$ $RMSE$ [kPa]		% increase relative to the CVC method	$10t_0$ $RMSE$ [kPa]		% increase relative to the CVC method
4	0.49	(0.34, 1.03)	23.47	(16.70, 38.54)	4,835.36%	23.21	(16.39, 38.03)	4,783.37%
6	0.76	(0.55, 1.16)	25.20	(15.26, 37.64)	3,323.03%	24.68	(14.59, 36.88)	3,254.89%
8	1.08	(0.90, 1.98)	24.92	(21.42, 41.24)	2,315.02%	24.07	(20.26, 40.25)	2,236.27%
10	1.34	(1.13, 2.97)	24.40	(20.55, 37.11)	1,815.63%	22.96	(18.77, 35.89)	1,708.33%
12	2.01	(1.40, 4.10)	24.27	(18.49, 39.65)	1,206.50%	22.77	(16.50, 37.54)	1,132.07%
14	3.04	(2.14, 6.40)	27.96	(23.24, 40.65)	919.10%	24.37	(18.39, 37.86)	800.88%
16	3.81	(2.68, 7.53)	25.28	(17.79, 38.37)	663.76%	21.84	(14.17, 35.31)	573.56%
18	5.23	(3.40, 12.68)	28.67	(24.45, 42.73)	547.66%	23.92	(15.89, 37.09)	457.02%
20	6.70	(4.37, 17.14)	27.41	(25.25, 49.85)	409.05%	22.63	(14.65, 35.50)	337.63%
25	10.40	(6.87, 30.69)	33.18	(26.72, 85.50)	319.03%	21.82	(17.42, 37.65)	209.80%
Average:					1,635.42%			1,549.38%

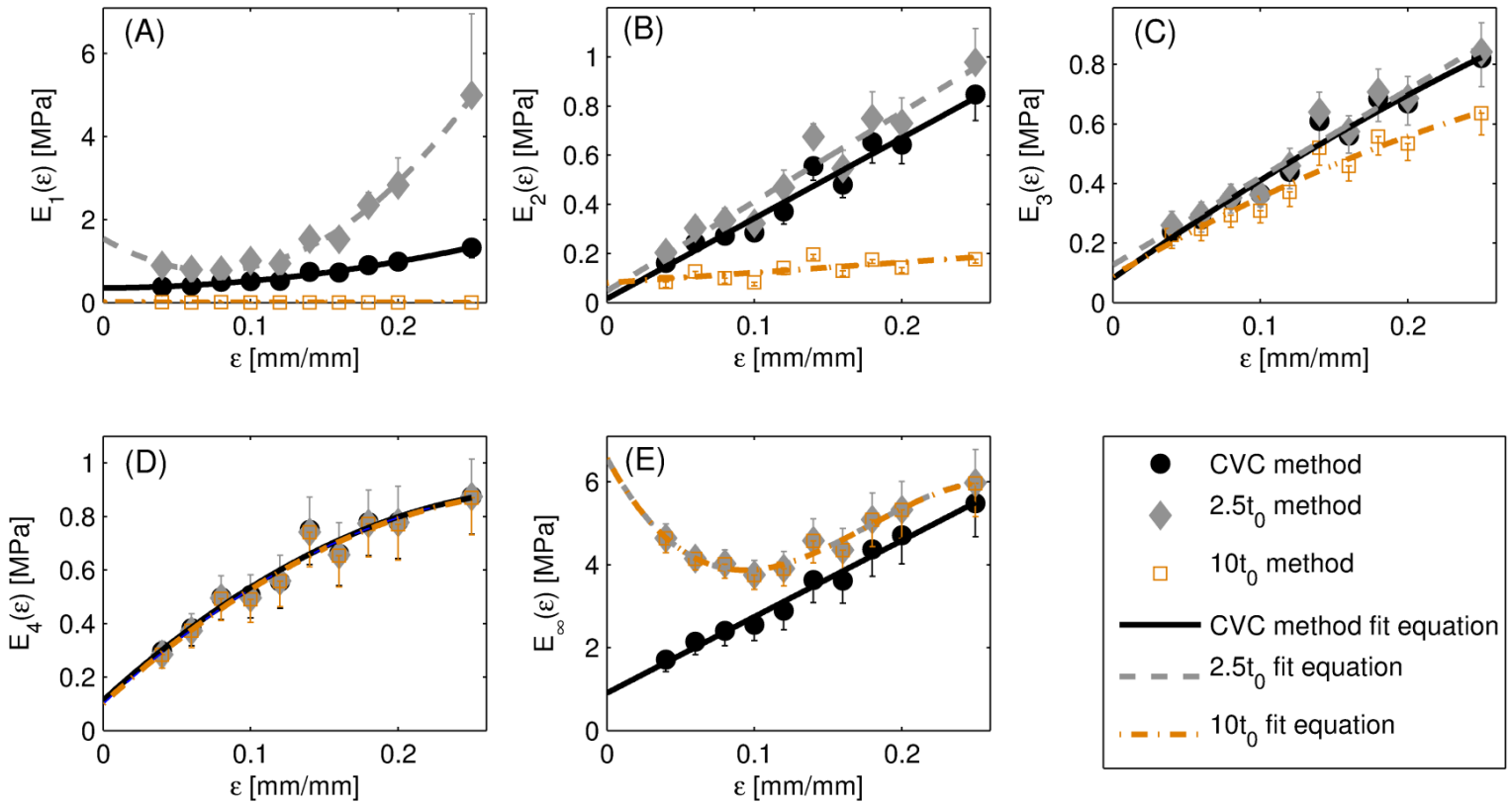

Figure 11: Summary of the fully nonlinear viscoelastic strain-dependent moduli [equation (29)] for each fitting method. The fitted equation for each moduli (not shown for brevity) was determined using a foreword selection method on a polynomial hierarchy, beginning with the intercept. The forward selection method was ceased when the coefficient associated with the highest polynomial degree was not statistically different from zero. Statistical analyses were performed using the SAS PROC MIXED procedure with an appropriate data transformation (square root or logarithmic) used to normalize the variance. These analyses indicated the $E_1(\varepsilon)$ equations were different for each fitting method (p≤0.005), the $E_2(\varepsilon)$ $10t_0$ method equation was different from both the CVC method equation and the $2.5t_0$ method equation (p≤0.024), and the $E_\infty(\varepsilon)$ CVC method equation was different than both the $10t_0$ and $2.5t_0$ method equations (p≥0.006). All other comparisons were not statistically different (p>0.05). Error bars indicate standard error of the mean.

2.3.4. Fully nonlinear viscoelastic cyclic predictions

A significant amount of error was observed for the $10t_0$ and the $2.5t_0$ cyclic predictions (Figure 12). The CVC method, however, predicted the cyclic data extremely well, with percent errors and $RMSE$ values that were an order of magnitude less than the experimental error (Table 6). The percent error and $RMSE$ values for the CVC method predictions were also at least an order of magnitude less than the $10t_0$ and the $2.5t_0$ predicted curves (Table 6). Except for the 15% strain amplitude, 1 Hz frequency, there were no statistical differences between the percent error for the $10t_0$ and the $2.5t_0$ method predictions.

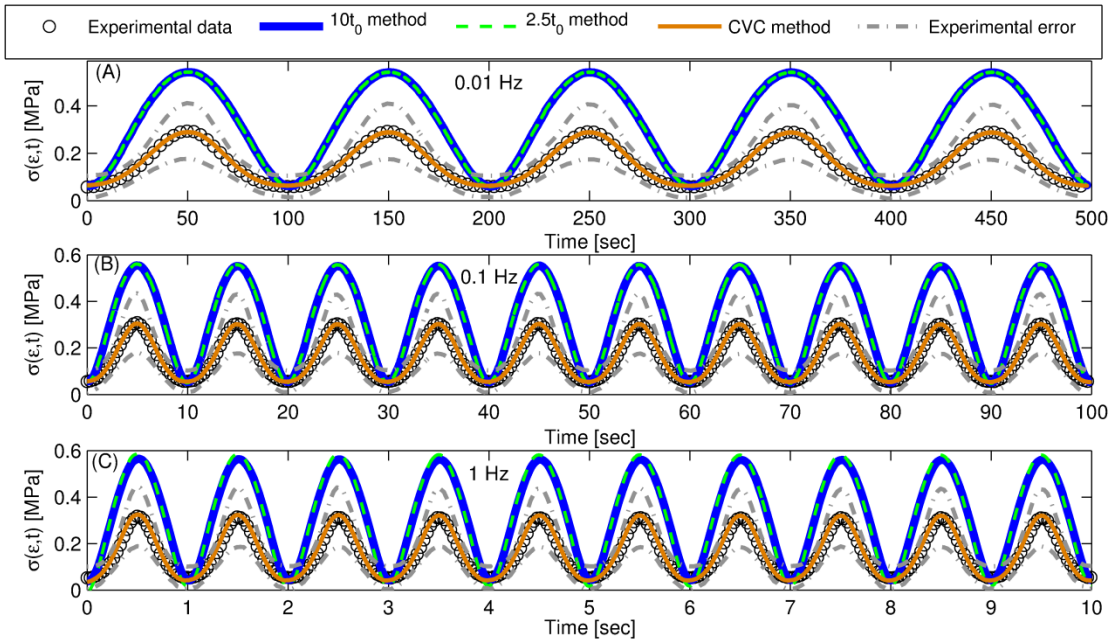

Figure 12: Comparison of the cyclic 10% strain amplitude predictions for the fully nonlinear viscoelastic fitting methods at the (A) 0.01 Hz, (B) 0.1 Hz, and (C) 1 Hz loading frequencies. The cyclic predictions for the 15% strain amplitude were similar. Experimental error was defined as one standard deviation from the experimental mean.

Table 6: Summary of the error calculations for the fully nonlinear viscoelastic cyclic predictions at (A) the 10% and (B) the 15% strain amplitudes. The CVC method parameters predicted the cyclic data extremely well, exhibiting median percent error (95% lower confidence limit, 95% upper confidence limit) and $RMSE$ values that were well within the bounds of experimental error (one standard deviation from the experimental mean) for both strain magnitudes and across all frequencies. Conversely, the parameters obtained from both of the $2.5t_0$ and the $10t_0$ fits poorly predicted the cyclic behavior. Statistical analyses were performed on the percent error by using a Kruskal-Wallis test within each strain amplitude and frequency grouping. *Post hoc* pairwise comparisons were performed by using a Wilcoxon rank-sum test with Bonferroni adjustment (statistical significance defined as p<0.008).

	Percent error [%]						$RMSE$ [MPa]		
	0.01 Hz		0.1 Hz		1 Hz		0.01 Hz	0.1 Hz	1 Hz
(A) 10% strain amplitude									
CVC method	**5.22**	**(5.18, 5.27)[a]**	**2.76**	**(2.67, 2.84)[a]**	**6.65**	**(6.17, 7.31)[a]**	**0.006**	**0.006**	**0.012**
Experimental error	40.17	(40.14, 40.20)[b]	42.30	(42.22, 42.41)[b]	40.36	(40.03, 40.77)[b]	0.071	0.076	0.074
$10t_0$ method	105.96	(105.08, 106.72)[c]	104.10	(102.46, 105.71)[c]	103.68	(98.14, 109.39)[c]	0.188	0.188	0.188
$2.5t_0$ method	105.96	(105.17, 106.78)[c]	104.44	(102.82, 105.97)[c]	104.75	(99.69, 110.18)[c]	0.188	0.189	0.197
(B) 15% strain amplitude									
CVC method	**6.48**	**(6.37, 6.58)[a]**	**6.16**	**(6.04, 6.28)[a]**	**6.06**	**(5.27, 9.18)[a]**	**0.019**	**0.025**	**0.032**
Experimental error	44.93	(44.87, 44.98)[b]	43.96	(43.83, 44.09)[b]	44.34	(44.07, 44.58)[b]	0.121	0.125	0.126
$10t_0$ method	78.45	(77.37, 79.61)[c]	85.65	(83.70, 87.93)[c]	82.55	(75.48, 88.21)[c]	0.192	0.190	0.189
$2.5t_0$ method	78.29	(77.25, 79.51)[c]	86.83	(84.78, 89.02)[c]	92.92	(85.47, 99.95)[d]	0.193	0.193	0.203

Superscript letters indicate statistical groupings within each strain amplitude and frequency; different letters indicate p<0.008

2.4. Discussion

Current viscoelastic characterization methods used for modeling biological soft tissues largely ignore the significant transient viscoelastic effects during loading. In order to address this shortcoming, this chapter interrogated the role of soft tissue relaxation during loading by introducing a novel, empirically-based method to correct for finite ramp time associated with stress relaxation experiments. Since this method is based on the shape of the relaxation curve, instead of the specific form of the constitutive equation, it can be applied to any viscoelastic formulation. Additionally, since the actual strain history is used as input for the integral form of the constitutive equation, no assumptions are made with regard to the applied strain history. Thus, this method is independent of the loading duration (i.e., can be applied to short or long ramp time experiments). Pilot stress relaxation experiments (data not presented) on viscoelastic leather strips demonstrated that the CVC methodology described the data very well across ramp times that ranged over three orders of magnitude (0.1 s, 1 s, and 10 s).

One objective of this chapter was to elucidate (quantitatively) the error associated with the assumption of a linear ramp strain history applied to a fast ramp experiment. Alarmingly, an apparently good fit (small $RMSE$) was produced under the linear strain ramp assumption, with $RMSE$ values that were comparable to those calculated using the CVC method (which incorporated the actual strain history). However, when the fitted coefficients obtained from the linear ramp assumption were input into the QLV integral formulation [equation (27)], with the actual strain history used as input, a significantly poor fit (demonstrated by an order of magnitude increase in $RMSE$) was observed. The poor stress relaxation prediction (Figure 8) and statistically different $G(t)$ parameters obtained using the linear ramp assumption (Table 2) suggests that a purely linear ramp assumption cannot accurately account for relaxation manifested during loading. The observed initial (apparently good) fit may mislead one into

believing that a linear ramp assumption is acceptable when, in fact, it is not. It is important to emphasize that the strain application for all stress relaxation experiments, especially at elevated strain rates, will deviate from a pure linear strain ramp due to the inertial effects of the testing device. Also, since these inertial effects are dependent on the design of experimental fixture, the CVC method presented herein removes the effect of variable fixturing between different laboratories because the actual strain history is used as input. Furthermore, these nonlinear inertial effects are representative of the loading patterns experienced by soft tissues *in vivo* during the acceleration/deceleration of different body mass components during physiologic motions.

Since no finite ramp time correction method has been developed for the fully nonlinear viscoelastic formulation commonly used to describe the viscoelastic behavior of biological tissues[117], fast ramp times are commonly used to approximate a true step function. Data in the initial ramping period is neglected, and the relaxation data is curve-fit beginning at multiples of 10 or 2.5 times the ramp time in order to negate errors associated with the transient load application[69-71,94,110,128]. This methodology is based on the viscoelastic characterization of typical engineering materials, such as glassy polymers in creep[128], which can more easily be tested for long experiment times (e.g., $>10^4$ s by a "hanging weight" experiment). However, viscoelastic experiments involving soft tissues are typically performed at substantially shorter experimental times[21,69-72,109] due to biological limitations such as tissue degradation[110]. Thus, negating the short-term behavior for these relatively brief experiments can greatly affect the accuracy of the fitted parameters. This error is exacerbated by the significant amount of relaxation these tissues exhibit in the initial short-term behavior (during loading), as indicated herein by the dominant short-term $E_1(\varepsilon)$ modulus. Neither the $10t_0$ nor the $2.5t_0$ fitting methods correctly

incorporated this short-term relaxation behavior, which resulted in the observed over-prediction of the long-term behavior, $E_\infty(\varepsilon)$.

Analogous to the aforementioned misleading conclusions of QLV linear ramp assumption, the $10t_0$ and $2.5t_0$ curve fitting methods may also result in a misinterpretation of the fitted parameters. Previous studies have reported high goodness-of-fit parameters, typically the r^2 value, when fitting data using these methods[70,71,74,94]. These relatively high r^2 values force the conclusion that the fitted coefficients are an acceptable model of the mechanical behavior. The results presented herein also produced high goodness-of-fit values (small $RMSE$) using the $10t_0$ and $2.5t_0$ fitting methods; however, when the fitted parameters were input back into the fully nonlinear integral formulation [equation (30)] to predict the entire experiment, a significant increase in error was observed. Therefore, although the coefficients obtained using the $10t_0$ and the $2.5t_0$ methods fit described the relaxation period of the data well, this apparently good curve fit does not imply that the fitted coefficients have accurately characterized the entire mechanical response of the tissue.

Since human cervical spine ligaments are known to exhibit fully nonlinear viscoelastic behavior[72], the validity of the CVC method developed in this chapter was supported by the ability of the fully nonlinear viscoelastic parameters to predict an independent cyclic data set consisting of multiple strain amplitudes and frequencies. The median percent error and $RMSE$ of the nonlinear viscoelastic cyclic predictions were well within the bounds of the experimental error across all frequencies and strain amplitudes. Abramowitch and Woo used a similar method to validate their finite ramp time correction method. Specifically, they utilized their fitted stress relaxation coefficients to predict the peak stresses of an independent cyclic stress relaxation experiment[100] and reported an average percent error of 6.3 ± 6.0%[109]. The median percent error of the nonlinear viscoelastic cyclic validation predictions is similar in magnitude to these

previously reported values. Additionally, the robust behavior of these cyclic predictions, as indicated by the relatively small percent error and $RMSE$ magnitudes across multiple strain amplitudes and frequencies, strongly suggests validity of our CVC method and the fully nonlinear viscoelastic constitutive model.

Although the QLV formulation is commonly used to model the viscoelastic behavior of connective tissues, it has recently received criticism with regard to its inability to predict mechanical behavior other than that used to fit the model[69,71,74,129]. Our results support this criticism by demonstrating that the QLV model fits the stress relaxation behavior well at a single strain magnitude (indicated by the low $RMSE$ values), but poorly predicts the tissue's cyclic mechanical behavior, regardless of frequency or strain amplitude (depicted in Figure 9 by the approximately 150% and 90% over-prediction of peak stresses across all frequencies for the Abramowitch and Woo and the CVC method methods, respectively). While the fully nonlinear $10t_0$ and the $2.5t_0$ fitting methods slightly improved the cyclic predictions when compared to the QLV predictions (approximately 85% over-prediction in peak stresses as depicted in Figure 12), the CVC method applied to the fully nonlinear formulation showed considerable improvement, with a negligible difference observed between the experimental data and the predicted curve. The greatly improved cyclic prediction of the fully nonlinear viscoelastic formulation suggests that the elastic and time-dependent aspects of soft tissue mechanical behavior are not separable, and it is therefore requisite to use a viscoelastic formulation that allows relaxation to occur as a function of strain magnitude (i.e., nonlinear viscoelasticity).

Overall, this study represents the first attempt to: (1) develop a method to incorporate relaxation manifested during loading that is independent of a specific viscoelastic formulation; (2) incorporate the actual strain history into this viscoelastic formulation in order to remove the effect of fixture inertia from the fitted coefficients; (3) develop a robust constitutive formulation

for soft tissues that can accurately and simultaneously describe both the static (stress relaxation) and dynamic (cyclic) soft tissue behavior; and (4) explicitly interrogate the errors associated with previously accepted viscoelastic formulations and characterization methods.

2.5. Conclusion

The results presented in this chapter demonstrate strong evidence for the following conclusions: (1) From a material characterization and modeling perspective, relaxation during soft tissue tensioning is significant and cannot be neglected if one is to accurately predict the transient material behavior under dynamic loading conditions; (2) A good curve fit under a single loading condition does not imply predictive power of the fitted parameters; (3) Quantitative validation studies under multiple loading conditions must be performed as part of the selection method for a particular viscoelastic constitutive model; (4) Fitting stress relaxation experimental data using a linear ramp history assumption may not accurately account for relaxation that occurred during the actual loading history.

3. Nonlinear Viscoelasticty Plays an Essential Role in the Functional Behavior of Spinal Ligaments

The data presented in chapter 3 has been published in the literature (Troyer KL, Puttlitz CM. Nonlinear viscoelasticity plays and essential role in the functional behavior of spinal ligaments. *Journal of Biomechanics*. 2012; 45(4):684–691).

3.1. Introduction

The stability of the spinal column and its ability to protect the spinal cord is partially dependent upon the mechanical behavior of the individual spinal ligaments. The functional role of these ligaments is to passively facilitate three-dimensional physiologic motion patterns and maintain vertebral postures while protecting the spinal cord by limiting excessive motion and absorbing additional energy during traumatic events[108]. Inclusion of all aspects of these functional roles requires consideration of the ligament's temporal (viscoelastic) mechanical behavior.

Despite the significant role ligament viscoelasticity plays in functional spinal biomechanics, previous research has primarily focused on characterization of their elastic (time-independent) mechanical behavior[14,53,107,130-137] and the relationship of this elastic behavior to the fibrous microstructure[49,50,138]. Several studies have implicitly incorporated spinal ligament viscoelasticty into the elastic properties by defining these properties as a function of the loading rate[14,107]. Although this rate-dependent behavior provides some insight into spinal ligament protective mechanisms, it does not provide a comprehensive description of spinal ligament viscoelasticity. Therefore, a more rigorous and explicit approach is requisite to elucidate, characterize, and model spinal ligament viscoelasticity.

Surprisingly, relatively few experimental studies have been performed to directly characterize human spinal ligament viscoelastic behavior[21,72,95,139]. These studies have very

restricted applications and interpretations due to over-simplified viscoelastic formulations or assumptions. For example, Yahia *et al*.[139] and Lucas *et al*.[21] characterized the stress relaxation behavior of spinal ligaments according to the quasi-linear viscoelastic (QLV) formulation proposed by Fung[59]. This formulation is a special (simplified) case of fully nonlinear viscoelasticity wherein it is assumed that the stress relaxation behavior is independent of the applied strain magnitude. Recent investigations have demonstrated strong experimental evidence which suggests that spinal ligaments violate this QLV assumption wherein the observed relaxation is a function of strain magnitude[72,73,95]. Additionally, current nonlinear viscoelastic models[72,73,95] are limited in that they do not incorporate relaxation manifested during loading events (i.e., during the ramping period of the experiment), an important physiological protective mechanism. As demonstrated in chapter 2, neglecting this important short-term behavior can greatly affect the accuracy and predictive power of the fitted constitutive model. Therefore, the purpose of the current chapter was to utilize the CVC method developed in chapter 2 to directly characterize the nonlinear viscoelastic behavior of three primary human spinal ligaments: the anterior longitudinal ligament (ALL), the posterior longitudinal ligament (PLL), and the ligamentum flavum (LF). The objectives of this chapter were: (1) to characterize the nonlinear viscoelastic constitutive behavior of the human spinal ALL, PLL, and LF via stress relaxation experiments at multiple strain magnitudes, and (2) to validate this constitutive relationship by quantifying its ability to predict an independent cyclic data set across multiple strain amplitudes and frequencies.

3.2. Materials and Methods

3.2.1. Experimental methods

The experimental methods for this chapter are described in detail elsewhere[72], and are outlined briefly in section 2.2.1 (page 24).

3.2.2. Constitutive formulation

Since human cervical spine ALL, PLL, and LF exhibit fully nonlinear viscoelastic behavior[72], the nonlinear viscoelastic constitutive formulation given by equation (28) was utilized for this study. The relaxation modulus was modeled using the Prony series given by equation (29). This Prony series representation is useful to parse the relaxation behavior contributions at specific time scales (specifically: τ_1 = 0.1 s, τ_2 = 1 s, τ_3 = 10 s, τ_4 = 100 s).

Stress relaxation fitting procedure

The ALL, PLL, and LF experimental stress relaxation data were fitted (MATLAB, version 7.11; TheMathWorks, Inc.; Natick, MA) using the novel CVC method developed and validated in chapter 2. This algorithm incorporates relaxation manifested during the fast (< 0.3 s) loading period of the stress relaxation experiments. Some of PLL and LF the curve-fits (15 out of 220, or < 7%) required the experimental data to be filtered in order to obtain mathematical convergence (moving average filter; maximum span: 50 out of 6,025 datum points). To interrogate any effect of this filtering on the resulting fitted parameters, data from the unfiltered ALL specimens at the strain magnitude extrema (4% and 25%) were filtered using the maximum moving average span, and the resulting fitted parameters were compared to the unfiltered parameters by performing a Wilcoxon Rank-sum test (statistical significance: $p<0.05$) using SAS statistical software. This comparison indicated that filtering the data did not significantly affect the determination of the fitted parameters ($p\geq0.345$).

As in section 2.2.5 (page 31), the goodness-of-fit for the stress relaxation curves was calculated using a weighted $RMSE$ [equation (35)]. The weighting function for these calculations is given by equation (36).

In order to determine the strain-dependent moduli equations [equation (29)], a forward selection regression analysis on a polynomial hierarchy was utilized in the SAS PROC MIXED

procedure (statistical significance: $p<0.05$). If required, an appropriate transformation (square root or logarithmic) was used to normalize the variance of these parameters.

Cyclic prediction procedure

In order to interrogate the validity of the proposed constitutive equation and its fitted parameters to model the dynamic viscoelastic behavior of these ligaments, the fitted parameters obtained from the transient stress relaxation fits were used to predict [via equation (30)] the cyclic experiments across the 0.01 Hz, 0.1 Hz, and 1 Hz frequencies and the 10% and 15% strain amplitudes. The 0.001 Hz frequency (ν) was not included in these predictions since it falls outside the spectrum of the chosen time constants ($\nu_4 = 1/\tau_4 = 0.01$ Hz). To quantify the ability of the fitted parameters to predict the cyclic behavior, a non-weighted $RMSE$ [i.e., equation (35) without the weighting function] and the percent error [equation (37)] were calculated for each strain amplitude and frequency and for each ligament. In order to compare the model predictions to the experimental variability, one standard deviation from the experimental mean was calculated as a percentage of the mean and its corresponding $RMSE$ and percent error were calculated. Within each strain amplitude and frequency the experimental error and the model prediction were compared using a Wilcoxon ranked sum test in SAS (statistical significance: $p<0.05$).

3.3. Results

The nonlinear viscoelastic constitutive equation fit both the short-term and long-term relaxation data well (Figure 13), producing very low $RMSE$ values (on the order of kilopascals) at each strain magnitude for each ligament type (Table 7).

The strain-dependent moduli were notability different for the ALL, PLL, and LF, and each polynomial formulation was unique to the specific ligament type ($p\leq0.038$ for all comparisons; Figure 14). For the ALL and the PLL, the relaxation modulus was dominated by both the steady-

state $E_\infty(\varepsilon)$ and the short-term $E_1(\varepsilon)$ moduli. The viscoelastic behavior of the LF was much more consistent than the longitudinal ligaments across the investigated temporal decades. Additionally, this consistent strain-dependent behavior of the LF was substantially reduced with respect to the longitudinal ligaments (ALL and PLL). This disparity may be indicative of differences in the ligaments' physiologic functions.

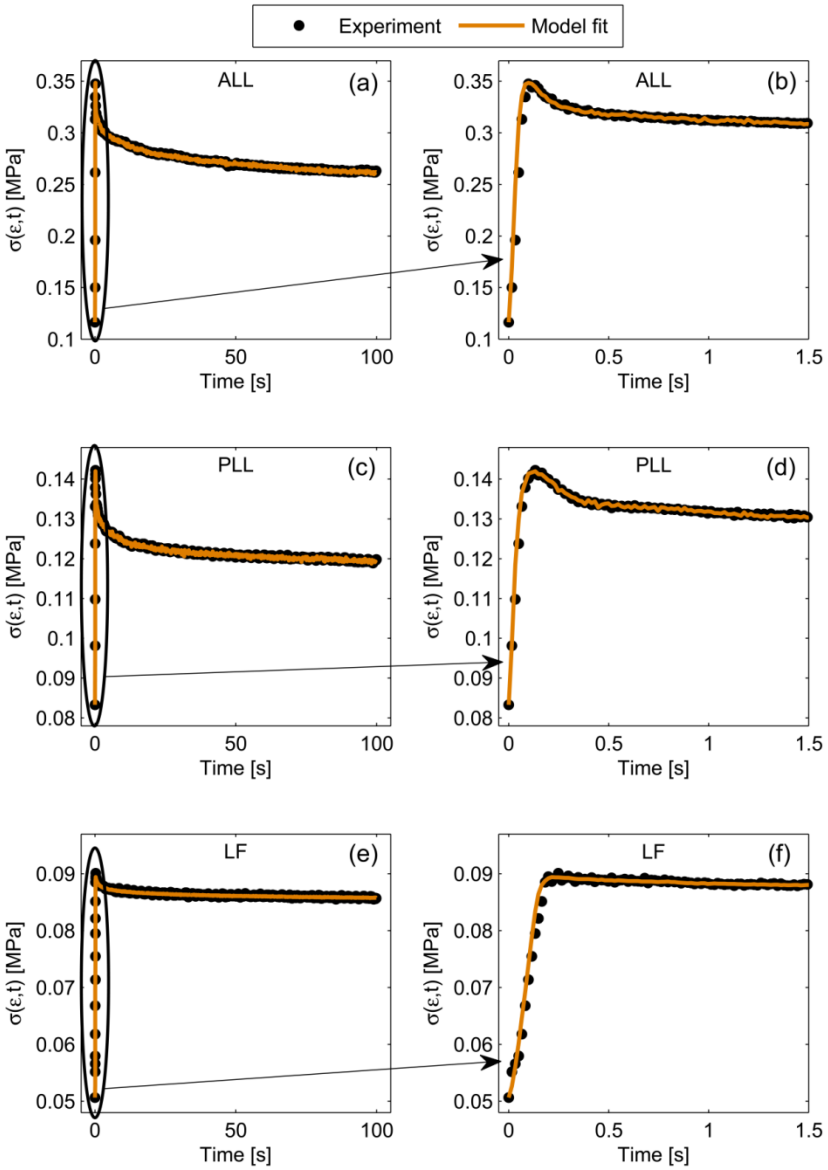

Figure 13: Curve-fits for a typical specimen from each ligament type: ALL shown in subplots (a) and (b), PLL shown in subplots (c) and (d), and LF shown in subplots in (e) and (f). The constitutive model fit the experimental stress relaxation data very well for both the long-term [subplots (a), (c), and (e)] and short-term [subplots (b), (d), and (f)] behavior.

Table 7: Median weighted $RMSE$ values (95% lower confidence limit, 95% upper confidence limit) derived from the stress relaxation experiments for each ligament type and strain level.

Strain [mm/mm]	ALL [kPa]		PLL [kPa]		LF [kPa]	
0.04	0.49	(0.34, 1.03)	0.29	(0.14, 1.47)	0.07	(0.05, 0.09)
0.06	0.76	(0.55, 1.16)	0.45	(0.17, 1.73)	0.11	(0.06, 0.13)
0.08	1.08	(0.90, 1.98)	0.65	(0.27, 2.57)	0.12	(0.06, 0.17)
0.10	1.34	(1.13, 2.97)	0.78	(0.18, 3.10)	0.11	(0.06, 0.19)
0.12	2.01	(1.40, 4.10)	1.05	(0.25, 3.19)	0.14	(0.07, 0.23)
0.14	3.04	(2.14, 6.40)	0.96	(0.28, 4.78)	0.26	(0.06, 0.56)
0.16	3.81	(2.68, 7.53)	1.04	(0.29, 6.47)	0.23	(0.07, 0.45)
0.18	5.23	(3.40, 12.68)	1.26	(0.34, 7.64)	0.46	(0.06, 1.17)
0.20	6.70	(4.37, 17.14)	1.19	(0.40, 9.69)	0.57	(0.07, 1.20)
0.25	10.40	(6.87, 30.69)	1.52	(0.54, 13.60)	1.03	(0.11, 1.88)

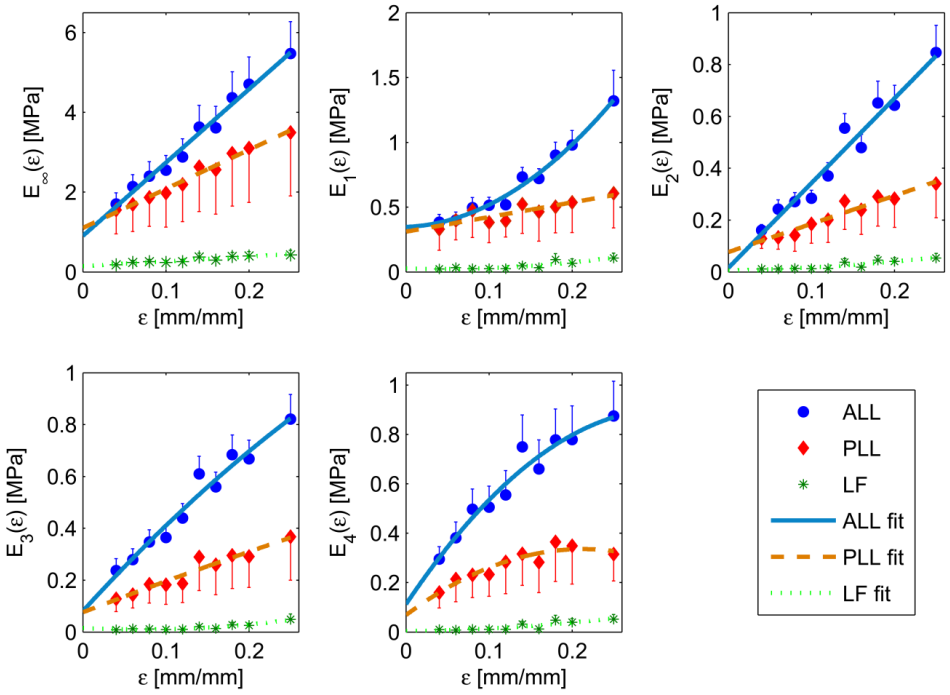

Figure 14: The mean strain-dependent relaxation moduli components [equation (29)] and the corresponding fitted equations (table below). The data indicate that the strain-dependent viscoelastic behavior was unique to each ligament type ($p \leq 0.038$ for all comparisons). Error bars represent standard error of the mean.

ALL	PLL	LF
$E_\infty(\varepsilon) = 18.38\varepsilon + 0.90$	$E_\infty(\varepsilon) = 9.79\varepsilon + 1.10$	$E_\infty(\varepsilon) = 1.20\varepsilon + 0.15$
$E_1(\varepsilon) = 14.70\varepsilon^2 + 0.24\varepsilon + 0.35$	$E_1(\varepsilon) = 1.13\varepsilon + 0.31$	$E_1(\varepsilon) = 2.03\varepsilon^2 - 0.17\varepsilon + 0.03$
$E_2(\varepsilon) = 3.28\varepsilon + 0.02$	$E_2(\varepsilon) = 1.09\varepsilon + 0.08$	$E_2(\varepsilon) = 0.53\varepsilon^2 + 0.07\varepsilon + 0.01$
$E_3(\varepsilon) = -2.16\varepsilon^2 + 3.51\varepsilon + 0.08$	$E_3(\varepsilon) = -0.30\varepsilon^2 + 1.23\varepsilon + 0.08$	$E_3(\varepsilon) = 1.17\varepsilon^2 - 0.17\varepsilon + 0.02$
$E_4(\varepsilon) = -7.95\varepsilon^2 + 5.02\varepsilon + 0.11$	$E_4(\varepsilon) = -5.89\varepsilon^2 + 2.51\varepsilon + 0.07$	$E_4(\varepsilon) = 0.68\varepsilon^2 + 0.04\varepsilon$

The constitutive equations determined from the stress relaxation experiments predicted the cyclic behavior well for each ligament type at each frequency and strain amplitude (ALL: Figure 15; PLL: Figure 16; LF: Figure 17), resulting in relatively low $RMSE$ values (at least 1 order of magnitude less than the peak stresses) and percent errors (less than 7.2%) (ALL: Table 8; PLL: Table 9; LF: Table 10). The error calculations indicated that all cyclic predictions were well within the bounds of the experimental error (at least one order of magnitude less).

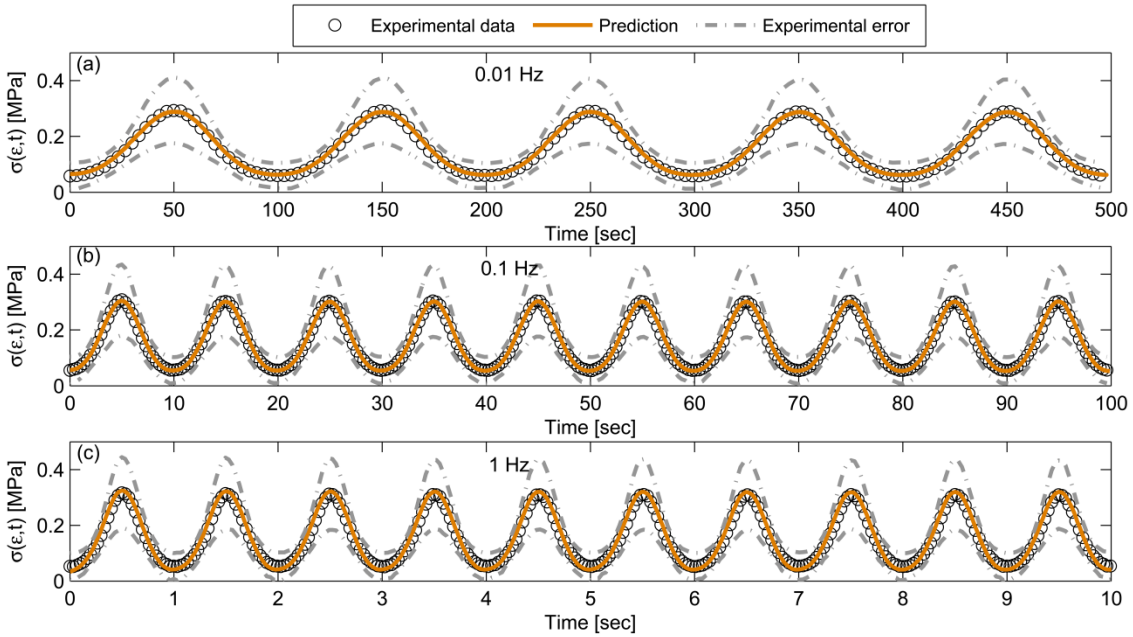

Figure 15: The ALL cyclic predictions at the (a) 0.01 Hz, (b) 0.1 Hz, and (c) 1 Hz for the 10% (peak-to-peak) strain amplitude. The constitutive equation predicted the data very well and was well within the bounds of experimental error (one standard deviation from the experimental mean) at each frequency and strain amplitude. The 15% strain amplitude predictions (not shown) were similar.

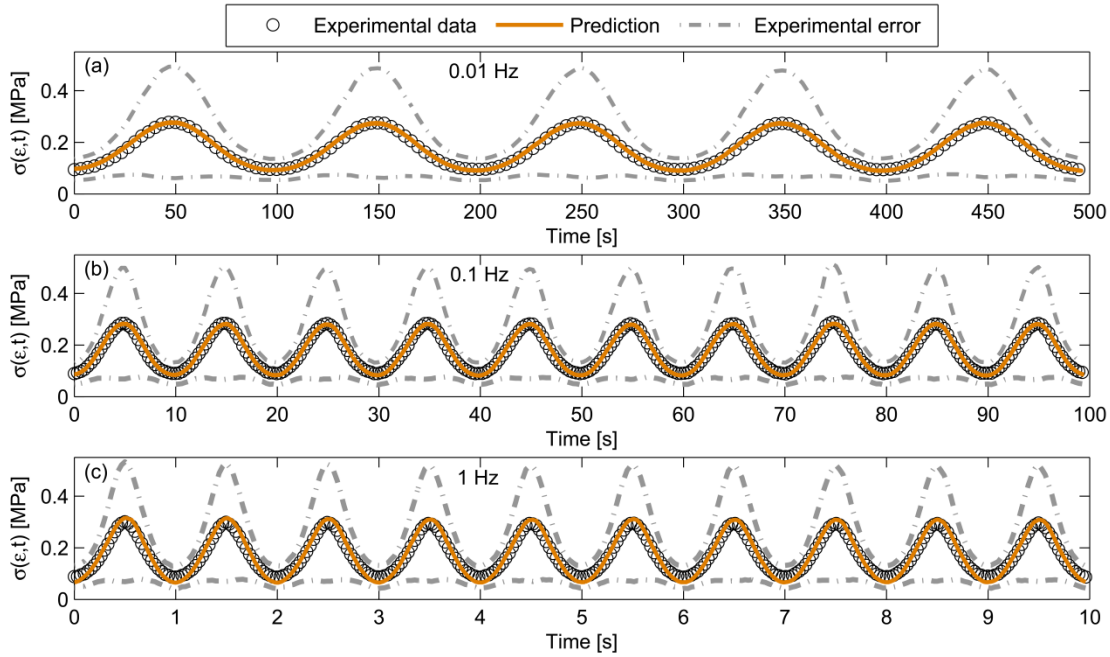

Figure 16: The PLL cyclic predictions at the (a) 0.01 Hz, (b) 0.1 Hz, and (c) 1 Hz for the 10% (peak-to-peak) strain amplitude. The constitutive equation predicted the data very well and was well within the bounds of experimental error (one standard deviation from the experimental mean) at each frequency and strain amplitude. The 15% strain amplitude predictions (not shown) were similar.

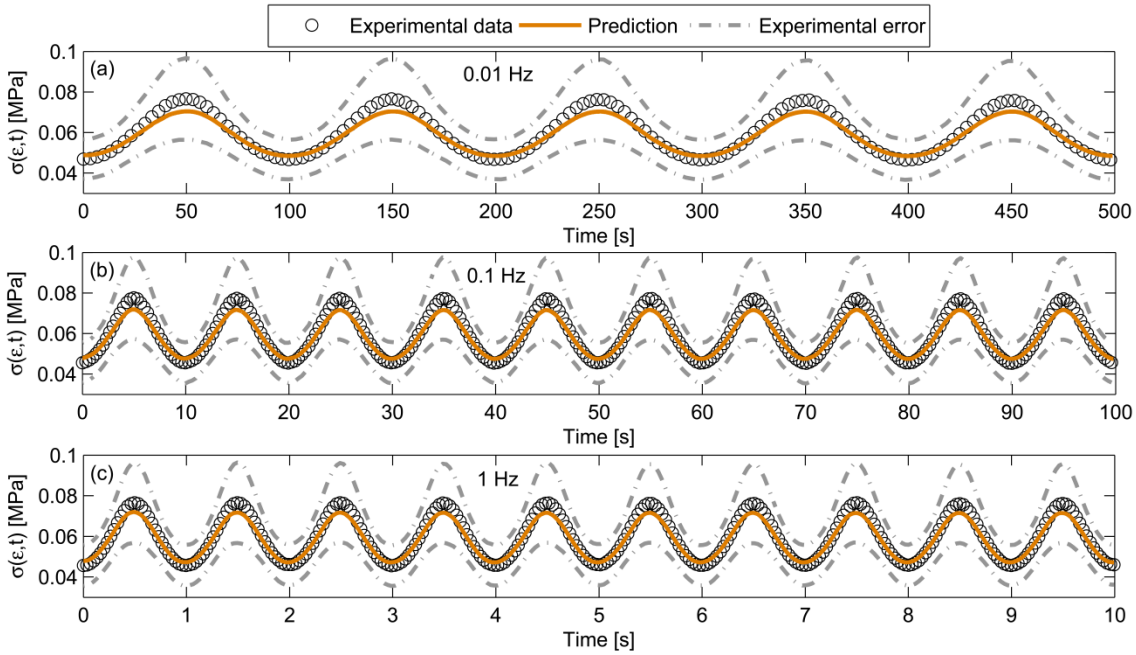

Figure 17: The LF cyclic predictions at the (a) 0.01 Hz, (b) 0.1 Hz, and (c) 1 Hz for the 10% (peak-to-peak) strain amplitude. The constitutive equation predicted the data very well and was well within the bounds of experimental error (one standard deviation from the experimental mean) at each frequency and strain amplitude. The 15% strain amplitude predictions (not shown) were similar.

Table 8: The percent error and $RMSE$ values for the ALL cyclic predictions indicate that the model predicted the cyclic behavior well across all frequencies at both (A) the 10% strain amplitude, and (B) the 15% strain amplitude. Both the percent error and $RMSE$ values were an order of magnitude smaller than the experimental error (one standard deviation from the experimental mean), indicating that the model prediction was well within the bounds of experimental error (p<0.001 for the percent error comparisons).

	Percent error [%]						$RMSE$ [kPa]		
	0.01 Hz		0.1 Hz		1 Hz		0.01 Hz	0.1 Hz	1 Hz
(A) 10% strain amplitude									
Model prediction	5.22	(5.18, 5.27)	2.76	(2.67, 2.84)	6.65	(6.17, 7.31)	6.33	6.06	11.76
Experimental error	40.17	(40.14, 40.20)	42.30	(42.22, 42.41)	40.36	(40.03, 40.77)	71.08	76.18	74.44
(B) 15% strain amplitude									
Model prediction	6.48	(6.37, 6.58)	6.16	(6.04, 6.28)	6.06	(5.27, 9.18)	19.08	24.58	32.14
Experimental error	44.93	(44.87, 44.98)	43.96	(43.83, 44.09)	44.34	(44.07, 44.58)	121.29	125.16	126.22

Percent error shown as: median (95% lower confidence limit, 95% upper confidence limit)

Table 9: The percent error and $RMSE$ values for the PLL cyclic predictions indicate that the model predicted the cyclic behavior well across all frequencies at both (A) the 10% strain amplitude, and (B) the 15% strain amplitude. Both the percent error and $RMSE$ values were an order of magnitude smaller than the experimental error (one standard deviation from the experimental mean), indicating that the model prediction was well within the bounds of experimental error ($p<0.001$ for the percent error comparisons).

	Percent error [%]						$RMSE$ [kPa]		
	0.01 Hz		0.1 Hz		1 Hz		0.01 Hz	0.1 Hz	1 Hz
(A) 10% strain amplitude									
Model prediction	2.36	(2.33, 2.39)	2.50	(2.40, 2.59)	5.74	(5.47, 6.12)	4.40	5.35	13.63
Experimental error	55.80	(55.49, 56.15)	55.50	(54.80, 56.32)	55.26	(53.24, 57.69)	124.28	125.58	127.87
(B) 15% strain amplitude									
Model prediction	3.72	(3.69, 3.74)	7.20	(6.85, 7.53)	5.47	(5.01, 6.07)	9.39	16.99	21.17
Experimental error	62.36	(61.89, 62.80)	63.12	(61.99, 64.26)	62.58	(59.06, 66.72)	206.24	210.99	213.30

Percent error shown as: median (95% lower confidence limit, 95% upper confidence limit)

Table 10: The percent error and $RMSE$ values for the LF cyclic predictions indicate that the model predicted the cyclic behavior well across all frequencies at both (A) the 10% strain amplitude, and (B) the 15% strain amplitude. Both the percent error and $RMSE$ values were an order of magnitude smaller than the experimental error (one standard deviation from the experimental mean), indicating that the model prediction was well within the bounds of experimental error (p<0.001 for the percent error comparisons).

	Percent error [%]						$RMSE$ [kPa]		
	0.01 Hz		0.1 Hz		1 Hz		0.01 Hz	0.1 Hz	1 Hz
(A) 10% strain amplitude									
Model prediction	3.51	(3.48, 3.54)	3.63	(3.54, 3.71)	2.85	(2.70, 3.05)	3.11	2.84	2.45
Experimental error	21.0	(20.99, 21.03)	21.4	(21.37, 21.48)	21.5	(21.37, 21.64)	13.96	13.91	13.74
(B) 15% strain amplitude									
Model prediction	3.44	(3.36, 3.51)	3.09	(2.96, 3.23)	3.40	(3.28, 3.52)	4.68	4.41	3.78
Experimental error	23.0	(23.01, 23.06)	23.7	(23.60, 23.78)	24.0	(23.69, 24.27)	17.35	17.56	17.39

Percent error shown as: median (95% lower confidence limit, 95% upper confidence limit)

3.4. Discussion

Human spinal ligaments facilitate and guide quasi-static and dynamic physiologic spinal motion patterns and absorb energy during traumatic events in order to protect the spinal cord. Thus, viscoelasticity is requisite to comprehensively model the functional mechanical behavior of these ligaments. The purpose of the current chapter was to directly characterize the nonlinear viscoelastic behavior of three primary spinal ligaments: the ALL, the PLL, and the LF. To the best of the author's knowledge, the results presented herein represent the first report to empirically derive a comprehensive constitutive equation at multiple strain magnitudes for spinal ligaments that can accurately model the entire physiologic stress relaxation response *and* predict their cyclic behavior. Additionally, the Prony series representation of the constitutive equation [equation (29)] provides a temporal decomposition of the viscoelastic properties of these ligaments to elucidate this behavior across multiple temporal decades.

All three ligament types (ALL, PLL, and LF) were observed to exhibit unique nonlinear viscoelastic behavior. This is likely attributed to the different morphologies and specific physiologic function of each ligament type. Structurally, the longitudinal ligaments are narrow fibrous bands with similar (relatively highly) collagenous compositions[49,140]. These ligaments serve similar physiologic roles; primarily to stabilize the spinal column during flexion-extension motions and to maintain intradiscal pressures by resisting disc bulge[108,118,119]. By temporally decomposing the relaxation modulus into its decade components, it can be observed that the ALL and PLL viscoelastic behavior is dominated by both the $E_\infty(\varepsilon)$ and the $E_1(\varepsilon)$ moduli. The dominant behavior of the steady-state $E_\infty(\varepsilon)$ modulus indicates that these ligaments maintain a substantial proportion of their initial applied load. This property may be attributed to the need for these ligaments to maintain mechanical integrity to support the spine during sustained postures. The dominant behavior of the short-term $E_1(\varepsilon)$ modulus of the ALL and PLL indicates

that these ligaments relax quickly, and that the relaxation during loading events is of vital importance. The large contribution of the $E_1(\varepsilon)$ modulus may be the mechanism for the significant rate-dependent elastic behavior previously observed[14,107], as this modulus corresponds to the loading period of the experiment. Additionally, this fast relaxation behavior may be important to minimize peri-spinous muscle expenditure during sustained postures since the majority of relaxation occurs quickly (on the order of 0.1 s).

The ALL exhibited the greatest amount of viscoelastic behavior of the longitudinal ligaments. This may be attributed to its anatomical location, which is further from the motion segment's center of rotation than the PLL. During extension the ALL experiences a greater amount of deformation than the PLL does in flexion[14]. Therefore, in order to maintain spinal stability during these larger deformations, it is requisite that the ALL maintain a greater amount of its initial stress than the PLL. Additionally, the increased damping characteristics observed for the ALL over the PLL [increased $E_1(\varepsilon)$, $E_2(\varepsilon)$, $E_3(\varepsilon)$, $E_4(\varepsilon)$ behavior] may be an adaptation that allows greater extension while imparting sufficient stability without becoming too stiff. Functionally, this is important because the ALL is the dominant ligamentous structure that resists excessive extension motion.

Contrary to the longitudinal ligaments, the LF is a thick, wide structure whose fibrous content is dominated by elastin[53]. This ligament exhibited significantly reduced steady-state and short-term viscoelastic behavior as compared to the ALL and PLL. The observation of the reduced steady-state behavior is consistent with the significantly reduced elastic modulus of the cervical LF reported previously[134]. This may be an adaptation of the LF since it is required to undergo a greater amount of deformation than the longitudinal ligaments due to its anatomical location (i.e., it is more remote from the spinal center of rotation)[14]. The reduced $E_1(\varepsilon)$, $E_2(\varepsilon)$, $E_3(\varepsilon)$, $E_4(\varepsilon)$ behavior indicates that the LF exhibits less viscoelastic behavior than the

longitudinal ligaments. The increased elastic behavior observed for the LF is congruent with the assertion that the primary role of the LF is not to provide mechanical support of the spine, but rather to protect the spinal cord from impingement during neck motion[14].

An important outcome of this study is the observation that spinal ligament relaxation is significantly dependent on strain magnitude across all temporal decades, behavior which has been previously neglected[21,139]. Physiologically, this adaptive relaxation behavior may be important to minimize muscular energy expenditure when maintaining a quasi-static posture. The stiffening effect that spinal ligaments exhibit when tensioned would require greater muscular energy to maintain postural attitudes at greater deformations. The increasing $E_1(\varepsilon)$, $E_2(\varepsilon)$, $E_3(\varepsilon)$, $E_4(\varepsilon)$ moduli indicate that the ligaments dissipate more of this elastic energy when a posture is maintained at higher strain magnitudes[49]. During physiologic motions, additional elastic energy is dissipated in order to reduce the muscular forces required to maintain a consistent posture. The dominant $E_1(\varepsilon)$ behavior, as compared to the $E_2(\varepsilon)$, $E_3(\varepsilon)$, and $E_4(\varepsilon)$ moduli, indicates that this energy is dissipated quickly, possibly to minimize the active muscular contribution required to stabilize the spine during this brief period of instability. Additionally, the increased viscoelastic properties of these ligaments with relatively greater deformation indicate that these ligaments store additional elastic energy that would help protect the spine during high strain and loading rate traumatic events.

The results presented herein may have important implications with regard to spinal stability. Typical curved column structures, which are geometrically similar to the spine, have a critical buckling load; below this load the structure is stable and above this load it demonstrates elastic instability. However, since the spine is a viscoelastic structure, its mechanical behavior includes a temporal component wherein its stability is also a function of the rate of load application and the time over which load is maintained[108]. The results presented herein

demonstrate that the load magnitude on the spinal ligaments significantly alters their temporal mechanical behavior due to their nonlinear viscoelastic characteristics. This complex behavior, which may result from rearrangement of the ligament microstructure[108], may be an intrinsic protective mechanism that restores structural stability of the ligamentous spine in a transient load environment.

3.5. Conclusion

The data from this chapter provides strong evidence of the following conclusions: (1) All three ligament types (ALL, PLL, and LF) exhibit a significant amount of relaxation during the loading period of the experiment; (2) Each ligament type displayed unique nonlinear viscoelastic behavior which may be attributed to its specific morphology; (3) The nonlinear viscoelastic behavior of the LF is substantially different from the longitudinal ligaments, suggesting a different functional role; (4) The adaptive (strain-dependent) viscoelastic behavior of these spinal ligaments may have important implications with regard to spinal stability and muscular expenditure.

4. Finite Element Implementation of Fully Nonlinear Viscoelasticity

4.1. Introduction

Developed over forty years ago, the quasi-linear viscoelastic (QLV) theory proposed by Fung[97] has been the widely-accepted gold-standard to describe the temporal mechanics of soft tissues[21,34,84,98-105]. Fundamentally, this theory assumes that the tissue's mechanical behavior can be separated into a nonlinear hyperelastic (time-independent) component and a linear time-dependent (strain-independent) component. Widespread use of QLV theory stems from its reduced mathematical interpretation (as compared to available fully nonlinear formulations) and the relative ease with which it can be incorporated into many commercial finite element (FE) software packages. For example, ABAQUS® includes typical strain energy functions to describe the tissue's hyperelastic component and permits direct input of the experimental stress relaxation curve to simulate the linear time-dependent component[141].

Despite its historical popularity, the linear time dependence assumption of QLV theory severely limits its applicability as a robust mechanical model for soft tissues because these tissues are subjected to temporally varying loading regimes *in vivo*. Recent studies have conclusively demonstrated that soft tissues violate the QLV assumption wherein fully nonlinear (and non-separable) viscoelastic behavior has been observed under various static and dynamic loading events. With specific reference to connective orthopaedic tissues, both ligament[70-73,142] and tendon[69] exhibit strain-dependent stress relaxation and stress-dependent creep behavior under constant (static) strain and stress magnitudes, respectively. In addition, it has been explicitly shown that ligament exhibits amplitude-dependent viscoelastic effects when subjected to dynamic oscillations[72,143]. Overall, these complex nonlinear phenomena cannot be captured by QLV theory, thereby significantly reducing the formulation's predictive accuracy under

physiologically germane loading conditions[69-71,142,144]. In addition, the characterization method used for experimentally-based nonlinear viscoelastic models can also have a substantial impact on the resultant model predictions. Specifically, it has recently been suggested that viscoelastic characterization techniques which incorporate relaxation manifested during the experimental loading (ramping) period are requisite to maintain predictive fidelity of the fitted model[144].

In order to shift the current FE modeling paradigm to include fully nonlinear viscoelastic behavior and accurately model physiologically-important static and dynamic loading regimes, the aims of this chapter were: (1) to experimentally characterize the nonlinear viscoelastic behavior of orthopaedic connective tissue under static (stress relaxation) loading conditions, (2) to develop a nonlinear viscoelastic constitutive relationship that accurately captures this experimental behavior and implement this formulation into FE algorithms (i.e., demonstrate computational tractability), and (3) to validate the predictive accuracy of the viscoelastic FE model under static and dynamic (cyclic) loading conditions.

4.2. Materials and Methods

4.2.1. Experimental data acquisition

Ovine Achilles tendon and its corresponding muscle belly and calcanei were immediately excised from ten (n=10) skeletally mature ewes euthanized for unrelated studies, wrapped in saline-soaked gauze, sealed in a plastic bag, and frozen (-20 °C). This tissue model was selected because of its relatively large size and constant cross-section. Before testing, each specimen was thawed to room temperature, the muscle belly was carefully removed, and the calcaneous was potted in polymethylmethacrylate bone cement. Thereafter, the potted specimen was wrapped in saline-soaked gauze, sealed in a plastic bag, and refrozen (-20 °C) until the day of testing. Similar careful refreezing procedures have been used[69] and shown to minimally affect the hydrated tissue's viscoelastic properties[145].

On the day of testing, the specimen was gradually thawed and placed in a warmed saline bath (ovine body temperature, 39 °C) for one hour to ensure hydrothermal equilibration. The specimen was subsequently attached to a servohydraulic materials testing machine (858 MiniBionix II; MTS; Eden Prairie, MN). The experimental apparatus included a translation (x-y) table, an environmental chamber (saline, 39 °C), and a six degree-of-freedom load cell (MC3A-1000; AMTI; Watertown, MA; axial capacity: 4,448 N) placed below the environmental chamber[72]. The potted calcaneous was rigidly attached to the fixed environmental chamber and the distal tendinous tissue was attached to the actuator via a custom-designed cryo-clamp to minimize tissue slippage[69,146,147].

The tendon's initial gage length was defined under a 10 N preload, and the tissue was allowed to relax at this length for 5 minutes. The specimen was cyclically (haversine) preconditioned with a peak-to-peak strain amplitude of 7% engineering strain for 50 cycles at 0.5 Hz followed by 50 cycles at 1 Hz. The tissue was allowed to recover for 1,000 s. Three (n=3) pilot specimens were subjected to repeated stress relaxation experiments following this preconditioning procedure (data presented in Appendix C, page 109), and demonstrated repeatable results that were within previously-defined boundaries[69]. Following preconditioning, seven (n=7) tendons were subjected to a series of physiologic[69] stress relaxation (randomized strain magnitudes: 1%, 2%, 3%, 4%, 5%, 6%, ramp rate: 10 mm/s, hold: 100 s, recover: 1,000 s, data capture rate: 102.4 Hz), dynamic (randomized strain amplitudes: 3% and 6%, frequencies: 1 Hz and 10 Hz, data capture rate: 204.8 Hz), and creep experiments (load rate: 1,000 N/s, hold: 100 s, recover: 1,000 s, data capture rate: 102.4 Hz). The order of stress relaxation, dynamic, and creep experiments was randomized for each specimen, with the restriction that creep did not occur first. If the order of the experiments was randomly selected as (1) dynamic, (2) creep, (3) stress relaxation, then the target forces for the creep experiments were obtained from the

maximum force observed from the 1 Hz (3% and 6%) cyclic experiments. Otherwise, the target forces were obtained from the maximum forces recorded during the 3% and 6% stress relaxation experiment. Cross-sectional area of each tendon was measured *post hoc* using an area micrometer technique (Appendix C)[148-151].

Due to experimental errors caused by high-frequency vibrations, the 10 Hz force data were not accurately captured by the six degree-of-freedom load cell. Data from a load cell placed above the specimen, between the cryoclamp and the MTS actuator, are presented in Appendix D. Additionally, attempts to interrelate the creep and stress relaxation data are presented in Appendix E. The current chapter presents data from the stress relaxation fits and the corresponding 1 Hz cyclic predictions.

4.2.2. Nonlinear viscoelastic formulations

Both the analytical and FE nonlinear viscoelastic formulations are described in the following two subsections. All fits and analytical predictions were performed with MATLAB (version 7.11; TheMathWorks, Inc.; Natick, MA), and the FE simulations were performed using ABAQUS (version 6.9; Simulia; Providence, RI).

Analytical formulation

Since tendon is a nonlinear viscoelastic material[69], the viscoelastic constitutive formulation given by equation (28) was utilized for this study. The relaxation modulus was modeled using the five-term Prony series given by equation (29) with fixed decadal time constants: τ_1 = 0.1 s, τ_2 = 1 s, τ_3 = 10 s, τ_4 = 100 s.

Stress relaxation data at each strain magnitude were fitted to equation (28) using two characterization techniques: (1) the comprehensive viscoelastic characterization (CVC) method developed in chapter 2, which incorporates viscoelastic effects during the loading event via an iterative algorithm[144], and (2) a previously used characterization technique [69,94,110] wherein strain

was assumed to be applied instantaneously (i.e., a Heaviside step application; thereby neglecting relaxation manifested during loading) and data fitting began after a multiple of 2.5 times the ramp time t_0 (referred to in the current chapter as the *2.5t_0 method*).

For each fitting method, the strain dependence of the moduli components were determined *post hoc* via a polynomial formulation[117,144,152-154]:

$$E(\varepsilon) = C_1\varepsilon + C_2\varepsilon^2 \tag{38}$$

where C_1 and C_2 were fit for each individual modulus component [$E_1(\varepsilon)$, $E_2(\varepsilon)$, $E_3(\varepsilon)$, $E_4(\varepsilon)$, $E_\infty(\varepsilon)$].

In order to interrogate any differences between these two characterization techniques, the coefficients from each method (and strain level) were input into the analytical formulation [equation (28)] with the actual (ramp and relax) strain history to predict the experimental stress relaxation curve[144].

The relaxation period fits and the full predicted curves were compared via calculation of an exponentially weighted root mean-squared error [$wRMSE$, equation (35)][127,144,154]. Statistical comparisons on the $wRMSE$ were performed using the PROC MIXED procedure in SAS (SAS Institute, Inc.; Cary, NC; statistical significance: $p<0.05$).

Finite element formulation

Consider a five-component mechanical model (Figure 1) composed of an elastic (steady-state) spring in parallel with four Maxwell components[126]. Under deformation, each component experiences the same strain ε, whereas the total stress σ is a summation of the stress in each individual component (σ_∞ and σ_i) plus any initial pretension σ_0:

$$\sigma = \sigma_\infty + \sum_{i=1}^{4} \sigma_i + \sigma_0 \tag{39}$$

The steady-state stress σ_∞ component is given by the purely elastic relationship:

$$\sigma_\infty = E_\infty(\varepsilon) \cdot \varepsilon \tag{40}$$

whereas the stress in each Maxwell component σ_i (i = 1, 2, 3, 4) is governed by the time-dependent differential equation[94]:

$$\dot{\sigma}_i + \frac{1}{\tau_i}\sigma_i = E_i(\varepsilon) \cdot \dot{\varepsilon} \tag{41}$$

where $[\dot{}]$ represents differentiation with respect to time and $E_\infty(\varepsilon)$, $E_i(\varepsilon)$, and τ_i are defined above (section 2.2.3, page 28).

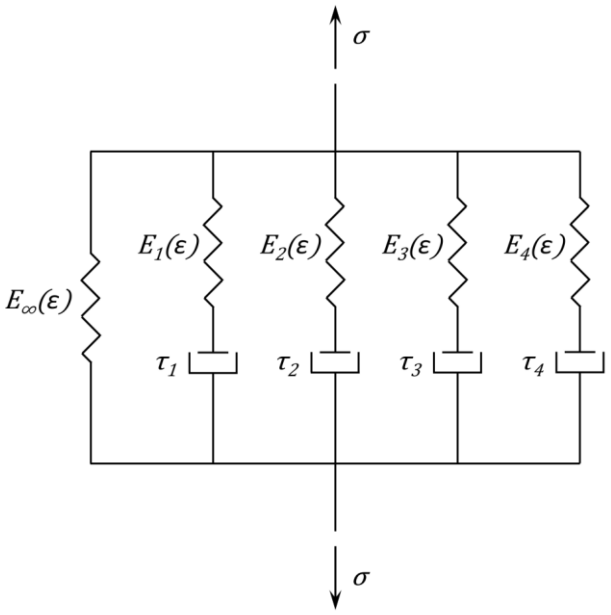

Figure 18: A five-component spring and dashpot nonlinear viscoelastic mechanical model. Nonlinearity of the spring constants $E_\infty(\varepsilon)$, $E_1(\varepsilon)$, $E_2(\varepsilon)$, $E_3(\varepsilon)$, and $E_4(\varepsilon)$ was modeled via a quadratic polynomial [equation (38)]. The dashpots are characterized by their respective time constants τ_i (i = 1, 2, 3, 4).

Equation (39) can be implemented numerically by use of the stable integration operator[141]:

$$\dot{f}_{t+\frac{1}{2}\Delta t} = \frac{\Delta f}{\Delta t}$$
$$f_{t+\frac{1}{2}\Delta t} = f^t + \frac{\Delta f}{\Delta t} \tag{42}$$

where f is an arbitrary function, f^t is its value at the current time, and Δf is the change in f over a time step Δt. Hence, by defining $\Delta f = f^t - f^{t-1}$, where f^{t-1} is the function value from the previous time step, the total stress at the current time [equation (39)] can be recast as:

$$\sigma^t(\varepsilon^t, t) = E_\infty(\varepsilon^t) \cdot \varepsilon^t + \sum_{i=1}^{4} \frac{1}{1 + \frac{\Delta t}{\tau_i} + \frac{\Delta t}{2\tau_i}} \left[E_i(\varepsilon^t) \cdot \Delta\varepsilon + \left(1 + \frac{\Delta t}{2\tau_i}\right) \sigma_i^{t-1} \right] + \sigma_0 \quad (43)$$

where ε^t is the strain at the current time, $\Delta\varepsilon$ is the strain increment, and σ_i^{t-1} is the ith Maxwell component stress [equation (41)] from the previous time step.

In addition to the stress definition [equation (43)], the FE solution procedure also requires definition of a tangent stiffness. Utilizing the relations in equations (39)-(42), the uniaxial tangent stiffness C^t can be cast as[141]:

$$C^t = \frac{\partial \Delta\sigma}{\partial \Delta\varepsilon} = E_\infty(\varepsilon^t) + \sum_{i=1}^{4} \left[\frac{1}{1 + \frac{\Delta t}{2\tau_i}} \right] E_i(\varepsilon^t) \quad (44)$$

4.2.3. Finite element model

A tension-only FE model of tendon was created in ABAQUS CAE using a single, two-node linear truss element (T3D2). This element is ideal for representing long, slender structures which support only axial loads and do not support bending/torsional moments[141]; a typical geometry and mechanical behavior exhibited by tendon and several other connective tissues. A custom-written (FORTRAN) user-defined subroutine (UMAT) was developed to calculate the stress and tangent stiffness [equations (43) and (44)] using the coefficients obtained from either the CVC method or the $2.5t_0$ method. Gage length and cross-sectional area measurements obtained experimentally were used in the model geometry definitions.

In order to interrogate the predictive accuracy of the FE model and the two characterization methods, the FE models with material coefficients obtained from the each method were used to predict the average dynamic behavior via input of the average experimental cyclic displacement history. Accuracy of these predictions were quantified via calculation of the non-weighted $RMSE$ [i.e., equation (35) without the weighting function] and the percent error [equation (37)][144,154]. For each strain amplitude, FE predictions for each

characterization technique were compared to their corresponding analytical predictions [obtained via equation (28)] and to the experimental variability (defined as one positive standard deviation from the experimental mean) using a Kruskal–Wallis test. *Post hoc* pairwise comparisons were performed using a Wilcoxon rank-sum test with Bonferroni adjustment (SAS, statistical significance: p<0.005).

4.3. Results

Both characterization methods fit the stress relaxation period well [Figure 19(a)] producing very low $wRMSE$ values in comparison to the peak stresses [Table 11(a)]. Statistical analyses indicated that the $wRMSE$ for the $2.5t_0$ method fit was lower than that of the CVC method (p<0.001). However, there was a significant increase in $wRMSE$ for $2.5t_0$ method prediction of the entire (ramping and relaxation periods) curve as compared to the CVC method [p<0.001, Table 11(b)].

The polynomial formulation [equation (38)] described the strain dependence of the moduli well (r^2≥0.89, Figure 20). Comparison of the two fitting techniques indicated that there was no statistical difference between the $E_\infty(\varepsilon)$, $E_2(\varepsilon)$, $E_3(\varepsilon)$, $E_4(\varepsilon)$ moduli components (p≥0.44, Table 12). However, the $E_1(\varepsilon)$ modulus, corresponding to the 0.1 s time constant, was observed to be highly sensitive to the fitting technique (p<0.001).

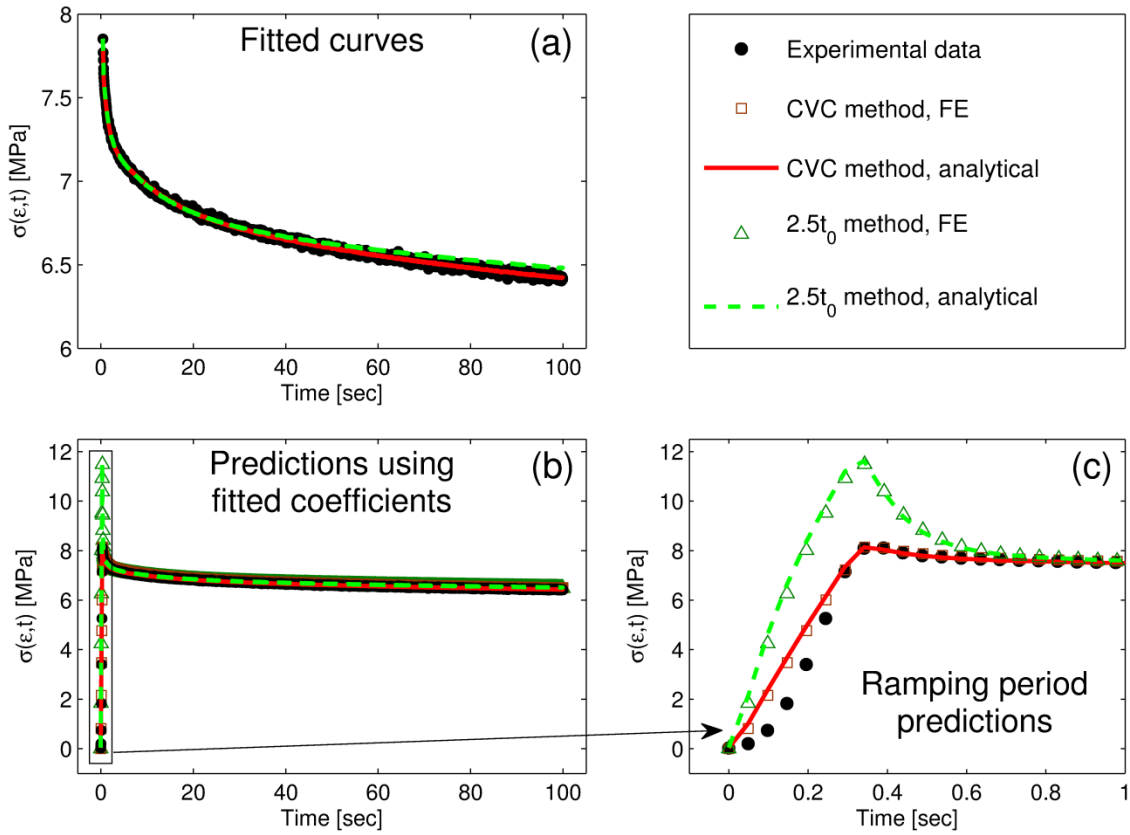

Figure 19: (a) A typical relaxation period curve fit (CVC method $wRMSE$ = 2.62 kPa, 2.5t_0 method $wRMSE$ = 1.33 kPa); (b) the corresponding full (ramping and relaxation periods) analytical and FE curve predictions (CVC method $wRMSE$ = 54.21 kPa, 2.5 t_0 method $wRMSE$ = 182.51 kPa); and (c) the ramping period only predictions. Since the inherent viscoelastic nonlinearity was determined *post hoc*, the CVC method predictions at individual strain magnitudes were not explicitly inclusive of the relaxation as a function of the applied strain. As a result, there was a minor disparity between the predicted stress relaxation behavior and the experimental ramping period [shown in (c)] that lead to an increase in $wRMSE$ with strain amplitude (Table 11). The FE model closely approximated the analytical solution of both characterization methods.

Table 11: Comparison of the median (95% lower confidence limit, 95% upper confidence limit) $wRMSE$ values for (a) the stress relaxation fits and (b) the full curve analytical predictions. Although the reduced magnitude (p<0.001) of the $2.5t_0$ $wRMSE$ indicates a better fit of the data [as shown in (a)], there was a substantial increase in error when the resulting fitted coefficients were used to predict the full curve [as shown in (b)]. The CVC method reduced the $wRMSE$ (p<0.001) by an order of magnitude for the 2%, 4%, 5%, and 6% strain as compared to the $2.5t_0$ method. Median peak stress (σ_{peak}) values are provided as a relative scale for the magnitude of the $wRMSE$ calculations.

Strain	*(a) Fit: relaxation period [kPa]*				*(b) Prediction: full (ramp and relax) curve [kPa]*				Median σ_{peak} [kPa]
	CVC method		$2.5t_0$ method		CVC method		$2.5t_0$ method		
0.01	2.54	(0.54, 4.17)	1.40	(0.29, 2.50)	2.63	(0.60, 4.32)	8.21	(4.27, 37.44)	452.31
0.02	2.67	(0.67, 4.25)	1.49	(0.35, 2.47)	6.98	(4.40, 14.56)	18.44	(7.61, 44.83)	1,968.80
0.03	2.67	(0.99, 4.19)	1.51	(0.47, 2.23)	33.48	(21.71, 40.15)	68.45	(49.647, 98.24)	4,803.20
0.04	3.51	(2.18, 4.02)	2.02	(1.22, 2.17)	63.25	(52.45, 74.95)	182.51	(91.30, 345.13)	8,161.60
0.05	2.83	(1.82, 3.88)	1.57	(0.75, 2.12)	89.27	(80.06, 116.79)	598.99	(428.11, 862.60)	11,658.00
0.06	2.84	(1.66, 3.96)	1.62	(1.08, 2.28)	116.85	(113.73, 159.69)	1,496.40	(978.82, 2151.10)	15,756.00

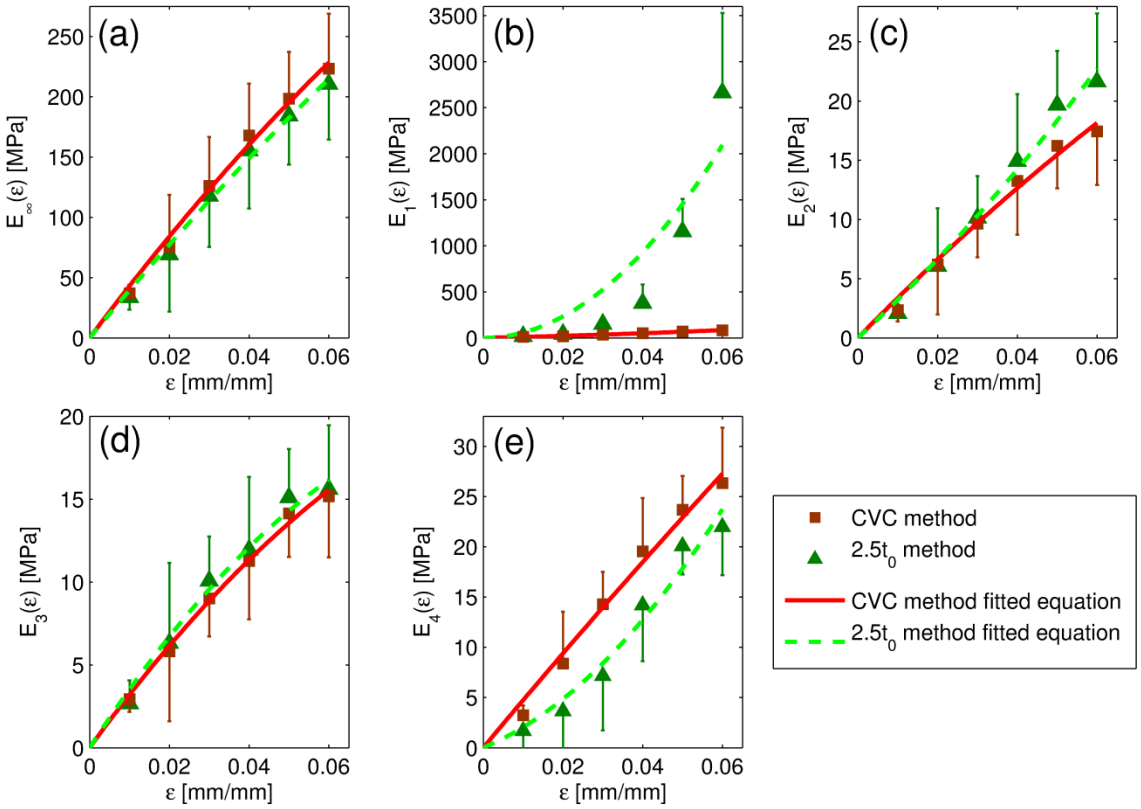

Figure 20: Average strain-dependent behavior of each moduli component with its corresponding fitted equation [equation (38)]. The data indicated that the $E_1(\varepsilon)$ coefficient (corresponding to τ_1 = 0.1 s) was highly dependent upon the fitting technique (Table 12). Error bars represent one standard deviation.

Table 12: Comparison of the strain-dependent moduli for each characterization technique. Statistical analyses indicated that the $E_1(\varepsilon)$ moduli, which corresponds to the τ_1 = 0.1 s time constant, was the only component that was dependent upon the fitting technique (p<0.001).

Modulus	CVC method			$2.5t_0$ method			p-value
	C_1 [MPa]	C_2 [MPa]	r^2	C_1 [MPa]	C_2 [MPa]	r^2	
$E_\infty(\varepsilon)$	4403.1	-9959.3	0.99	4008.3	-7179.7	0.99	0.93
$\boldsymbol{E_1(\varepsilon)}$	**901.1**	**8437.0**	**0.99**	**0.0**	**5.8E5**	**0.89**	**<0.001**
$E_2(\varepsilon)$	343.5	-684.1	0.99	309.7	1147.3	0.99	0.90
$E_3(\varepsilon)$	331.2	-1201.2	0.99	368.2	-1650.4	0.99	0.59
$E_4(\varepsilon)$	476.5	-363.4	0.99	165.7	3828.6	0.97	0.44

The FE model predictions for each fitting method closely approximated the average cyclic analytical solution at both the 3% (Figure 21) and the 6% (Figure 22) strain amplitudes (Table 13). Data taken from the last full cycle [Figures 21(b) and 22(b), Table 13] indicated that the material coefficients obtained using the CVC method: (1) fell within the bounds of experimental variability, (2) closely approximated the average experimental peak stress (within the bounds of experimental variability), and (3) was in-phase with the average experimental data (Table 13). Conversely, the coefficients obtained from the $2.5t_0$ method could not comprehensively capture these three criteria at either strain amplitude.

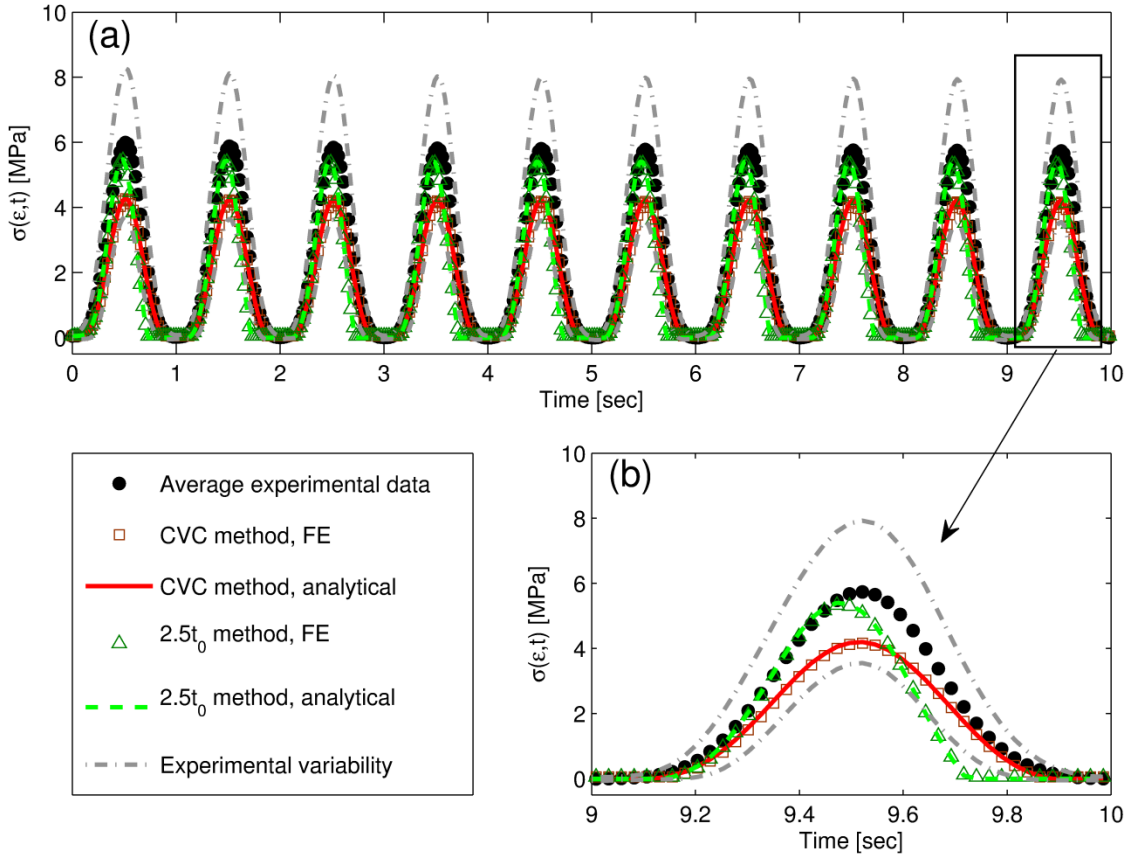

Figure 21: Average 3% strain amplitude cyclic behavior and the corresponding analytical and FE predictions from the two fitting techniques for (a) the full experiment and (b) the last full cycle. Although the $2.5t_0$ method predictions closely approximated the loading phase of the dynamic behavior, its peak stress magnitude was out-of-phase from the average experimental data. Conversely, the CVC method predictions were within the bounds of experimental variability and in-phase with the average experimental data.

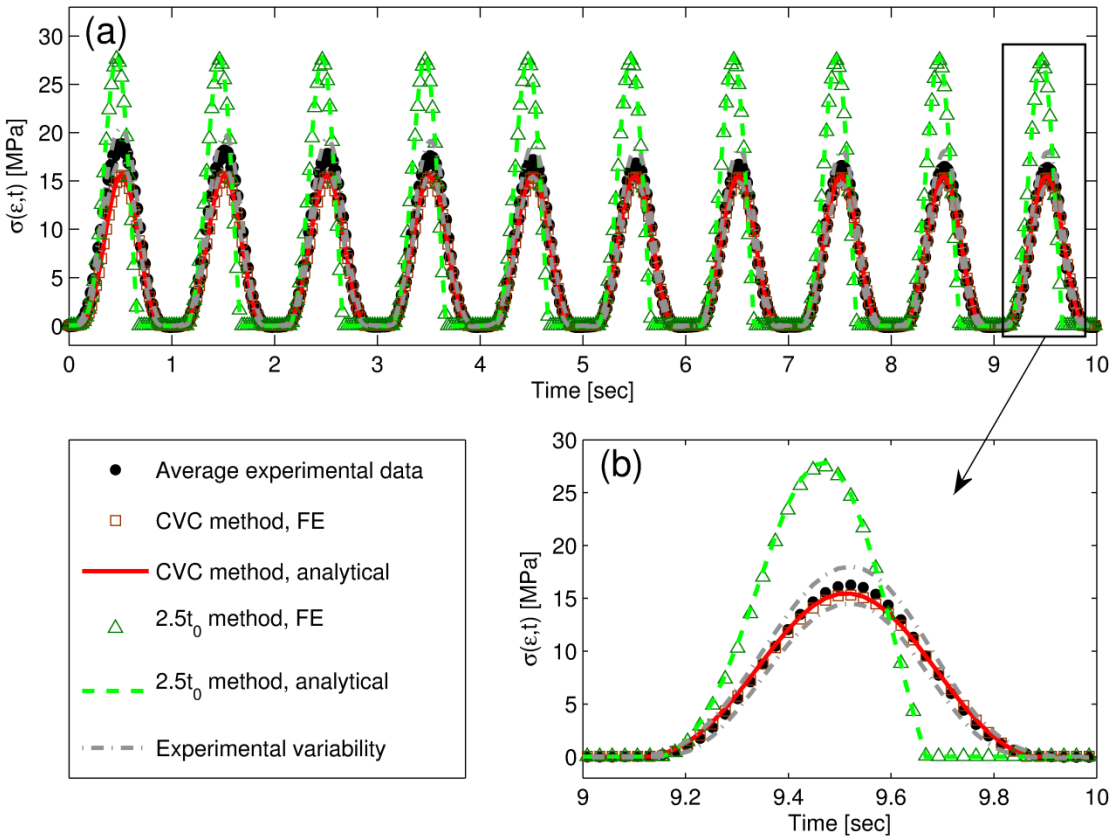

Figure 22: Average 6% strain amplitude cyclic behavior and the corresponding analytical and FE predictions from the two fitting techniques for (a) the full experiment and (b) the last full cycle. The $2.5t_0$ method predictions poorly approximated both the magnitude of the average experimental data and its phase. Conversely, the CVC method predictions were within the bounds of experimental variability and in-phase with the average experimental data.

Table 13: Summary of (a) the 3% and (b) the 6% strain amplitude cyclic prediction error metrics. For the last cycle, peak stresses (σ_{peak}) and their corresponding time shifts are provided as a reference for the magnitude of the $RMSE$ values and phase considerations, respectively. Quantitative error metrics (percent error and $RMSE$) indicated that the CVC method analytical and FE predictions were well within the bounds of experimental variability and were in-phase with the average cyclic behavior at both strain amplitudes. In contrast, the 2.5t_0 method was unable to comprehensively capture this dynamic behavior (both amplitude and phase) at either strain amplitude.

	All cycles		Last full cycle			
	Percent error [%]	$RMSE$ [MPa]	Percent error [%]	$RMSE$ [MPa]	σ_{peak} [MPa]	Time shift
(a) 3% strain amplitude						
Average experimental data	--	--	--	--	5.74	--
Experimental variability	16.43 (15.05, 17.89)[a]	1.33	16.60 (11.97, 21.76)[a]	1.30	7.93	0
CVC method, analytical prediction	**5.70 (5.08, 6.41)[b]**	**0.80**	**5.34 (4.00, 7.84)[b]**	**0.76**	**4.20**	**<Δt**
CVC method, FE prediction	**5.95 (5.30, 6.65)[b]**	**0.81**	**5.84 (4.38, 8.53)[b]**	**0.78**	**4.15**	**<Δt**
2.5t_0 method, analytical prediction	2.93 (2.86, 3.01)[c]	0.91	2.97 (2.75, 3.33)[c]	0.89	5.40	>7Δt
2.5t_0 method, FE prediction	3.52 (3.38, 3.61)[c]	0.90	3.25 (2.20, 3.81)[c]	0.87	5.34	>7Δt
(b) 6% strain amplitude						
Average experimental data	--	--	--	--	16.26	--
Experimental variability	4.78 (4.47, 5.07)[a]	1.05	5.40 (4.17, 6.61)[a]	1.06	17.00	0
CVC method, analytical prediction	**1.39 (1.27, 1.52)[b]**	**0.96**	**1.45 (1.07, 2.01)[b]**	**0.39**	**15.47**	**<Δt**
CVC method, FE prediction	**1.23 (1.12, 1.34)[b]**	**0.99**	**1.27 (0.87, 1.58)[b]**	**0.40**	**15.30**	**<Δt**
2.5t_0 method, analytical prediction	11.70 (9.96, 13.67)[c]	5.59	14.12 (8.03, 22.19)[c]	5.89	27.86	>7Δt
2.5t_0 method, FE prediction	10.96 (9.33, 12.95)[c]	5.42	13.24 (7.13, 21.23)[c]	5.68	27.46	>7Δt

Superscript letters depict statistical groupings; different letters indicate p<0.005.
Percent error is presented as: median (95% lower confidence limit, 95% upper confidence limit)
The temporal resolution of the experiment was: Δt = 0.0049 s.

4.4. Discussion

Soft tissues exhibit fully nonlinear viscoelastic properties under varying strain magnitudes. This behavior cannot be captured using the popular QLV formulation. Recent work from our laboratory[72,154] and several others[69-71,73,110,142,153] have observed substantial errors in the predictive fidelity of QLV formulations under multiple loading conditions. Implementation of more accurate, fully nonlinear viscoelastic models has been hindered by the lack of available material models that can be directly input into a FE algorithm. Previous studies have recommended the use of the single integral modified nonlinear superposition formulation [equation (28)] for soft tissues because of its simplicity and its ability to accurately model nonlinear viscoelastic behavior[117]. To the best of the author's knowledge, the current study is the first to develop and validate a material model with an accompanying experimental characterization technique for this formulation which can be directly implemented into FE algorithms.

Data generated in the current chapter demonstrate the importance of considering the viscoelastic effects during loading events. Current nonlinear viscoelastic characterization methodologies rapidly apply the deformation (t_0 on the order of milliseconds), then begin data fitting at a specified time-point that is temporally remote from the experimental ramp time (e.g. $2.5t_0$). As demonstrated herein, the coefficients obtained using the $2.5t_0$ method fit the stress relaxation data well (Tables 11 and 12; Figures 19 and 20). However, this technique poorly predicted the material behavior under different (dynamic) loading conditions, which is congruent with our previous observations[144]. These poor predictions are likely a result of the $2.5t_0$ method inaccurately capturing the important short-term behavior, as indicated by the statistically different $E_1(\varepsilon)$ moduli which describes the mechanical behavior on the order of 0.1 s.

Although a significant amount of cyclic preconditioning was performed, a noticeable stress decay (approximately 25% reduction in amplitude) in the 6% strain amplitude average cyclic data was observed *post hoc*. This irreversible behavior was not accurately captured by the nonlinear viscoelastic formulation utilized herein (Figure 22). Previous work has reported similar behavior in which stress decay was observed in tendon after many repeated cycles without reaching steady-state[155,156]. These previous findings were also more pronounced at larger strain magnitudes[155], a trend also observed in the current study. In order to capture these decay effects, it has been postulated that consideration of a constituent-based model (which would allow for the incorporation of transient component contributions such as collagen fiber recruitment) may be required[156]. However, our predictions of the entire dynamic loading regime curve were within the bounds of experimental variability (Table 13), and the errors (percent errors and $RMSE$ values) from these full predictions were similar in magnitude to previously published acceptance criteria[84,144,154].

An important advantage of the proposed differential FE formulation [equation (43)] with regard to computational efficiency is that it requires storage of a single (axial) stress value from the previous step rather than the entire stress history [as necessitated by equation (28)]. Even for FE models with relatively few elements, storage of the entire stress history at each integration point may be computationally expensive or intractable. Similar methods have been previously developed for an integral formulation, but its applicability has been restricted to QLV theory[157].

The constitutive formulae presented herein are limited to uniaxial (one-dimensional) tensile deformations. Nevertheless, both the integral [equation (28)] and the differential [equation (43)] formulations may be generalized to multiaxial stress states[96], although tendon and ligament anisotropy is rarely considered in whole joint simulations. Current whole joint FE

investigations, such as those of the cervical spine[158,159], the lumbar spine[160,161], the knee[162,163], the sacroiliac joint[164], and the pelvic joint[165] typically model these connective tissues as one-dimensional elastic spring or truss elements in order to reduce computational cost. Three dimensional, continuum-based material models have been put forth in an attempt to more accurately represent connective tissue anisotropic nonlinear viscoelasticity[166-168]. However, these continuum formulations require very complicated experimental characterization techniques owing to the relatively large number of required material coefficients, and implementation of these anisotropic derivations into whole joint FE model has, to date, been shown to be largely intractable.

4.5. Conclusion

To conclude, this study was the first attempt to develop and validate a computationally tractable, fully nonlinear viscoelastic formulation that can be directly implemented into FE algorithms. It is expected that adaptation of this formulae and associated characterization technique will greatly improve the predictive fidelity of soft tissue transient internal mechanical parameters for whole joint FE simulations subjected to temporally fluctuating loading regimes.

5. Overall Conclusions

The overall conclusions of this dissertation are:

- The comprehensive viscoelastic characterization (CVC) technique developed in chapter 2 significantly improves the predictive fidelity of the fitted material coefficients for musculoskeletal soft tissues under static and dynamic loading regimes as compared to previously accepted characterization methods.
- The short-term aspect (on the order of 0.1 s) of spinal ligament and tendon viscoelasticity is highly important under temporally fluctuating (static and dynamic) loading conditions.
- The proposed strain-dependent Prony series relaxation modulus with fixed time constants described spinal ligament and tendon viscoelasticty well (within the bounds of experimental variability) under multiple loading conditions, indicating that this model accurately captures the nonlinear viscoelastic behavior of multiple musculoskeletal tissue types.
- The finite element formulation developed herein offers a fully nonlinear viscoelastic material model that can be directly implemented into whole joint musculoskeletal models.

6. Future Work

While this dissertation represents a significant advancement in our ability to characterize the viscoelastic behavior of biological tissues, further investigations are warranted to develop more sophisticated models. The following sections detail several possible future investigations.

6.1. Anisotropic Nonlinear Viscoelastic Characterization

Although the nonlinear viscoelastic formulae developed herein [equations (28) and (29)] accurately captured the one-dimensional temporal behavior of various musculoskeletal soft tissues, theses tissues are known to exhibit a significant amount of mechanical anisotropy due their fiber-composite microstructure. Previous efforts have developed microstructural (fiber-level)[167,169-172] and multiphasic-based viscoelastic models to describe this anisotropic behavior[173]. Unfortunately, the available microstructural-based formulae are either restricted to utilizing over-simplified QLV formulations[169-172] or are burdened with an inordinate number of material coefficients whereby implementation into FE codes becomes intractable[167]. Additionally, multiphasic representations are complicated by the appropriate prescription of the constituent (namely fluid) boundary conditions as would be present *in vivo*[174]. Although these constituent-based models offer insight into the origins of tissue viscoelasticity, they are not particularly necessary to describe tissue-level (phenomenological) behavior.

Several tissue-level anisotropic phenomenological formulations have been suggested for modeling ligament viscoelasticity[95,157,175,176]. Nonetheless, most of the these models are based on over-simplified QLV assumptions which cannot accurately capture nonlinear viscoelastic behavior[157,175,176]. However, a possible fully nonlinear viscoelastic formulation proposed by

Rajagopal and Wineman[174] may offer the generality necessary to describe multidimensional soft tissue nonlinear viscoelasticity:

$$\boldsymbol{T} = -p\mathbf{1} + \boldsymbol{F}(t)\left\{\boldsymbol{R}[\boldsymbol{C}(t), 0] + \int_0^t \frac{\partial}{\partial(t-\tau)}\boldsymbol{R}[\boldsymbol{C}(\tau), t-\tau]d\tau\right\}\boldsymbol{F}^T(t) \tag{45}$$

where $\boldsymbol{T}$ is the Cauchy stress tensor, $-p\mathbf{1}$ is the indeterminate stress (due to the incompressibility constraint), $\boldsymbol{F}(t)$ is the time-dependent deformation gradient, $\boldsymbol{C}(\tau)$ is the right Cauchy-Green deformation tensor, and $\boldsymbol{R}[\boldsymbol{C}(\tau), t-\tau]$ is the tensorial relaxation modulus. Equation (45) is similar in form to the one-dimensional nonlinear superposition formulation utilized herein [equation (28)].

Implementation of equation (45) is not straightforward. Several experimental and computational challenges exist, such as: (1) the explicit definition of the form of the tensoral relaxation modulus $\boldsymbol{R}$, (2) the protocol for conducting multiaxial nonlinear stress relaxation experiments (at multiple strain magnitudes) under controlled hydrothermal conditions, and (3) the complex (simultaneous) fitting of the multidimensional stress relaxation data to determine the material coefficients of $\boldsymbol{R}$. It is likely that appropriate material symmetries (such as transverse isotropy) are requisite in order to reduce the number of tensoral components of equation (45) and make the definition of $\boldsymbol{R}$ tractable[177]. Additionally, the form of $\boldsymbol{R}$ must satisfy previously established thermodynamic feasibility requirements[93,94]. It is postulated that fitting the mulitaxial experimental data to equation (45) may be carried out by developing FE model of the experimental specimen (based on physical measurements) where the actual experimental forces and/or displacements can be used as the input FE boundary conditions. This FE model, which includes a custom user-defined material (UMAT) that implements equation (45), can be used to create the predicted curves [step (b)] in the CVC algorithm (page 30). This protocol would be similar to a previous study that combined analytical and computational models to achieve the optimum coefficients for an anisotropic QLV model for brain stem[178].

6.2. Interrogation of Various Nonlinear Viscoelastic Formulations

Although several studies have demonstrated that the single integral nonlinear superposition model [equation (28)] can accurately capture the nonlinear viscoelastic effects of soft tissues subjected to temporally varying (stress relaxation and cyclic) loading conditions[69-73,117,144,179], recent evidence suggests that this formulation demonstrates reduced accuracy when describing other viscoelastic effects such as stress recovery[179] and creep (Appendix E). A single integral formulation developed by Schapery[180] may be more applicable to describe soft tissue recovery than equation (28)[179]. In addition, multiple-integral nonlinear viscoelastic models, which contain more general nonlinear material definitions than the single integral models[94,96], may offer the ability to represent numerous soft tissue viscoelastic effects. To the best of the author's knowledge, there has been no effort to implement multiple integral formulations into soft tissue viscoelasticity.

Additionally, there are a number of relaxation moduli proposed to describe musculoskeletal soft tissue viscoelasticity, including Prony series [e.g., equation (29)] and power law formulations[69-71,110,117,153]. To date, there has been no general agreement in the literature over which specific form the relaxation modulus must take to describe soft tissue viscoelasticity.

References

1. Davis SJ, Teresi LM, Bradley WG, Jr., Ziemba MA, Bloze AE. Cervical spine hyperextension injuries: MR findings. *Radiology*. 1991; 180(1):245-251.

2. Jonsson H, Bring G, Rauschning W, Sahlstedt B. Hidden cervical-spine injuries in traffic accident victims with skull fractures. *Journal of Spinal Disorders*. 1991; 4(3):251-263.

3. Panjabi MM, Pearson AM, Ito S, Ivancic PC, Gimenez SE, Tominaga Y. Cervical spine ligament injury during simulated frontal impact. *Spine (Phila Pa 1976)*. 2004; 29(21):2395-2403.

4. Ito S, Ivanvic PC, Panjabi MM, Cunningham BW. Soft tissue injury threshold during simulated whiplash - a biomechanical investigation. *Spine*. 2004; 29(9):979-987.

5. Pearson AM, Panjabi MM, Ivancic PC, Ito S, Cunningham BW, Rubin W, et al. Frontal impact causes ligamentous cervical spine injury. *Spine*. 2005; 30(16):1852-1858.

6. Panjabi MM, Nibu K, Cholewicki J. Whiplash injuries and the potential for mechanical instability. *European Spine Journal*. 1998; 7(6):484-492.

7. Ivancic PC, Pearson AM, Panjabi MM, Ito S. Injury of the anterior longitudinal ligament during whiplash simulation. *European Spine Journal*. 2004; 13(1):61-68.

8. Panjabi MM, Cholewicki J, Nibu K, Grauer JN, Babat LB, Dvorak J. Mechanism of whiplash injury. *Clinical Biomechanics*. 1998; 13(4-5):239-249.

9. Yoganandan N, Pintar FA, Kleinberger M. Whiplash injury - biomechanical experimentation. *Spine*. 1999; 24(1):83-85.

10. Majewski M, Susanne H, Klaus S. Epidemiology of athletic knee injuries: a 10-year study. *Knee*. 2006; 13(3):184-188.

11. Griffin LY, Agel J, Albohm MJ, Arendt EA, Dick RW, Garrett WE, et al. Noncontact anterior cruciate ligament injuries: risk factors and prevention strategies. *Journal of the American Academy of Orthopaedic Surgeons*. 2000; 8(3):141-150.

12. Clarke KS. Epidemiology of athletic neck injury. *Clinics in Sports Medicine*. 1998; 17(1):83-97.

13. Torg JS, Guille JT, Jaffe S. Injuries to the cervical spine in American football players. *Journal of Bone and Joint Surgery - American Volume*. 2002; 84-A(1):112-122.

14. Ivancic PC, Coe MP, Ndu AB, Tominaga Y, Carlson EJ, Rubin W, et al. Dynamic mechanical properties of intact human cervical spine ligaments. *The Spine Journal*. 2007; 7(6):659-665.

15. Lauder TD, Baker SP, Smith GS, Lincoln AE. Sports and physical training injury hospitalizations in the army. *American Journal of Preventive Medicine*. 2000; 18(3):118-128.

16. Gwinn DE, Wilckens JH, Mcdevitt ER, Ross G, Kao TC. The relative incidence of anterior cruciate ligament injury in men and women at the United States Naval Academy. *American Journal of Sports Medicine*. 2000; 28(1):98-102.

17. Owens BD, Mountcastle SB, Dunn WR, Deberardino TM, Taylor DC. Incidence of anterior cruciate ligament injury among active duty US military servicemen and servicewomen. *Military Medicine*. 2007; 172(1):90-91.

18. Kaufman KR, Brodine S, Shaffer R. Military training-related injuries - surveillance, research, and prevention. *American Journal of Preventive Medicine*. 2000; 18(3):54-63.

19. Boos N, Khazim R, Kerslake RW, Webb JK, Mehdian H. Atlanto-axial dislocation without fracture - case report of an ejection injury. *Journal of Bone and Joint Surgery-British Volume*. 1997; 79B(2):204-205.

20. Schall DG. Non-ejection cervical spine injuries due to +Gz in high-performance aircraft. *Aviation Space and Environmental Medicine*. 1989; 60(5):445-456.

21. Lucas SR, Bass CR, Salzar RS, Oyen ML, Planchak C, Ziemba A, et al. Viscoelastic properties of the cervical spinal ligaments under fast strain-rate deformations. *Acta Biomaterialia*. 2008; 4(1):117-125.

22. Bass CR, Lucas SR, Salzar RS, Oyen ML, Planchak C, Shender BS, et al. Failure properties of cervical spinal ligaments under fast strain rate deformations. *Spine (Phila Pa 1976)*. 2007; 32(1):E7-13.

23. Lohmander LS, Ostenberg A, Englund M, Roos H. High prevalence of knee osteoarthritis, pain, and functional limitations in female soccer players twelve years after anterior cruciate ligament injury. *Arthritis and Rheumatism*. 2004; 50(10):3145-3152.

24. Felson DT. The epidemiology of knee osteoarthritis - results from the framingham osteoarthritis study. *Seminars in Arthritis and Rheumatism*. 1990; 20(3):42-50.

25. Felson DT, Zhang YQ. An update on the epidemiology of knee and hip osteoarthritis with a view to prevention. *Arthritis and Rheumatism*. 1998; 41(8):1343-1355.

26. Fleming BC, Hulstyn MJ, Oksendahl HL, Fadale PD. Ligament injury, reconstruction and osteoarthritis. *Current Opinion in Orthopaedics*. 2005; 16(5):354-362.

27. Gillquist J, Messner K. Anterior cruciate ligament reconstruction and the long term incidence of gonarthrosis. *Sports Medicine*. 1999; 27(3):143-156.

28. Anderson DD, Chubinskaya S, Guilak F, Martin JA, Oegema TR, Olson SA, et al. Post-traumatic osteoarthritis: Improved understanding and opportunities for early intervention. *Journal of Orthopaedic Research*. 2011; 29(6):802-809.

29. Brown TD, Johnston RC, Saltzman CL, Marsh JL, Buckwalter JA. Posttraumatic osteoarthritis: a first estimate of incidence, prevalence, and burden of disease. *Journal of Orthopaedic Trauma*. 2006; 20(10):739-744.

30. Dirschl DR, Marsh JL, Buckwalter JA, Gelberman R, Olson SA, Brown TD, et al. Articular fractures. *Journal of the American Academy of Orthopaedic Surgeons*. 2004; 12(6):416-423.

31. Simon SR, American Academy of Orthopaedic Surgeons. Orthopaedic basic science. Rosemont, Ill.: *American Academy of Orthopaedic Surgeons*; 1994.

32. Kadler KE, Holmes DF, Trotter JA, Chapman JA. Collagen fibril formation. *Biochemical Journal*. 1996; 316(Pt. 1):1-11.

33. Kastelic J, Galeski A, Baer E. Multicomposite structure of tendon. *Connective Tissue Research*. 1978; 6(1):11-23.

34. Weiss JA, Gardiner JC. Computational modeling of ligament mechanics. *Critical Reviews in Biomedical Engineering*. 2001; 29(3):303-371.

35. Tanzer ML, Waite JH. Collagen cross-linking. *Collagen and Related Research*. 1982; 2(2):177-180.

36. Woo SLY, Johnson GA, Smith BA. Mathematical-modeling of ligaments and tendons. *Journal of Biomechanical Engineering*. 1993; 115(4):468-473.

37. Viidik A. Structure and function of normal and healing tendons and ligaments. In: Mow VC, Ratcliffe A, Woo SL-Y, editors. Biomechanics of diarthrodial joints. New York: *Springer-Verlag*; 1990. p. 3-38.

38. Walsh WR. Repair and regeneration of ligaments, tendons, and joint capsule. Totowa, N.J.: *Humana Press*; 2006.

39. Lujan TJ, Underwood CJ, Jacobs NT, Weiss JA. Contribution of glycosaminoglycans to viscoelastic tensile behavior of human ligament. *Journal of Applied Physiology*. 2009; 106(2):423-431.

40. Rumian AP, Wallace AL, Birch HL. Tendons and ligaments are anatomically distinct but overlap in molecular and morphological features - a comparative study in an ovine model. *Journal of Orthopaedic Research*. 2007; 25(4):458-464.

41. Danielson KG, Baribault H, Holmes DF, Graham H, Kadler KE, Iozzo RV. Targeted disruption of decorin leads to abnormal collagen fibril morphology and skin fragility. *Journal of Cell Biology*. 1997; 136(3):729-743.

42. Nakamura N, Hart DA, Boorman RS, Kaneda Y, Shrive NG, Marchuk LL, et al. Decorin antisense gene therapy improves functional healing of early rabbit ligament scar with enhanced collagen fibrillogenesis in vivo. *Journal of Orthopaedic Research*. 2000; 18(4):517-523.

43. Scott JE. Proteodermatan and proteokeratan sulfate (decorin, lumican/fibromodulin) proteins are horseshoe shaped. Implications for their interactions with collagen. *Biochemistry*. 1996; 35(27):8795-8799.

44. Pins GD, Christiansen DL, Patel R, Silver FH. Self-assembly of collagen fibers. Influence of fibrillar alignment and decorin on mechanical properties. *Biophysical Journal*. 1997; 73(4):2164-2172.

45. Birk DE, Trelstad RL. Extracellular compartments in tendon morphogenesis - collagen fibril, bundle, and macroaggregate formation. *Journal of Cell Biology*. 1986; 103(1):231-240.

46. Olsen BR. Collagen biosynthesis. In: Hay ED, editor. Cell biology of extracellular matrix. 2nd ed ed. New York: *Plenum*; 1991. p. 177-220.

47. Yang G, Crawford RC, Wang JH. Proliferation and collagen production of human patellar tendon fibroblasts in response to cyclic uniaxial stretching in serum-free conditions. *Journal of Biomechanics*. 2004; 37(10):1543-1550.

48. Frank CB. Ligament structure, physiology and function. *Journal of Musculoskeletal and Neuronal Interactions*. 2004; 4(2):199-201.

49. Hukins DW, Kirby MC, Sikoryn TA, Aspden RM, Cox AJ. Comparison of structure, mechanical properties, and functions of lumbar spinal ligaments. *Spine*. 1990; 15(8):787-795.

50. Kirby MC, Sikoryn TA, Hukins DWL, Aspden RM. Structure and mechanical-properties of the longitudinal ligaments and ligamentum flavum of the spine. *Journal of Biomedical Engineering*. 1989; 11(3):192-196.

51. Aims AA. Biomechanics of bone, tendon, and ligament. In: Hughes S, Mccarthy ID, editors. Sciences basic to orthopaedics. London: *Saunders*; 1998. p. 232-239.

52. Arms S, Boyle J, Johnson R, Pope M. Strain-measurement in the medial collateral ligament of the human knee - an autopsy study. *Journal of Biomechanics*. 1983; 16(7):491-496.

53. Nachemson AL, Evans JH. Some mechanical properties of the third human lumbar interlaminar ligament (ligamentum flavum). *Journal of Biomechanics*. 1968; 1(3):211-220.

54. Pintar FA, Yoganandan N, Myers T, Elhagediab A, Sances A. Biomechanical properties of human lumbar spine ligaments. *Journal of Biomechanics*. 1992; 25(11):1351-1356.

55. Panjabi MM, Goel VK, Takata K. Physiologic strains in the lumbar spinal ligaments - an in vitro biomechanical study. *Spine*. 1982; 7(3):192-203.

56. Johansson H, Sjolander P, Sojka P. Activity in receptor afferents from the anterior cruciate ligament evokes reflex effects on fusimotor neurons. *Neuroscience Research*. 1990; 8(1):54-59.

57. Reider B, Arcand MA, Diehl LH, Mroczek K, Abulencia A, Stroud CC, et al. Proprioception of the knee before and after anterior cruciate ligament reconstruction. *Arthroscopy - The Journal of Arthroscopic and Related Surgery*. 2003; 19(1):2-12.

58. Fung YC. Elasticity of soft tissues in simple elongation. *American Journal of Physiology*. 1967; 213(6):1532-1544.

59. Fung YC. Biomechanics: mechanical properties of living tissues. 2nd ed. New York: *Springer-Verlag*; 1993.

60. Viidik A. Simultaneous mechanical and light microscopic studies of collagen fibers. *Anatomy and Embryology*. 1972; 136(2):204-212.

61. Mosler E, Folkhard W, Knorzer E, Nemetschekgansler H, Nemetschek T, Koch MHJ. Stress-induced molecular rearrangement in tendon collagen. *Journal of Molecular Biology*. 1985; 182(4):589-596.

62. Ciarletta P, Micera S, Accoto D, Dario P. A novel microstructural approach in tendon viscoelastic modelling at the fibrillar level. *Journal of Biomechanics*. 2006; 39(11):2034-2042.

63. Puxkandl R, Zizak I, Paris O, Keckes J, Tesch W, Bernstorff S, et al. Viscoelastic properties of collagen: synchrotron radiation investigations and structural model. *Philosophical Transactions of the Royal Society of London Series B-Biological Sciences*. 2002; 357(1418):191-197.

64. Henninger HB, Underwood CJ, Ateshian GA, Weiss JA. Effect of sulfated glycosaminoglycan digestion on the transverse permeability of medial collateral ligament. *Journal of Biomechanics*. 2010; 43(13):2567-2573.

65. Hewitt J, Guilak F, Glisson R, Vail TP. Regional material properties of the human hip joint capsule ligaments. *Journal of Orthopaedic Research*. 2001; 19(3):359-364.

66. Lynch HA, Johannessen W, Wu JP, Jawa A, Elliott DM. Effect of fiber orientation and strain rate on the nonlinear uniaxial tensile material properties of tendon. *Journal of Biomechanical Engineering*. 2003; 125(5):726-731.

67. Yin LH, Elliott DM. A biphasic and transversely isotropic mechanical model for tendon: application to mouse tall fascicles in uniaxial tension. *Journal of Biomechanics*. 2004; 37(6):907-916.

68. Taylor DC, Dalton JD, Seaber AV, Garrett WE. Viscoelastic properties of muscle-tendon units - the biomechanical effects of stretching. *American Journal of Sports Medicine*. 1990; 18(3):300-309.

69. Duenwald SE, Vanderby R, Jr., Lakes RS. Viscoelastic relaxation and recovery of tendon. *Annals of Biomedical Engineering*. 2009; 37(6):1131-1140.

70. Hingorani RV, Provenzano PP, Lakes RS, Escarcega A, Vanderby R, Jr. Nonlinear viscoelasticity in rabbit medial collateral ligament. *Annals of Biomedical Engineering*. 2004; 32(2):306-312.

71. Provenzano P, Lakes R, Keenan T, Vanderby R, Jr. Nonlinear ligament viscoelasticity. *Annals of Biomedical Engineering*. 2001; 29(10):908-914.

72. Troyer KL, Puttlitz CM. Human cervical spine ligaments exhibit fully nonlinear viscoelastic behavior. *Acta Biomater*. 2011; 7(2):700-709.

73. Ambrosetti-Giudici S, Gedet P, Ferguson SJ, Chegini S, Burger J. Viscoelastic properties of the ovine posterior spinal ligaments are strain dependent. *Clinical Biomechanics*. 2010; 25(2):97-102.

74. Thornton GM, Oliynyk A, Frank CB, Shrive NG. Ligament creep cannot be predicted horn stress relaxation at low stress: A biomechanical study of the rabbit medial collateral ligament. *Journal of Orthopaedic Research*. 1997; 15(5):652-656.

75. Natali AN, Pavan PG, Carniel EL, Lucisano ME, Taglialavoro G. Anisotropic elasto-damage constitutive model for the biomechanical analysis of tendons. *Medical Engineering and Physics*. 2005; 27(3):209-214.

76. Panjabi MM, Yoldas E, Oxland TR, Crisco JJ. Subfailure injury of the rabbit anterior cruciate ligament. *Journal of Orthopaedic Research*. 1996; 14(2):216-222.

77. Provenzano PP, Heisey D, Hayashi K, Lakes R, Vanderby R. Subfailure damage in ligament: a structural and cellular evaluation. *Journal of Applied Physiology*. 2002; 92(1):362-371.

78. Laws G, Walton M. Fibroblastic healing of grade-II ligament injuries - histological and mechanical studies in the sheep. *Journal of Bone and Joint Surgery - British Volume*. 1988; 70(3):390-396.

79. Duenwald-Kuehl SE, Kondratko J, Vanderby R, Lakes R. Characterization of tendon mechanics following subfailure damage. In: Proulx T, editor. Mechanics of Biological Systems and Materials, Volume 2: *Springer New York*; 2011. p. 213-217.

80. Provenzano PP, Hayashi K, Kunz DN, Markel MD, Vanderby R. Healing of subfailure ligament injury: comparison between immature and mature ligaments in a rat model. *Journal of Orthopaedic Research*. 2002; 20(5):975-983.

81. Thornton GM, Leask GP, Shrive NG, Frank CB. Early medial collateral ligament scars have inferior creep behaviour. *Journal of Orthopaedic Research*. 2000; 18(2):238-246.

82. Woo SLY, Abramowitch SD, Kilger R, Liang R. Biomechanics of knee ligaments: injury, healing, and repair. *Journal of Biomechanics*. 2006; 39(1):1-20.

83. Frank C, Woo SLY, Amiel D, Harwood F, Gomez M, Akeson W. Medial collateral ligament healing - a multidisciplinary assessment in rabbits. *American Journal of Sports Medicine*. 1983; 11(6):379-389.

84. Abramowitch SD, Woo SLY, Clineff TD, Debski RE. An evaluation of the quasi-linear viscoelastic properties of the healing medial collateral ligament in a goat model. *Annals of Biomedical Engineering*. 2004; 32(3):329-335.

85. Abramowitch SD, Papageorgiou CD, Debski RE, Clineff TD, Woo SLY. A biomechanical and histological evaluation of the structure and function of the healing medial collateral ligament in a goat model. *Knee Surgery Sports Traumatology Arthroscopy*. 2003; 11(3):155-162.

86. Ohno K, Pomaybo AS, Schmidt CC, Levine RE, Ohland KJ, Woo SLY. Healing of the medial collateral ligament after a combined medial collateral and anterior cruciate ligament injury and reconstruction of the anterior cruciate ligament - comparison of repair and nonrepair of medial collateral ligament tears in rabbits. *Journal of Orthopaedic Research*. 1995; 13(3):442-449.

87. Hart DP, Dahners LE. Healing of the medial collateral ligament in rats - the effects of repair, motion, and secondary stabilizing ligaments. *Journal of Bone and Joint Surgery-American Volume*. 1987; 69A(8):1194-1199.

88. Weiss JA, Woo SLY, Ohland KJ, Horibe S, Newton PO. Evaluation of a new injury model to study medial collateral ligament healing - primary repair versus nonoperative treatment. *Journal of Orthopaedic Research*. 1991; 9(4):516-528.

89. Inoue M, Woo SL, Gomez MA, Amiel D, Ohland KJ, Kitabayashi LR. Effects of surgical-treatment and immobilization on the healing of the medial collateral ligament - a long-term multidisciplinary study. *Connective Tissue Research*. 1990; 25(1):13-26.

90. Loitz-Ramage BJ, Frank CB, Shrive NG. Injury size affects long term strength of the rabbit medial collateral ligament. *Clinical Orthopaedics and Related Research*. 1997; 337):272-280.

91. Aims AA. Artificial ligaments. In: Walsh WR, editor. Repair and regeneration of ligaments, tendons, and joint capsule. Totowa, N.J.: *Humana Press*; 2006. p. 233-256.

92. Woo SLY, Kanamori A, Zeminski J, Yagi M, Papageorgiou C, Fu FH. The effectiveness of reconstruction of the anterior cruciate ligament with hamstrings and patellar tendon - A cadaveric study comparing anterior tibial and rotational loads. *Journal of Bone and Joint Surgery-American Volume*. 2002; 84A(6):907-914.

93. Christensen RM. Restrictions upon viscoelastic relaxation functions and complex moduli. *Transactions of the Society of Rheology*. 1972; 16(4):603-614.

94. Lakes RS. Viscoelastic solids. Boca Raton: *CRC Press*; 1999.

95. Little JS, Khalsa PS. Material properties of the human lumbar facet joint capsule. *Journal of Biomechanical Engineering*. 2005; 127(1):15-24.

96. Findley WN, Lai JS, Onaran K. Creep and relaxation of nonlinear viscoelastic materials, with an introduction to linear viscoelasticity. Amsterdam: *Elsevier/North Holland*; 1976.

97. Fung YC. Stress-strain-history relations of soft tissues in simple elongation. In: Fung YC, Perrone N, Anliker M, editors. Biomechanics: its foundations and objectives. Englewood Cliffs, NJ: *Prentice-Hall*; 1972. p. 181–207.

98. Funk JR, Hall GW, Crandall JR, Pilkey WD. Linear and quasi-linear viscoelastic characterization of ankle ligaments. *Journal of Biomechanical Engineering*. 2000; 122(1):15-22.

99. Kwan MK, Lin TH, Woo SL. On the viscoelastic properties of the anteromedial bundle of the anterior cruciate ligament. *Journal of Biomechanics*. 1993; 26(4-5):447-452.

100. Woo SL, Gomez MA, Akeson WH. The time and history-dependent viscoelastic properties of the canine medical collateral ligament. *Journal of Biomechanical Engineering*. 1981; 103(4):293-298.

101. Woo SL, Simon BR, Kuei SC, Akeson WH. Quasi-linear viscoelastic properties of normal articular cartilage. *Journal of Biomechanical Engineering*. 1980; 102(2):85-90.

102. Toms SR, Dakin GJ, Lemons JE, Eberhardt AW. Quasi-linear viscoelastic behavior of the human periodontal ligament. *Journal of Biomechanics*. 2002; 35(10):1411-1415.

103. Elliott DM, Robinson PS, Gimbel JA, Sarver JJ, Abboud JA, Iozzo RV, et al. Effect of altered matrix proteins on quasilinear viscoelastic properties in transgenic mouse tail tendons. *Annals of Biomedical Engineering*. 2003; 31(5):599-605.

104. Johnson GA, Tramaglini DM, Levine RE, Ohno K, Choi NY, Woo SLY. Tensile and viscoelastic properties of human patellar tendon. *Journal of Orthopaedic Research*. 1994; 12(6):796-803.

105. Iatridis JC, Setton LA, Weidenbaum M, Mow VC. The viscoelastic behavior of the non-degenerate human lumbar nucleus pulposus in shear. *Journal of Biomechanics*. 1997; 30(10):1005-1013.

106. Neumann P, Keller TS, Ekstrom L, Hansson T. Effect of strain rate and bone mineral on the structural properties of the human anterior longitudinal ligament. *Spine (Phila Pa 1976)*. 1994; 19(2):205-211.

107. Yoganandan N, Pintar F, Butler J, Reinartz J, Sances A, Jr., Larson SJ. Dynamic response of human cervical spine ligaments. *Spine (Phila Pa 1976)*. 1989; 14(10):1102-1110.

108. White AA, Panjabi MM. Clinical biomechanics of the spine. 2nd ed. Philadelphia: *Lippincott*; 1990.

109. Abramowitch SD, Woo SL. An improved method to analyze the stress relaxation of ligaments following a finite ramp time based on the quasi-linear viscoelastic theory. *Journal of Biomechanical Engineering*. 2004; 126(1):92-97.

110. Duenwald SE, Vanderby R, Lakes RS. Constitutive equations for ligament and other soft tissue: evaluation by experiment. *Acta Mechanica*. 2009; 205(1-4):23-33.

111. Gimbel JA, Sarver JJ, Soslowsky LJ. The effect of overshooting the target strain on estimating viscoelastic properties from stress relaxation experiments. *Journal of Biomechanical Engineering*. 2004; 126(6):844-848.

112. Yang W, Fung TC, Chian KS, Chong CK. Viscoelasticity of esophageal tissue and application of a QLV model. *Journal of Biomechanical Engineering*. 2006; 128(6):909-916.

113. Sorvari J, Malinen M, Hamalainen J. Finite ramp time correction method for non-linear viscoelastic material model. *International Journal of Non-Linear Mechanics*. 2006; 41(9):1050-1056.

114. Myers BS, Mcelhaney JH, Doherty BJ. The viscoelastic responses of the human cervical spine in torsion: experimental limitations of quasi-linear theory, and a method for reducing these effects. *Journal of Biomechanics*. 1991; 24(9):811-817.

115. Nigul I, Nigul U. On algorithms of evaluation of Fung's relaxation function parameters. *Journal of Biomechanics*. 1987; 20(4):343-352.

116. Nordin LO, Varna J. Methodology for parameter identification in nonlinear viscoelastic material model. *Mechanics of Time-Dependent Materials*. 2005; 9(4):259-280.

117. Provenzano PP, Lakes RS, Corr DT, Vanderby R, Jr. Application of nonlinear viscoelastic models to describe ligament behavior. *Biomechanics and Modeling in Mechanobiology*. 2002; 1(1):45-57.

118. Heuer F, Schmidt H, Wilke HJ. Stepwise reduction of functional spinal structures increase disc bulge and surface strains. *Journal of Biomechanics*. 2008; 41(9):1953-1960.

119. Heuer F, Schmidt H, Klezl Z, Claes L, Wilke HJ. Stepwise reduction of functional spinal structures increase range of motion and change lordosis angle. *Journal of Biomechanics*. 2007; 40(2):271-280.

120. Goel VK, Clausen JD. Prediction of load sharing among spinal components of a C5-C6 motion segment using the finite element approach. *Spine*. 1998; 23(6):684-691.

121. Lucas SR, Bass CR, Crandall JR, Kent RW, Shen FH, Salzar RS. Viscoelastic and failure properties of spine ligament collagen fascicles. *Biomechanics and Modeling in Mechanobiology*. 2009; 8(8):487-498.

122. Abramowitch SD, Zhang X, Curran M, Kilger R. A comparison of the quasi-static mechanical and non-linear viscoelastic properties of the human semitendinosus and gracilis tendons. *Clinical Biomechanics*. 2010; 25(4):325-331.

123. Kohandel M, Sivaloganathan S, Tenti G. Estimation of the quasi-linear viscoelastic parameters using a genetic algorithm. *Mathematical and Computer Modelling*. 2008; 47(3-4):266-270.

124. Mirani RD, Pratt J, Iyer P, Madihally SV. The stress relaxation characteristics of composite matrices etched to produce nanoscale surface features. *Biomaterials*. 2009; 30(5):703-710.

125. Xu F, Seffen K, Lu TJ. A quasi-linear viscoelastic model for skin tissue. *Theoretical and Experimental Aspects of Continuum Mechanics*. 2008; 14-21.

126. Pryse KM, Nekouzadeh A, Genin GM, Elson EL, Zahalak GI. Incremental mechanics of collagen gels: new experiments and a new viscoelastic model. *Annals of Biomedical Engineering*. 2003; 31(10):1287-1296.

127. Ott L, Longnecker M. An introduction to statistical methods and data analysis. 5th ed. Pacific Grove, CA: *Duxbury*; 2001.

128. Turner S. Creep in glassy polymers. In: Haward RN, editor. The physics of glassy polymers. New York: *Wiley*; 1973. p. 238-244.

129. Defrate LE, Li G. The prediction of stress-relaxation of ligaments and tendons using the quasi-linear viscoelastic model. *Biomechanics and Modeling in Mechanobiology*. 2007; 6(4):245-251.

130. Dumas GA, Beaudoin L, Drouin G. In situ mechanical behavior of posterior spinal ligaments in the lumbar region. An in vitro study. *Journal of Biomechanics*. 1987; 20(3):301-310.

131. Chazal J, Tanguy A, Bourges M, Gaurel G, Escande G, Guillot M, et al. Biomechanical properties of spinal ligaments and a histological study of the supraspinal ligament in traction. *Journal of Biomechanics*. 1985; 18(3):167-176.

132. Myklebust JB, Pintar F, Yoganandan N, Cusick JF, Maiman D, Myers TJ, et al. Tensile strength of spinal ligaments. *Spine*. 1988; 13(5):526-531.

133. Neumann P, Keller TS, Ekstrom L, Perry L, Hansson TH, Spengler DM. Mechanical properties of the human lumbar anterior longitudinal ligament. *Journal of Biomechanics*. 1992; 25(10):1185-1194.

134. Yoganandan N, Kumaresan S, Pintar FA. Geometric and mechanical properties of human cervical spine ligaments. *Journal of Biomechanical Engineering*. 2000; 122(6):623-629.

135. Przybylski GJ, Carlin GJ, Patel PR, Woo SL. Human anterior and posterior cervical longitudinal ligaments possess similar tensile properties. *Journal of Orthopaedic Research*. 1996; 14(6):1005-1008.

136. Waters RL, Morris JM. An in vitro study of normal and scoliotic interspinous ligaments. *Journal of Biomechanics*. 1973; 6(4):343-348.

137. Tkaczuk H. Tensile properties of human lumbar longitudinal ligaments. *Acta Orthopaedica Scandinavica*. 1968; Suppl 115:111+.

138. Hukins DWL, Meakin JR. Relationship between structure and mechanical function of the tissues of the intervertebral joint. *American Zoologist*. 2000; 40(1):42-52.

139. Yahia LH, Audet J, Drouin G. Rheological properties of the human lumbar spine ligaments. *Journal of Biomedical Engineering*. 1991; 13(5):399-406.

140. Nakagawa H, Mikawa Y, Watanabe R. Elastin in the human posterior longitudinal ligament and spinal dura. A histologic and biochemical study. *Spine*. 1994; 19(19):2164-2169.

141. Abaqus. Abaqus analysis user's manual (version 6.9). Providence, RI: *Dassault Systèmes Simulia Corp.*; 2009.

142. Thornton GM, Oliynyk A, Frank CB, Shrive NG. Ligament creep cannot be predicted from stress relaxation at low stress: a biomechanical study of the rabbit medial collateral ligament. *Journal of Orthopaedic Research*. 1997; 15(5):652-656.

143. Bonifasi-Lista C, Lake SP, Small MS, Weiss JA. Viscoelastic properties of the human medial collateral ligament under longitudinal, transverse and shear loading. *Journal of Orthopaedic Research*. 2005; 23(1):67-76.

144. Troyer KL, Estep DJ, Puttlitz CM. Viscoelastic effects during loading play an integral role in soft tissue mechanics. *Acta Biomaterialia*. 2012; 8(1):234–243.

145. Moon DK, Woo SL, Takakura Y, Gabriel MT, Abramowitch SD. The effects of refreezing on the viscoelastic and tensile properties of ligaments. *Journal of Biomechanics*. 2006; 39(6):1153-1157.

146. Santoni BG, Mcgilvray KC, Lyons AS, Bansal M, Turner AS, Macgillivray JD, et al. Biomechanical analysis of an ovine rotator cuff repair via porous patch augmentation in a chronic rupture model. *American Journal of Sports Medicine*. 2010; 38(4):679-686.

147. Hee CK, Dines JS, Dines DM, Roden CM, Wisner-Lynch LA, Turner AS, et al. Augmentation of a rotator cuff suture repair using rhPDGF-BB and a type I bovine collagen matrix in an ovine model. *American Journal of Sports Medicine*. 2011; 39(8):1630-1639.

148. Butler DL, Grood ES, Noyes FR, Zernicke RF, Brackett K. Effects of structure and strain-measurement technique on the material properties of young human tendons and fascia. *Journal of Biomechanics*. 1984; 17(8):579-596.

149. Shetye SS, Malhotra K, Ryan SD, Puttlitz CM. Determination of mechanical properties of canine carpal ligaments. *American Journal of Veterinary Research*. 2009; 70(8):1026-1030.

150. Gibbons MJ, Butler DL, Grood ES, Bylskiaustrow DI, Levy MS, Noyes FR. Effects of gamma-irradiation on the initial mechanical and material properties of goat bone-patellar tendon-bone allografts. *Journal of Orthopaedic Research*. 1991; 9(2):209-218.

151. Mcgilvray KC, Santoni BG, Turner AS, Bogdansky S, Wheeler DL, Puttlitz CM. Effects of ^{60}Co gamma radiation dose on initial structural biomechanical properties of ovine bone--patellar tendon--bone allografts. *Cell Tissue Bank*. 2011; 12(2):89-98.

152. Lakes RS, Vanderby R. Interrelation of creep and relaxation: a modeling approach for ligaments. *Journal of Biomechanical Engineering*. 1999; 121(6):612-615.

153. Oza A, Vanderby R, Lakes RS. Interrelation of creep and relaxation for nonlinearly viscoelastic materials: application to ligament and metal. *Rheologica Acta*. 2003; 42(6):557-568.

154. Troyer KL, Puttlitz CM. Nonlinear viscoelasticty plays an essential role in the functional behavior of spinal ligaments. *Journal of Biomechanics*. 2012; 45(4):684-691.

155. Sverdlik A, Lanir Y. Time-dependent mechanical behavior of sheep digital tendons, including the effects of preconditioning. *Journal of Biomechanical Engineering*. 2002; 124(1):78-84.

156. Einat R, Yoram L. Recruitment viscoelasticity of the tendon. *Journal of Biomechanical Engineering*. 2009; 131(11):

157. Puso MA, Weiss JA. Finite element implementation of anisotropic quasi-linear viscoelasticity using a discrete spectrum approximation. *Journal of Biomechanical Engineering*. 1998; 120(1):62-70.

158. Brolin K, Halldin P. Development of a finite element model of the upper cervical spine and a parameter study of ligament characteristics. *Spine*. 2004; 29(4):376-385.

159. Womack W, Leahy PD, Patel VV, Puttlitz CM. Finite element modeling of kinematic and load transmission alterations due to cervical intervertebral disc replacement. *Spine (Phila Pa 1976)*. 2011; 36(17):E1126-1133.

160. Rohlmann A, Burra NK, Zander T, Bergmann G. Comparison of the effects of bilateral posterior dynamic and rigid fixation devices on the loads in the lumbar spine: a finite element analysis. *European Spine Journal*. 2007; 16(8):1223-1231.

161. Ayturk UM, Puttlitz CM. Parametric convergence sensitivity and validation of a finite element model of the human lumbar spine. *Computer Methods in Biomechanics and Biomedical Engineering*. 2011; 14(8):695-705.

162. Bae JY, Park KS, Seon JK, Kwak DS, Jeon I, Song EK. Biomechanical analysis of the effects of medial meniscectomy on degenerative osteoarthritis. *Medical and Biological Engineering and Computing*. 2012; 50(1):53-60.

163. Baldwin MA, Clary CW, Fitzpatrick CK, Deacy JS, Maletsky LP, Rullkoetter PJ. Dynamic finite element knee simulation for evaluation of knee replacement mechanics. *Journal of Biomechanics*. 2012; 45(3):474-483.

164. Eichenseer PH, Sybert DR, Cotton JR. A finite element analysis of sacroiliac joint ligaments in response to different loading conditions. *Spine*. 2011; 36(22):E1446-E1452.

165. Phillips ATM, Pankaj P, Howie CR, Usmani AS, Simpson AHRW. Finite element modelling of the pelvis: inclusion of muscular and ligamentous boundary conditions. *Medical Engineering and Physics*. 2007; 29(7):739-748.

166. Holzapfel GA, Gasser TC. A viscoelastic model for fiber-reinforced composites at finite strains: Continuum basis, computational aspects and applications. *Computer Methods in Applied Mechanics and Engineering*. 2001; 190(34):4379-4403.

167. Nguyen TD, Jones RE, Boyce BL. A nonlinear anisotropic viscoelastic model for the tensile behavior of the corneal stroma. *Journal of Biomechanical Engineering*. 2008; 130(4):

168. Pena E, Pena JA, Doblare M. On modelling nonlinear viscoelastic effects in ligaments. *Journal of Biomechanics*. 2008; 41(12):2659-2666.

169. Lanir Y. Constitutive equations for fibrous connective tissues. *Journal of Biomechanics*. 1983; 16(1):1-12.

170. Bischoff JE. Reduced parameter formulation for incorporating fiber level viscoelasticity into tissue level biomechanical models. *Annals of Biomedical Engineering*. 2006; 34(7):1164-1172.

171. Bischoff JE, Arruda EM, Grosh K. A rheological network model for the continuum anisotropic and viscoelastic behavior of soft tissue. *Biomechanics and Modeling in Mechanobiology*. 2004; 3(1):56-65.

172. Vena P, Gastaidi D, Contro R. A constituent-based model for the nonlinear viscoelastic behavior of ligaments. *Journal of Biomechanical Engineering*. 2006; 128(3):449-457.

173. Mow VC, Kuei SC, Lai WM, Armstrong CG. Biphasic creep and stress-relaxation of articular-cartilage in compression - theory and experiments. *Journal of Biomechanical Engineering*. 1980; 102(1):73-84.

174. Rajagopal KR, Wineman AS. Response of anisotropic nonlinearly viscoelastic solids. *Mathematics and Mechanics of Solids*. 2009; 14(5):490-501.

175. Taylor ZA, Comas O, Cheng M, Passenger J, Hawkes DJ, Atkinson D, et al. On modelling of anisotropic viscoelasticity for soft tissue simulation: numerical solution and GPU execution. *Medical Image Analysis*. 2009; 13(2):234-244.

176. Johnson GA, Livesay GA, Woo SLY, Rajagopal KR. A single integral finite strain viscoelastic model of ligaments and tendons. *Journal of Biomechanical Engineering*. 1996; 118(2):221-226.

177. Boehler J-P. Applications of tensor functions in solid mechanics. Wien; New York: *Springer-Verlag*; 1987.

178. Ning XG, Zhu QL, Lanir Y, Margulies SS. A transversely isotropic viscoelastic constitutive equation for Brainstem undergoing finite deformation. *Journal of Biomechanical Engineering*. 2006; 128(6):925-933.

179. Duenwald SE, Vanderby R, Lakes RS. Stress relaxation and recovery in tendon and ligament: experiment and modeling. *Biorheology*. 2010; 47(1):1-14.

180. Schapery RA. On Characterization of Nonlinear Viscoelastic Materials. *Polymer Engineering and Science*. 1969; 9(4):295-310.

181. Butler DL, Grood ES, Noyes FR, Zernicke RF, Brackett K. Effects of structure and strain measurement technique on the material properties of young human tendons and fascia. *Journal of Biomechanics*. 1984; 17(8):579-596.

182. Woo SLY, Danto MI, Ohland KJ, Lee TQ, Newton PO. The use of a laser micrometer system to determine the cross-sectional shape and area of ligaments - a comparative-study with 2 existing methods. *Journal of Biomechanical Engineering*. 1990; 112(4):426-431.

183. Park SW, Schapery RA. Methods of interconversion between linear viscoelastic material functions. Part I - a numerical method based on Prony series. *International Journal of Solids and Structures*. 1999; 36(11):1653-1675.

184. Lakes RS. Viscoelastic materials. Cambridge; New York: *Cambridge University Press*; 2009.

185. Taylor RL. Inversion of prony series characterization for viscoelastic stress analysis. *International Journal for Numerical Methods in Engineering*. 1973; 5(3):499-502.

Appendix A: Uniqueness of a Prony Series with Fixed Time Constants

Since the general Prony series formulation $E(t) = \sum_{i=1}^{n} E_i e^{-t/\tau_i}$ with fitted coefficients E_i and τ_i is non-unique[59], it is of interest to verify that the mathematical form of the proposed relaxation modulus [a Prony series with fixed τ_i time constants, equation (29)] yields a unique solution. The author gratefully acknowledges Professor Donald Estep (Departments of Mathematics and Statistics; Colorado State University; Fort Collins, Colorado) for providing the following proof, which demonstrates uniqueness of the relaxation modulus [equation (29)] utilized throughout this dissertation.

A.1. Proof of Uniqueness of a Prony Series With Fixed Time Constants

Consider a Prony series expansion of the relaxation modulus under the assumption of fixed time constants $\tau_1 < \tau_2 < \tau_3 < \tau_4$:

$$E(\varepsilon, t) = E_\infty(\varepsilon) + \sum_{i=1}^{4} E_i(\varepsilon) e^{-t/\tau_i} \tag{46}$$

Assume that the function $E(\varepsilon, t)$ allows another expansion with possibly different coefficients:

$$E(\varepsilon, t) = \hat{E}_\infty(\varepsilon) + \sum_{i=1}^{4} \hat{E}_i(\varepsilon) e^{-t/\tau_i} \tag{47}$$

Subtracting equations (47) and (46) yields:

$$0 = \delta_\infty(\varepsilon) + \sum_{i=1}^{4} \delta_i(\varepsilon) e^{-t/\tau_i} \tag{48}$$

where $\delta_i = \hat{E}_i - E_i$. If it is shown that $\delta_i = 0$ for all i, then the expansion coefficients are unique. This argument uses the fact that fixing the time constants $\tau_1 < \tau_2 < \tau_3 < \tau_4$ means that the expansion is linear in the coefficients that vary.

If we take the limit of equation (48) as $t \to \infty$, then all of the exponential terms in the sum converge to zero. This yields $0 = \delta_\infty(\varepsilon)$. Hence, now consider:

$$0 = \sum_{i=1}^{4} \delta_i(\varepsilon) e^{-t/\tau_i} \tag{49}$$

Multiplying equation (49) by e^{t/τ_4}, yields:

$$0 = \delta_4(\varepsilon) + \sum_{i=1}^{3} \delta_i(\varepsilon) e^{-(\tau_4 - \tau_i)t/\tau_4\tau_i} \tag{50}$$

Note that the terms in the summation all have negative coefficients in the exponent. Hence, taking the limit as $t \to \infty$ yields $0 = \delta_4(\varepsilon)$. Subsequently, we consider the equation:

$$0 = \sum_{i=1}^{3} \delta_i(\varepsilon) e^{-t/\tau_i} \tag{51}$$

and return the same mathematical procedure. Proceeding successively using the same argument after multiplying by e^{t/τ_3}, e^{t/τ_2}, and e^{t/τ_1}, and taking the limit as $t \to \infty$ each time, it is concluded that $0 = \delta_i(\varepsilon)$ for each i, thereby proving uniqueness of a Prony series with fixed time constants.

Appendix B: Interrogation of Inertial Artifacts

B.1. Introduction

For the spinal ligament experiments (chapters 2 and 3), the load cell was placed above the specimen, between the actuator of the testing device and a custom upper fixture (Figure 23). While this setup permitted convenient attachment of the specimen to the testing device and has been utilized in recent transient viscoelastic investigations (with ramp times similar in magnitude that used in chapters 2 and 3)[69,70,110,179], the mass of the upper fixture may have induced inertial force artifacts during the brief periods of acceleration/deceleration. Therefore, the specific aim of this appendix was to directly elucidate the potential inertial artifacts generated by the experimental setup used in chapters 2 and 3.

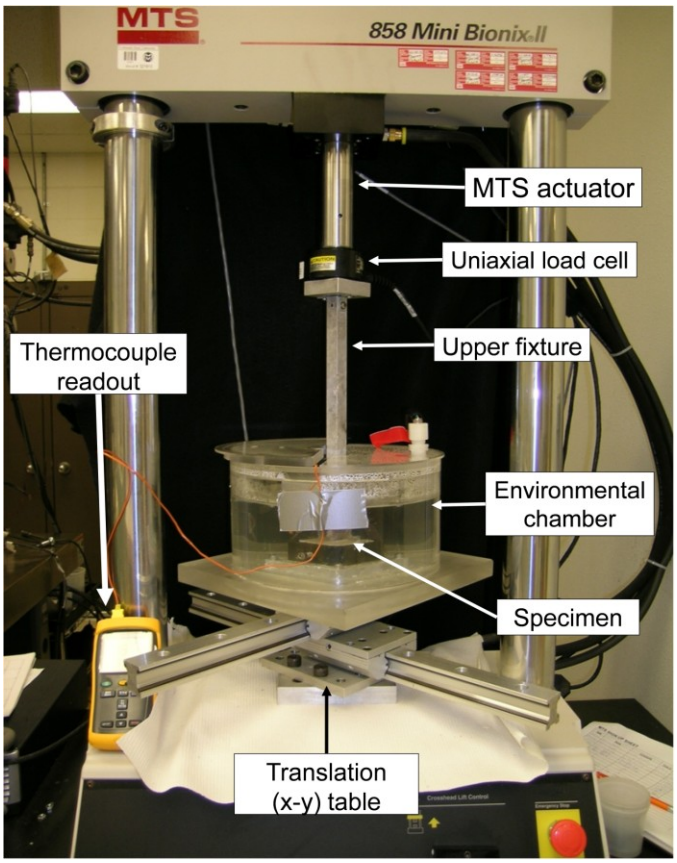

Figure 23: Setup for spinal ligament viscoelasticity experiments. Placement of the uniaxial load cell above the specimen may have caused inertial artifacts in the recorded force readout during the brief periods of acceleration/deceleration.

B.2. Materials and Methods

B.2.1. Experimental data capture

A series of fast-ramp (5 mm/s) and slow-ramp (0.1 mm/s) stress relaxation experiments were conducted on a representative leather strip specimen. The fast-ramp velocity was chosen to be identical to the rate used in chapters 2 and 3; the slow ramp velocity was chosen to be an order of magnitude less than the fast-ramp velocity in order to minimize the inertial effects. Potential slippage of the specimen was reduced by wrapping its ends around a metal fixture, which were secured with bolts and washers, and potting each end in polymethylmethacrylate (PMMA) (Figure 24). After the PMMA cured, the potted leather strip was attached to an experimental setup that was identical to that of the spinal ligament experiments (Figure 23) with the addition of a six degree of freedom load cell (MC3A-1000; AMTI; Watertown, MA) placed between the specimen and the translation table. Both load cells were zeroed by lowering the MTS actuator until there was visible slack in the specimen.

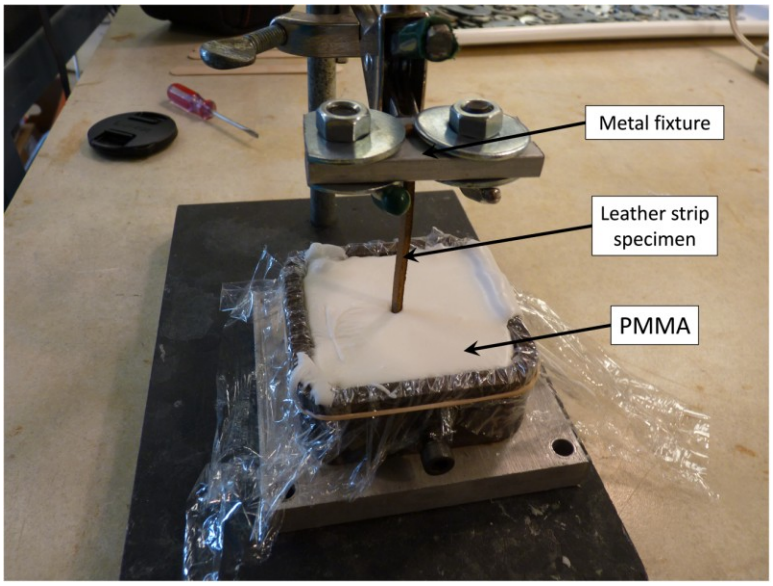

Figure 24: Picture of the leather strip specimen during potting. This potting procedure was performed in order to eliminate potential slippage of the specimen during testing.

Analogous to the spinal ligament experiments, the specimen was ramped to 5 N of pretension at a rate of 0.1 mm/s and held at the resulting displacement for 1,000 s. The gage

length (53.64 mm) was defined in this configuration as the distance between the potting fixtures. Following the 1,000 s hold, the specimen was preconditioned at frequency of 0.5 Hz and a peak-to-peak strain amplitude of 10% engineering strain, then returned to its reference configuration for 1,000 s of recovery. Subsequently, the specimen was subjected to two repeated fast-ramp stress relaxation experiments (strain magnitude: 10%, hold: 100 s, recover: 1,000 s). Following the recovery period of the second fast-ramp experiment, a single slow-ramp stress relaxation experiment was performed (strain magnitude: 10%, hold: 100 s). Force data between the two load cells were synchronized *post hoc* via the peak stress from each stress relaxation experiment.

B.2.2. Repeatability error quantification

In order to quantify the repeatability of the stress relaxation behavior, an exponentially weighted and non-weighted root mean-squared error [$wRMSE$: equation (35), $RMSE$: equation (35) without the weighting function, respectively] was calculated between the two repeated experiments. The percent error [equation (37)] between these two experiments was also calculated.

B.2.3. Inertial artifact quantification

The inertial artifact was quantified by comparing the $wRMSE$, the $RMSE$, and the percent error between the upper and lower load cell readouts from the second fast-ramp and the slow-ramp experiments.

B.3. Results

B.3.1. Repeatability

The stress relaxation data from both load cells were highly repeatable at both the long-term [Figure 25, (a) and (c)] and short-term [Figure 25, (b) and (d)] behavior. The quantitative error metrics for the upper and lower load cells are given in Table 14.

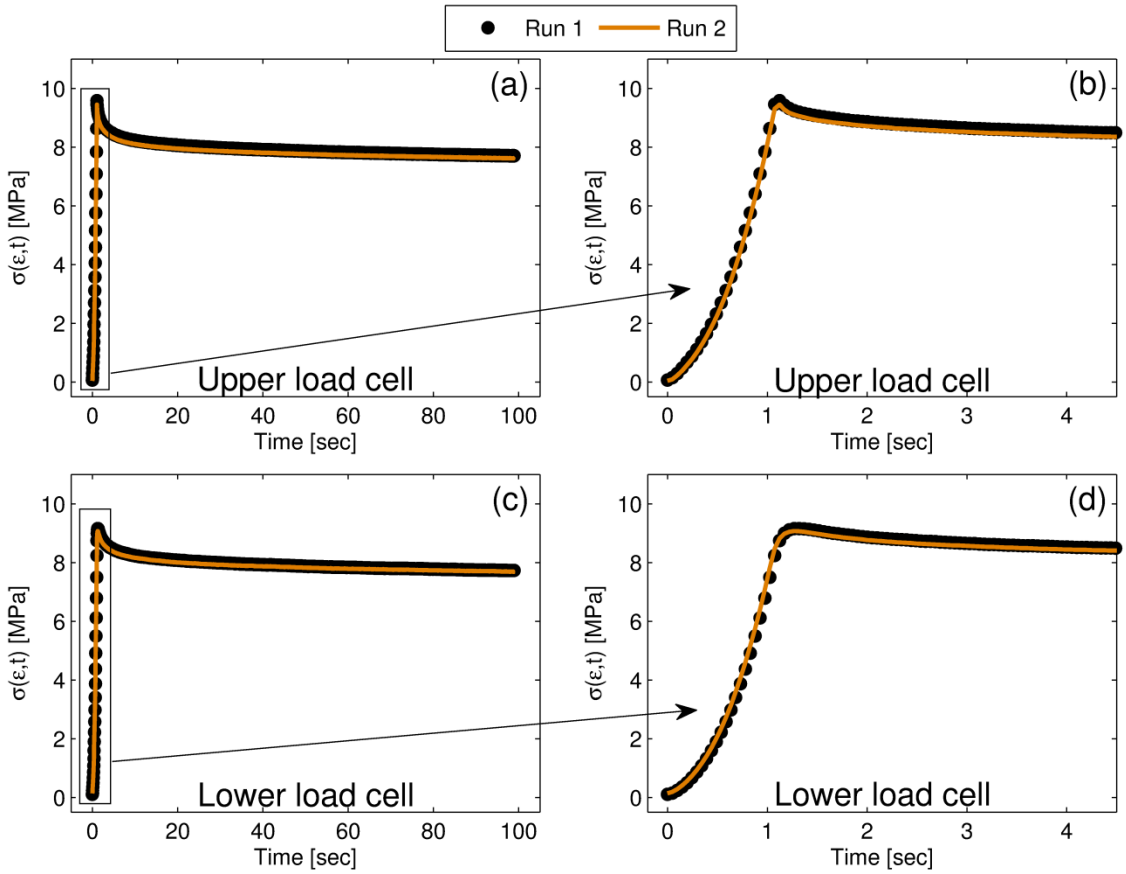

Figure 25: Long-term [(a) and (c)] and short-term [(b) and (d)] repeatability for the upper and lower load cells.

Table 14: Error metrics calculated between the two repeated runs for the upper and lower load cells.

	$wRMSE$ [kPa]	$RMSE$ [kPa]	Percent error [%]		
			Median	Maximum	Minimum
Upper load cell	24.5	104.1	1.29	52.62	0.91
Lower load cell	18.0	61.3	0.67	28.79	0.05

B.3.2. Error between upper and lower load cells

The upper and lower load cell data from the fast-ramp and slow-ramp experiments demonstrated comparable behavior (Figure 26). The quantitative error metrics between the two load cells were similar in magnitude for both the fast-ramp and the slow-ramp protocols (Table 15).

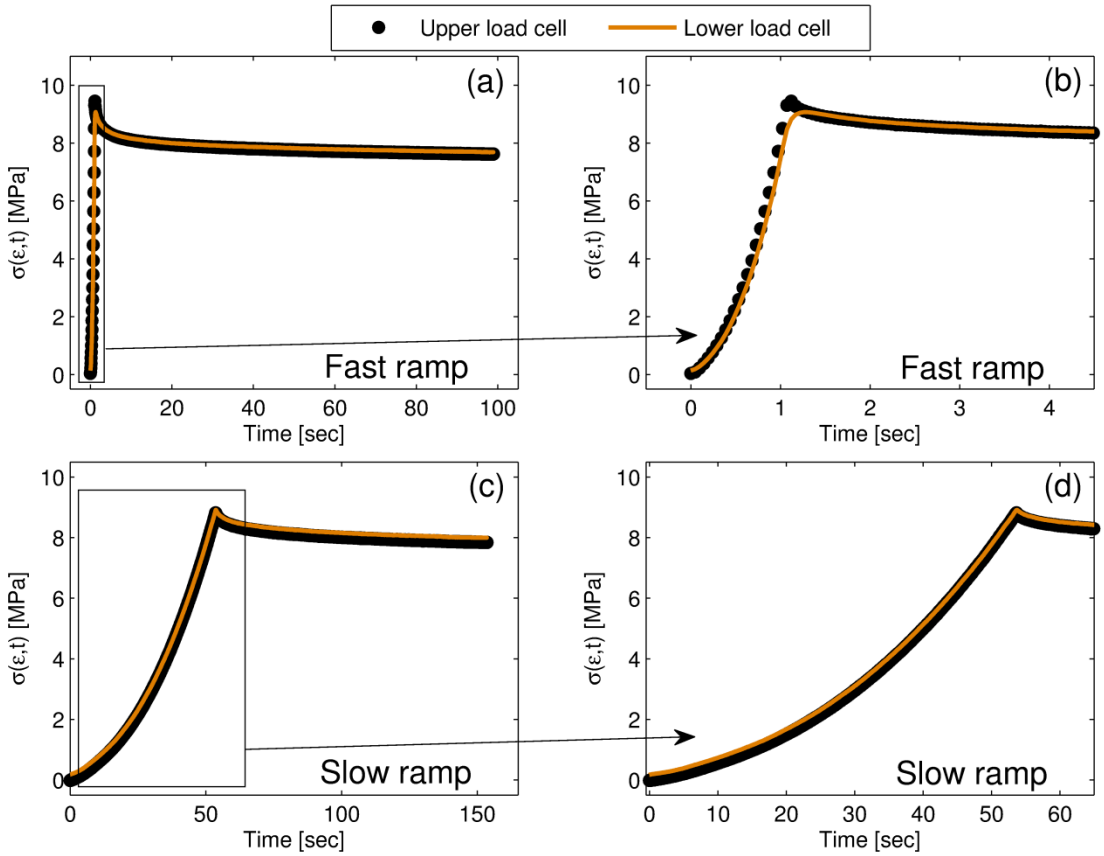

Figure 26: Comparison of the long term [(a) and (c)] and short term [(b) and (d)] upper and lower load cell data for the fast-ramp and slow-ramp experiments.

Table 15: Error metrics between upper and lower load cell readout for the fast ramp and slow ramp experiments.

	$wRMSE$ [kPa]	$RMSE$ [kPa]	Percent error [%]		
			Median	Maximum	Minimum
Fast ramp	27.6	76.9	0.82	70.10	0.08
Slow ramp	29.2	147.8	1.83	114.21	0.96

B.4. Discussion

Fast- and slow-ramp stress relaxation experiments were performed to directly elucidate any inertial artifacts in upper load cell readout caused by the mass of the upper fixture (Figure 23). Repeatability of the stress relaxation behavior was quantified by performing two identical fast-ramp experiments. For comparison, a slow-ramp experiment, which contained minimal inertial effects, was performed and compared to the fast ramp data via quantative error metrics.

The relatively low $wRMSE$ and $RMSE$ values reported for the repeatability experiments (maximum $RMSE$ = 104.1 kPa, Table 14) and low median percent error (< 1.3%) indicate a high degree of repeatability (i.e., similar curve shapes) for the fast-ramp loading protocol.

In addition, the $wRMSE$, $RMSE$, and percent error metrics between the upper and lower load cell readouts were similar in magnitude for both the fast and slow ramp experiments. A significant inertial artifact would have caused the fast-ramp quantities to be greatly increased with respect to the slow-ramp quantities.

B.5. Conclusion

The similar magnitude of the error metrics between the upper and lower load cells for both the fast-ramp and slow-ramp experiments strongly suggests that the mass of the upper fixture and the acceleration rate utilized in the spinal ligament studies did not significantly affect the outcome of the stress relaxation data therein.

Appendix C: Pilot Experiments—Repeatability and Cross-Sectional Area Measurement

C.1. Repeatability

C.1.1. Materials and methods

In order to verify that the preconditioning protocol effectively removed the irreversible component of the viscoelastic behavior[155,156], and that sufficient recovery time was allotted between each viscoelastic experiment (stress relaxation, dynamic, and creep) to recover from load history effects, a set of pilot repeatability experiments was performed on three (n=3) ovine Achilles tendon specimens. Each tendon was subjected to the initial length definition and cyclic preconditioning procedures outlined above (section 4.2.1, page 64), and then allowed to recover for 1,000 s. Thereafter, each specimen was subjected to five repeated stress relaxation protocols at the 6% strain magnitude. This procedure closely followed the experimental stress relaxation protocol used to obtain the fitted material coefficients (section 4.2.1, page 64).

For each specimen, force relaxation data the five repeated experiments were averaged at specific time points (0.1 s, 1 s, 10 s, 100 s), and the variability (standard deviation) within the repeated tests was calculated as a percentage of the mean. The results were compared to previously accepted values[69].

C.1.2. Results and discussion

Results indicated that the stress relaxation experiments were very repeatable (Table 16), where the largest variability [Table 16(c), Figure 27] was similar in magnitude to previously accepted values[69].

Table 16: Repeatability statistics for each of the three (a, b, and c) pilot experiments. For each specimen, the standard deviation between the repeated experiments was small in comparison to the average force.

	Time points			
	0.1 s	1 s	10 s	100 s
(a) Specimen 1				
Average [N]	1,481.62	1,432.24	1,375.28	1,274.14
Standard deviation [N]	41.14	41.52	41.43	43.83
% of average	**2.78**	**2.90**	**3.01**	**3.44**
(b) Specimen 2				
Average [N]	1,503.20	1,447.02	1,394.14	1,308.86
Standard deviation [N]	25.55	22.94	21.14	15.88
% of average	**1.70**	**1.59**	**1.52**	**1.21**
(c) Specimen 3				
Average [N]	978.06	932.70	875.57	805.99
Standard deviation [N]	68.58	62.05	59.45	54.93
% of average	**7.01**	**6.65**	**6.79**	**6.82**

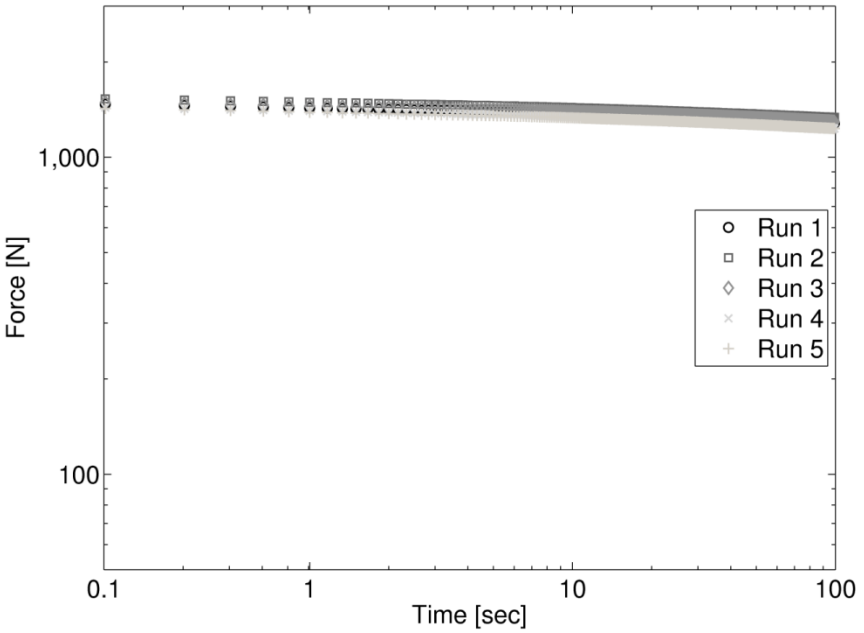

Figure 27: Repeated stress relaxation curves for the specimen with the greatest amount of variability [specimen 3, Table 16(c)]

C.1.3. Conclusion

Although there is conflicting data for and against the use of preconditioning protocols to obtain the viscoelastic behavior of orthopaedic connective tissues[70-74], a substantial loss in

repeatability was observed for this tendinous tissue if no preconditioning was performed (data not presented). Differences in the literature may be a result of the specific tissue being tested. For tendon, previous studies have demonstrated that significant, irreversible preconditioning effects are present during loading, but these effects can be removed by static (stress relaxation) or cyclic preconditioning protocols which subject the tissue to strain magnitudes that are greater (by 1%) than the strain during the measured experiment[69,155,156]. Since the cyclic preconditioning protocol herein was observed to yield highly repeatable results that were comparable to previously published data, this preconditioning procedure was utilized before each series of experiments (stress relaxation, cyclic, and creep).

C.2. Cross-sectional Area Measurement

C.2.1. Materials and methods

In order to determine an accurate representation of the tendon's cross-sectional geometry for engineering stress calculations and finite element implementation, the cross-sectional area of each pilot specimen (n=3) was determined using two independent methods: (1) a custom-designed area micrometer[149-151,181] and (2) *post hoc* digital image capture[72]. The area micrometer measured the width and height of the hydrated tendon when placed in rectangular slot of known width and applying a constant pressure of 0.12 MPa to a plunger attached to a high-resolution (0.0254 mm) micrometer (Figure 28)[149-151,181]. Height measurements from the micrometer were recorded five minutes after pressure application to allow for the pressure-induced creep to reach steady-state. Measurements were taken at two regions along the length of the tendon (proximal and distal) towards end of the tendinous tissue) and averaged. The cross-sectional geometry was then approximated by a circle, with a radius determined from the average proximal and distal areas.

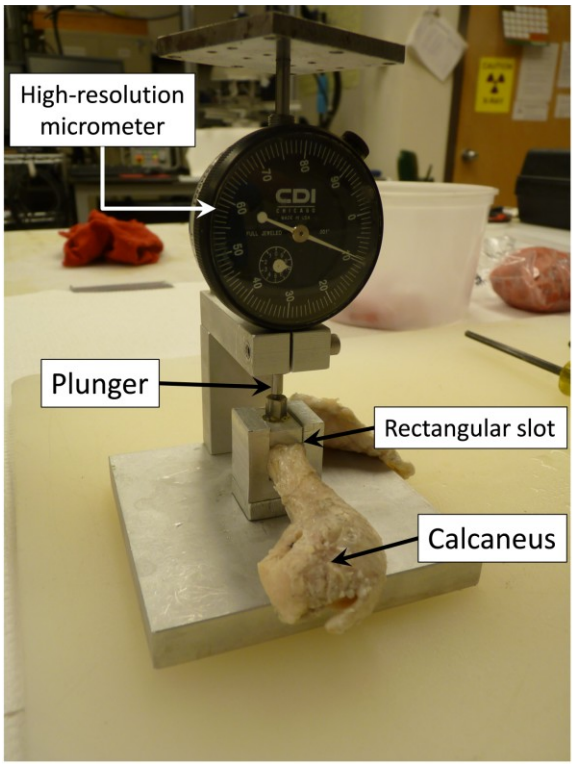

Figure 28: Picture of tendon area measurement using the area micrometer technique.

Following measurement using the area micrometer technique, the tendon was carefully transected approximately between the proximal and distal measured regions described above using a scalpel. Digital images of the hydrated cross-section were then captured under a dissection microscope (image resolution > 85 pixels/mm) mounted perpendicular to the cross-section, and the area was calculated from these images using ImageJ software (version 1.45s; National Institutes of Health; Bethseda, MD). By utilizing precision-machined block gages of known area, it has been previously demonstrated that this digital image capture technique is highly accurate (within 0.55% of the known area)[72].

C.2.2. Results and discussion

The areas calculated using the two methods were similar in magnitude; however, the area measured using the area micrometer was slightly reduced those measured from digital image capture (Table 17). This reduced area may be a result of the constant pressure applied to the tissue during the area micrometer measurement[182], which is requisite in order to ensure

that the tissue's cross-section has conformed to the shape of the rectangular slot. Despite this small (approximately 7%) reduction in area, the area micrometer closely approximated the shape of the cross section (Figure 29). This circular approximation is advantageous in the development of the finite element model because it permits a simple, cylindrical geometry to be utilized. The complex (and irregular) cross-section obtained using digital image capture would significantly complicate the mesh, and may result in poor element quality.

Table 17: The average and standard deviation (SD) of the cross-sectional areas calculated using the area micrometer (A_{AM}) and digital image capture (A_{DIC}) methods.

	A_{AM} [mm^2]	A_{DIC} [mm^2]	Percent difference† [%]
Average	104.81	112.50	7.08
SD	15.00	15.19	1.26

†The percent difference was calculated as: $\left|\frac{A_{AM}-A_{DIC}}{(A_{AM}+A_{DIC})/2}\right| * 100\%$

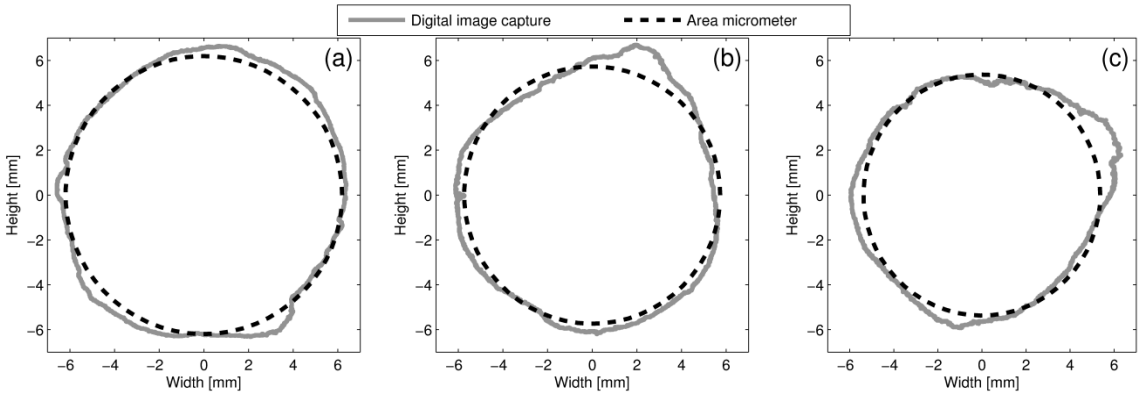

Figure 29: The circular approximation determined from the area micrometer (black dashed line) approximated the cross-section obtained from digital image capture (solid grey line) well for each of the three pilot specimens [(a), (b), and (c)].

C.2.3. Conclusion

It was observed that a circular approximation determined using the area micrometer was in good agreement with the actual cross-section geometry determined from digital image capture. Therefore, the cross-sectional area from all specimens in chapter 4 were determined using the area micrometer technique, and the cross-sectional geometry was assumed to be circular.

Appendix D: High Frequency (10 Hz) Cyclic Predictions

D.1. Introduction

The ovine Achilles tendons were subjected to cyclical loading regimes at two peak-to-peak strain amplitudes (3% and 6%) and two frequencies (1 Hz and 10 Hz). *Post hoc* data analysis elucidated significant errors in the lower load cell force data at the 10 Hz frequency which were likely caused by high-frequency vibrations induced in the experimental setup. These errors were consistent across all specimens and strain amplitudes. As a result, the force data was obtained from the upper load cell and, therefore, includes inherent inertial artifacts caused by the mass of the cryoclamp and the relatively fast accelerations required to achieve the 10 Hz oscillations. With these artifacts in mind, the specific aim of the current appendix was to interrogate the ability of the coefficients achieved from the stress relaxation experiments (section 4.2.1, page 64) to predict the high frequency (10 Hz) behavior of ovine Achilles tendon.

D.2. Materials and Methods

As outlined in section 4.2.2 (page 66), the fitted coefficients obtained from both stress relaxation fitting techniques (the CVC method and the $2.5t_0$ method) were used as input for both the analytical formulation [equation (28)] and the FE model in order to predict the average 10 Hz cyclic behavior at both strain amplitudes. Within each strain amplitude, the analytical and FE predictions from each fitting technique were compared to the average experimental data and to the experimental variability (defined as one standard deviation from the experimental mean) via calculation of the $RMSE$ [equation (35) without the weighting function] and percent error [equation (37)]. Statistical comparisons were performed on the percent error using a Kruskal–Wallis test (SAS; *post hoc* comparisons: Wilcoxon rank-sum test with Bonferroni adjustment; statistical significance: $p<0.005$).

D.3. Results

The 10 Hz frequency predictions followed trends that were similar to the 1 Hz predictions (section 4.3 , page 70). The peak magnitudes from the CVC method predictions were within the bounds of experimental variability for both the 3% (Figure 30) and 6% (Figure 31) strain amplitudes while the $2.5t_0$ method did not consistently capture these peaks. Statistical analyses indicated that the CVC method predictions of the full experimental curves (all cycles) were within the bounds of experimental variability for both strain amplitudes, whereas the 6% strain predictions from the $2.5t_0$ method were well outside of these bounds [$p<0.001$ for all significant comparisons, Table 18(a)]. No statistical difference was found between any of the predictions and the experimental variability when only the last cycle was considered ($p\geq0.168$).

D.4. Discussion

The data presented in this appendix indicate reduction in the predictive accuracy of the fitted coefficients at the 10 Hz frequency. All predictions at this high frequency were slightly out-of-phase from the average experimental data, and the overall error metrics (Table 18) were larger in magnitude than the 1 Hz cyclic predictions (Table 13). This reduction in fidelity may be a result of the specific discrete (Prony series) formulation utilized herein [equation (29)]. In a previous study, Lucas et al.[21] characterized the viscoelastic properties of human spinal ligaments under very fast strain applications (wherein strain onset was at least an order of magnitude faster than the ramping period of the current study) using fixed time constants that were two orders of magnitude smaller than those utilized herein (i.e., τ_1 = 0.001 s, τ_2 = 0.01 s, τ_3 = 0.1 s, τ_4 = 1 s). Using these reduced time constants, Lucas et al. achieved a high degree of predictive accuracy at 2 Hz and 20 Hz frequencies. Taken together, the results from the current study and from Lucas et al. suggest that a continuous spectrum relaxation function may be more applicable to describe a very broad range of soft tissue viscoelasticity at both physiologic and

injurious strain rates. However, to the best of the author's knowledge, no fully nonlinear viscoelastic continuous spectrum relaxation modulus has been developed for soft tissues that can simultaneously describe both static and dynamic temporal mechanics.

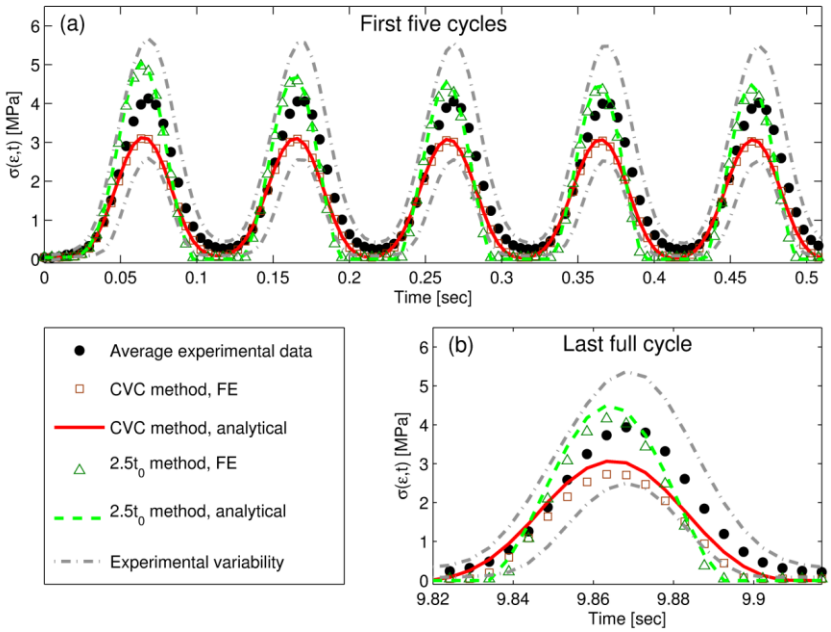

Figure 30: Depiction of (a) the first five cycles and (b) the last full cycle of the 3% strain amplitude, 10 Hz frequency predictions.

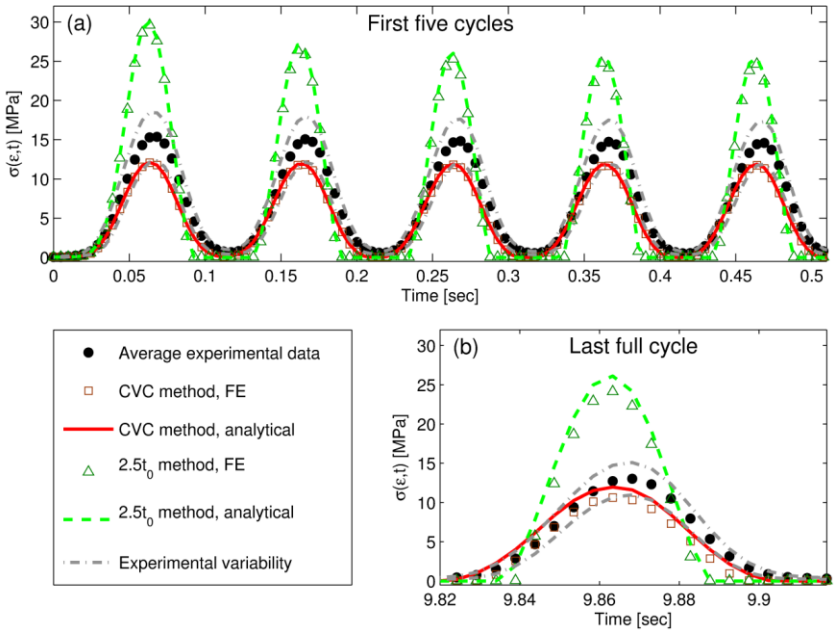

Figure 31: Depiction of (a) the first five cycles and (b) the last full cycle of the 6% strain amplitude, 10 Hz frequency predictions.

Table 18: Summary of (a) the 3% and (b) the 6% strain amplitude cyclic prediction error metrics for the 10 Hz frequency. Peak stresses (σ_{peak}) and their corresponding time shifts for the last full cycle are provided as a reference for the magnitude of the $RMSE$ values and for phase considerations, respectively. Quantitative error metrics (percent error and $RMSE$) indicated that the analytical and FE all cycle predictions from the CVC method were typically within the bounds of experimental variability (defined as one positive standard deviation from the experimental mean) at both strain amplitudes. Conversely, error metrics for the $2.5t_0$ method analytical and FE predictions were typically greater than those of the CVC method at both strain amplitudes.

	All cycles		Last full cycle			
	Percent error [%]	$RMSE$ [MPa]	Percent error [%]	$RMSE$ [MPa]	σ_{peak} [MPa]	Time shift
(a) 3% strain amplitude						
Average experimental data	--	--	--	--	3.94	--
Experimental variability	23.86 (21.85, 25.98)[a]	1.33	20.26 (5.99, 31.00)[a]	0.90	5.37	0
CVC method, analytical prediction	**7.33 (6.92, 7.65)[b]**	**0.52**	**7.70 (4.02, 15.83)[a]**	**0.50**	**3.06**	**>Δt**
CVC method, FE prediction	**8.66 (7.88, 9.56)[c]**	**0.63**	**10.72 (5.16, 22.91)[a]**	**0.70**	**2.89**	**>Δt**
$2.5t_0$ method, analytical prediction	10.77 (10.26, 11.29)[d]	0.63	11.73 (6.03, 19.49)[a]	0.63	4.50	>Δt
$2.5t_0$ method, FE prediction	9.93 (9.37, 10.39)[c]	0.62	10.72 (5.16, 14.54)[a]	0.62	4.32	>Δt
(b) 6% strain amplitude						
Average experimental data	--	--	--	--	13.04	--
Experimental variability	5.84 (5.46, 6.19)[a]	1.05	7.15 (2.63, 13.08)[a]	1.25	15.10	0
CVC method, analytical prediction	**5.65 (5.47, 5.84)[b]**	**1.35**	**6.26 (2.92, 10.31)[a]**	**1.08**	**11.98**	**>Δt**
CVC method, FE prediction	**5.27 (4.64, 5.93)[b]**	**1.68**	**5.46 (2.46, 16.76)[a]**	**1.67**	**10.89**	**>Δt**
$2.5t_0$ method, analytical prediction	14.85 (13.52, 16.27)[c]	5.92	12.93 (5.86, 52.57)[a]	6.13	26.12	>Δt
$2.5t_0$ method, FE prediction	14.91 (13.54, 16.15)[d]	5.24	12.47 (3.41, 40.53)[a]	5.19	24.40	>Δt

Superscript letters depict statistical groupings; different letters indicate $p<0.005$.
Percent error presented as: median (95% lower confidence limit, 95% upper confidence limit).
The temporal resolution of the experiment was: Δt = 0.0049 s.

D.5. Conclusion

Given the relative loss in predictive accuracy for the 10 Hz cyclic predictions compared to the 1 Hz predictions (section 4.3, page 70), it can be postulated that the higher frequency predictions were near the upper bound of the temporal spectrum defined by the fixed time constants. These findings demonstrate the importance of either: (1) developing a continuous spectrum relaxation modulus that can capture a relatively large temporal spectrum, or (2) selecting a discrete formulation and experimental characterization procedure that are appropriate for the time scales of interest.

Appendix E: Creep Predictions

E.1. Introduction

This appendix presents an introduction to the interrelationship between the creep compliance and the relaxation modulus for linear and fully nonlinear viscoelastic materials. The applicability of the fully nonlinear viscoelastic formulation is interrogated by the ability of the creep compliance (determined from the stress relaxation modulus fits in chapter 4) to predict the independent creep experiments.

E.1.1. Relationship between creep and stress relaxation: linear viscoelasticity

For a linear viscoelastic material, the relationship between the relaxation modulus $E(t)$ and creep compliance $J(t)$ is typically achieved via a Laplace transform in order to simplify analysis. The Laplace transform $\mathcal{L}\{s\}$ of the linear viscoelastic formulation [equation (15)] can be written as:

$$\mathcal{L}\{\sigma(t)\} = \sigma(s) = \mathcal{L}\left\{\int_0^t E(t-\tau)\varepsilon'(\tau)d\tau\right\} \tag{52}$$

where s is the transformed variable and $\varepsilon'(\tau) = d\varepsilon(\tau)/d\tau$. Utilizing the convolution property of the Laplace transform, equation (52) reduces to:

$$\sigma(s) = E(s) \cdot \mathcal{L}\{\varepsilon'(\tau)\} \tag{53}$$

where $E(s) = \mathcal{L}\{E(t)\}$. Further simplification is provided by the derivative property:

$$\begin{aligned} \sigma(s) &= E(s) \cdot [s \cdot \varepsilon(s) - \varepsilon(0)] \\ &= sE(s)\varepsilon(s) \end{aligned} \tag{54}$$

for $\varepsilon(0) = 0$. Similarly, the Laplace transform of the creep formulation:

$$\varepsilon(t) = \int_0^t J(t-\tau)\frac{d\sigma(\tau)}{d\tau}d\tau \tag{55}$$

is given by:

$$\varepsilon(s) = sJ(s)\sigma(s) \tag{56}$$

By re-writing the relations given by equations (54) and (56) as the ratio of stress and strain:

$$\frac{\sigma(s)}{\varepsilon(s)} = sE(s) = \frac{1}{sJ(s)} \tag{57}$$

a relationship between the transformed relaxation modulus and creep compliance can be established:

$$E(s)J(s) = \frac{1}{s^2} \tag{58}$$

By use of the convolution theorem and the inverse transform $\mathcal{L}^{-1}\{1/s^2\} = t$, equation (58) can be transformed into the time domain, yielding the implicit relationship between the relaxation modulus and the creep compliance for a linear viscoelastic material[94]:

$$\int_0^t E(t-\tau)J(\tau)\,d\tau = \int_0^t J(t-\tau)E(\tau)\,d\tau = t \tag{59}$$

Equation (59) is implicit because it does not contain explicit functions for the relaxation modulus nor the creep compliance.

E.1.2. Relationship between creep and stress relaxation: nonlinear viscoelasticity

Laplace transforms cannot be applied to nonlinear viscoelastic formulations. However, Lakes and Vanderby[152] recently developed an interrelation between the creep compliance and relaxation modulus for the nonlinear superposition formulation used throughout this dissertation [equation (28)]. While this formulation was successful at interrelating the experimental creep and stress relaxation periods for ligament[152,153], its applicability towards the interrelating the physiologically important loading period remains largely unknown. Additionally, it is unknown if this relationship is valid for soft tissues other than ligament. Therefore, the specific aim of this appendix was to interrogate the applicability of the nonlinear viscoelastic creep and stress relaxation interrelationship developed by Lakes and Vanderby[152] towards

describing the entire (ramp and creep) average nonlinear creep behavior of ovine Achilles tendon based on coefficients obtained from stress relaxation fits.

E.2. Materials and Methods

For a nonlinear viscoelastic material subjected to a constant stress (σ_c), the relationship between the time- and strain-dependent relaxation modulus $E(\varepsilon, t)$ and the time- and stress-dependent creep compliance $J(\sigma_c, t)$ can be given by[152,153]:

$$1 = J(\sigma_c, 0)E(\varepsilon, t) + \int_0^t E[\varepsilon(\tau), t-\tau]\frac{\partial J(\sigma_c, \tau)}{\partial \tau}d\tau \tag{60}$$

where t is time, $\varepsilon(\tau)$ is the applied strain history, and τ is a time variable of integration. The relationship in equation (60) is implicit unless specific functions are given for $E(\varepsilon, t)$ and $J(\sigma, t)$. Therefore, a stress-dependent generalization for the creep compliance, which is analogous to the strain-dependent Prony series generalization for the relaxation modulus [equation (29)], the nonlinear creep compliance can be cast as[183]:

$$J(\sigma, t) = J_g(\sigma) + \sum_{i=1}^{4} J_i(\sigma)\left(1 - e^{-\frac{t}{\tau_i}}\right) \tag{61}$$

where $J_c(\sigma)$ is the stress-dependent instantaneous (glassy) compliance and $J_i(\sigma)$ represent the stress-dependent compliance components corresponding to the τ_i time constants. For this study, the creep and relaxation time constants were assumed to be equivalent: τ_1 = 0.1 s, τ_2 = 1 s, τ_3 = 10 s, τ_4 = 100 s. Analogous to the relaxation moduli formulations [equation (38)], the stress-dependent creep compliance components were assumed to have a quadratic polynomial form[152,153]:

$$J(\varepsilon) = D_1\varepsilon + D_2\varepsilon^2 \tag{62}$$

where D_1 and D_2 were fit for each individual component $[J_1(\sigma), J_2(\sigma), J_3(\sigma), J_4(\sigma), J_g(\sigma)]$. Since equation (60) is in terms of a constant stress (σ_c), an instantaneous stress application of the average creep behavior from each creep experiment was assumed by using the $2.5t_0$

method described above (section 2.2.3, page 28)[69,110,184]. The average creep behavior at both stress magnitudes (denoted as "$\sigma_{3\%}$" and "$\sigma_{6\%}$" for the creep experiments corresponding to the peak stresses the 3% and 6% displacement-controlled experiments, respectively) were individually determined in MATLAB (version 7.11; TheMathWorks, Inc.; Natick, MA) by minimizing the objective function:

$$f(\theta) = \sum_{k} \left[\left(J(0;\theta)E(t,\varepsilon) + \int_0^t E[\varepsilon(\tau), t-\tau] \frac{\partial J(\tau, \sigma_c; \theta)}{\partial \tau} d\tau \right) - 1 \right]^2 \quad (63)$$

where k is the number of datum points and θ represents the set of fitted coefficients [equation (62)]. One set of coefficients was determined for the $\sigma_{3\%}$ experiment and another (separate) set was determined for the $\sigma_{6\%}$ experiment. In order to satisfy thermodynamic restrictions[94], all fitted coefficients were constrained (via MATLAB's *fmincon* function) to ensure equation (62) was positive and monotonically increasing with stress magnitude. In equation (63), the explicit form of the relaxation modulus was determined from the corresponding set of stress relaxation experiments (section 4.2.2, page 66). Finally, the sensitivity of the fitted parameters to the initial guess required by the fitting algorithm was investigated by fixing each of the initial guesses to a value of 0.01, 0.1, 1, 10 or 100 and observing any differences in the resulting fitted coefficients.

In order to elucidate the predictive accuracy of the fitted creep model, the coefficients determined from the abovementioned characterization procedure were used to predict the entire (ramp and creep) average nonlinear creep behavior using the relation[153]:

$$\varepsilon(\sigma, t) = \int_0^t J[\sigma(\tau), t-\tau] \frac{d\sigma(\tau)}{d\tau} d\tau \quad (64)$$

where $\sigma(\tau)$ is the applied stress history. Percent error [equation (37)] and $wRMSE$ [equation (35)] values were calculated between the predictions and the average $\sigma_{3\%}$ and $\sigma_{6\%}$ behavior and compared to the experimental variability (defined as one positive standard deviation from

the average creep behavior). Percent error calculations were compared to the experimental variability using a Wilcoxon ranked sum test (SAS, statistical significance: $p<0.05$)[154].

E.3. Results

E.3.1. Sensitivity of creep coefficients to the initial guess

The results indicated that the $\sigma_{3\%}$ creep coefficients were insensitive to the initial guess over a five decade range. Therefore, these fitted coefficients were deemed to be the global minimum of $f(\theta)$ (Table 19) and used to predict the average creep behavior. Although the $\sigma_{6\%}$ fitted coefficients varied slightly over the five decade range, the fitted coefficients corresponding to the minimum $f(\theta)$ (initial guesses of 0.1 and 10) were insensitive to the initial guess (Table 20). Therefore, these coefficients were deemed to be the global minimum of $f(\theta)$ and used to predict the average $\sigma_{6\%}$ behavior.

Table 19: Dependence of the $\sigma_{3\%}$ fitted creep coefficients on the initial guess. The fitted creep coefficients were independent of the initial guess over a five decade range (0.01 to 100).

	Fitted coefficients $[kPa]^{-1}$										
Initial guess	D_1^g	D_2^g	D_1^1	D_2^1	D_1^2	D_2^2	D_1^3	D_2^3	D_1^4	D_2^4	$f(\theta)$
100	2.45	-0.26	0.55	-0.06	0.17	-0.02	0.11	-0.01	0.20	-0.02	0.00217
10	2.45	-0.26	0.55	-0.06	0.17	-0.02	0.11	-0.01	0.20	-0.02	0.00217
1	2.45	-0.26	0.55	-0.06	0.17	-0.02	0.11	-0.01	0.20	-0.02	0.00217
0.1	2.45	-0.26	0.55	-0.06	0.17	-0.02	0.11	-0.01	0.20	-0.02	0.00217
0.01	2.45	-0.26	0.55	-0.06	0.17	-0.02	0.11	-0.01	0.20	-0.02	0.00217

Table 20: Dependence of the $\sigma_{6\%}$ fitted creep coefficients on the initial guess. The fitted creep coefficients varied slightly over the five decade range of initial guesses (0.01 to 100). The coefficients from the initial guesses of 0.1 and 10 corresponded to a minimum of $f(\theta)$.

	Fitted coefficients $[kPa]^{-1}$										
Initial guess	D_1^g	D_2^g	D_1^1	D_2^1	D_1^2	D_2^2	D_1^3	D_2^3	D_1^4	D_2^4	$f(\theta)$
100	0.34	-0.01	0.08	0.00	0.02	0.00	-0.05	0.00	0.01	0.00	0.00472
10	**0.36**	**-0.01**	**0.10**	**0.00**	**0.04**	**0.00**	**0.00**	**0.00**	**0.00**	**0.00**	**0.00451**
1	0.36	-0.01	0.10	0.00	0.03	0.00	-0.02	0.00	0.01	0.00	0.00456
0.1	**0.36**	**-0.01**	**0.10**	**0.00**	**0.04**	**0.00**	**0.00**	**0.00**	**0.00**	**0.00**	**0.00451**
0.01	0.36	-0.01	0.10	0.00	0.03	0.00	-0.01	0.00	0.01	0.00	0.00452

E.3.2. Average creep prediction: entire curve

Analytical predictions [via equation (64)] of the entire average $\sigma_{3\%}$ and $\sigma_{6\%}$ creep behavior are shown in Figures 32 and 33, respectively. The percent error and $wRMSE$ values indicated that the $\sigma_{3\%}$ prediction was within the bounds of experimental variability, while the $\sigma_{6\%}$ prediction was outside of these bounds (Table 21, p<0.001 for all percent error comparisons).

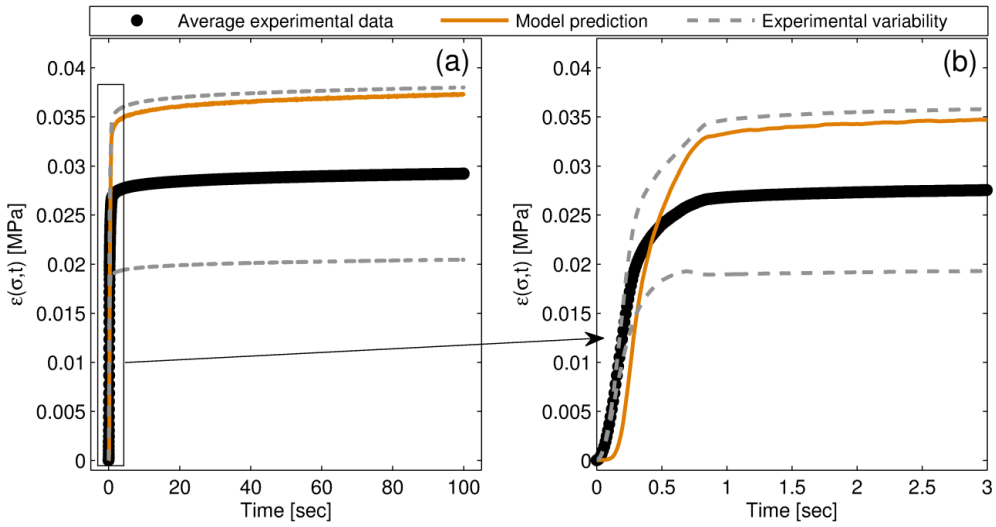

Figure 32: Long-term (a) and short-term (b) prediction of the average $\sigma_{3\%}$ behavior. The skewed shape of ramping period of the average experimental data is an artifact of averaging creep curves with different ramp times.

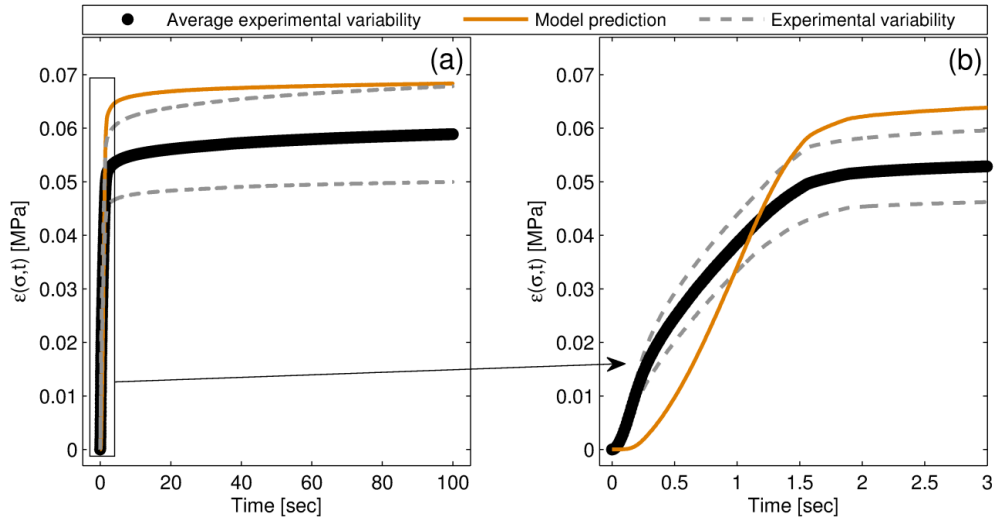

Figure 33: Long-term (a) and short-term (b) prediction of the average $\sigma_{6\%}$ behavior. The skewed shape of ramping period of the average experimental data is an artifact of averaging creep curves with different ramp times.

Table 21: Goodness-of-fit metrics for the (a) $\sigma_{3\%}$ and (b) and $\sigma_{6\%}$ creep model predictions compared to the experimental variability.

	Percent error [%]	$wRMSE$ [μm/μm]
(a) $\sigma_{3\%}$ creep		
Model prediction	26.90 (26.89, 26.92)*	1.55
Experimental variability	29.70 (29.69, 29.71)	1.74
(b) $\sigma_{6\%}$ creep		
Model prediction	17.09 (17.05, 17.11)*	2.21
Experimental variability	14.20 (14.18, 14.23)	1.55

Percent error reported as: median (95% confidence limit)
* represents p<0.001 when compared to the experimental variability

E.3.3. Average creep prediction: creep period only

In order to compare the creep predictions (Figures 32 and 33) to the results provided by Lakes and Vanderby[152], the average $\sigma_{3\%}$ and $\sigma_{6\%}$ data and their corresponding predictions were plotted beginning at 10 times the average experimental ramp time, and normalized by the peak strain (Figure 34). The correlation (R) between the normalized experimental data and creep predictions was R=0.998 for both the $\sigma_{3\%}$ and the $\sigma_{6\%}$ behavior, which is similar in magnitude to the correlations reported by Lakes and Vanderby[152].

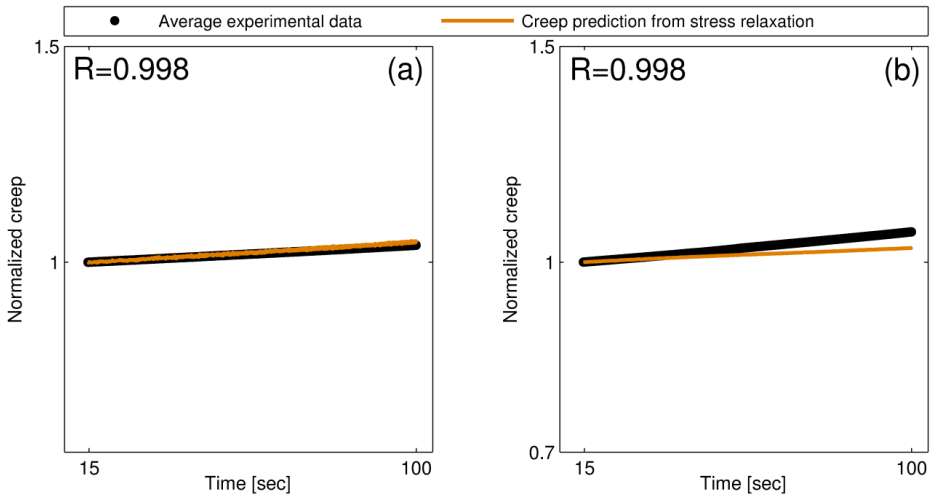

Figure 34: Normalized creep prediction of the average (a) $\sigma_{3\%}$ and (b) $\sigma_{6\%}$ behavior beginning at ten times the average experimental ramp time. Data are plotted on a log-log scale.

E.4. Discussion

The results in this appendix represent the first attempt to predict creep behavior from stress relaxation using a nonlinear viscoelastic formulation based on a Prony series. It was observed that the goodness-of fit metrics for these creep predictions were increased from the displacement-controlled 1 Hz cyclic predictions using the same relaxation modulus (section 4.3, page 70). Some of this increased error may be due to the assumption of equivalent creep and relaxation time constants. Previous studies have suggested that the time constants for creep are greater than the corresponding relaxation time constants (i.e., creep occurs at a slower rate than stress relaxation)[153,183]. With regard to linear viscoelastic materials, several previous attempts have determined the creep time constants by permitting these values to be fitted during the characterization procedure[183,185]. However, we have previously demonstrated that fixed time constants are necessary to achieve a unique solution during fitting (Appendix A)[144]. Therefore, by permitting these values to be fitted, the coefficients determined from these previous studies may be non-unique[59]. Currently, there is no objective method to select the time constants for the creep compliance other than to assume that they are equivalent to the relaxation modulus time constants.

Additionally, it is important to note that the fitted creep coefficients at the $\sigma_{3\%}$ and $\sigma_{6\%}$ stress levels were substantially different, indicating that the same coefficients could not be used to describe the creep behavior at both levels. The nonlinear viscoelastic creep and stress relaxation interrelationship proposed by Lakes and Vanderby[152] was developed by use of creep and stress relaxation data provided by Thronton et al.[74], in which the experimental stress relaxation and creep data at a single strain and a single stress level, respectively. Therefore, the interrelationship given by equation (60) was not tested at varying levels of creep and/or stress relaxation. Since a single set of coefficients could not be obtained to describe both constants

stress levels, equation (60) may not be applicable to materials wherein creep properties change significantly with stress magnitude.

Additionally, the applicability of equation (60) to related creep and stress relaxation was previously justified by calculating a high correlation (R) between the predicted creep or stress relaxation curves and the experimental data[152]. It is important to note that a high correlation between the predicted creep curves and the average experimental data was also achieved in the current study for both creep stress magnitudes, despite a clear disparity between the model prediction at the $\sigma_{6\%}$ stress magnitude [Figure 34(b)].

E.5. Conclusion

Numerical analyses were performed to interrogate the applicability of the stress relaxation and creep interrelationship proposed by Lakes and Vanderby[152] to describe the creep behavior of ovine Achilles tendon. Given the significant increase in error for the creep predictions as compared to the displacement-controlled 1 Hz cyclic predictions, and the observation that a single set of coefficients could not be achieved to describe the creep behavior at multiple stress magnitudes, the formulation provided by equation (60) may not be applicable to describe tendon creep behavior based on stress relaxation coefficients.

Appendix F: Applied Integration Techniques

F.1. Introduction

As described in detail in section 1.3 (page 12), the current stress state for linear and nonlinear viscoelastic materials subjected to a general strain history is represented respectively as convolution integrals:

$$\sigma(t) = \int_0^t E(t-\tau)\frac{d\varepsilon(\tau)}{d\tau}d\tau + \sigma_0 \tag{65}$$

$$\sigma(\varepsilon, t) = \int_0^t E[\varepsilon(\tau), t-\tau]\frac{d\varepsilon(\tau)}{d\tau}d\tau + \sigma_0 \tag{66}$$

Numerical implementation of these formulations into computational algorithms is complicated by the integration over the entire strain history and by the differentiation of this strain history because the explicit functional form of $\varepsilon(\tau)$ is unknown and arbitrary. To circumvent these complications, many researchers approximate the applied strain history by assuming simplified strain profiles (e.g., an instantaneous strain application or a pure linear ramp and hold) in order to obtain closed-form solutions. However, as demonstrated in chapters 2, 3, and 4, such assumptions may have an adverse affect on the predictive accuracy of the fitted coefficients. Therefore, the specific aim of the current appendix is to present the application of several integration techniques which can be used to evaluate equations (65) and (66) in their general, integral forms.

F.2. Materials and Methods

All fits in this appendix were performed using MATLAB (version 7.11, TheMathWorks, Inc.; Natick, MA).

Two applied numerical integration techniques are presented in the following subsections: (1) an adaptive Gauss-Kronrod quadrature (QUADGK) technique, and (2) a

convolution matrix technique. Since numerical differentiation (of the strain history) is known to decrease the signal-to-noise ratio of experimentally-captured data, two equivalent formulations within each technique were interrogated: (a) one that utilized integration by parts (IBP), in order to remove the differential operator from the strain history; and (b) one that differentiated the strain history using MATLAB's built-in differentiation function (*fnder*). Each of the four integration techniques was implemented [in step (b) of the of the CVC algorithm] to fit the stress relaxation data presented in chapter 2 at two individual strain magnitudes (4% and 25%). The resulting fitted coefficients were compared across the four formulations using a one-way ANOVA (statistical significance: $p<0.05$).

F.2.1. Adaptive Gauss-Kronrod quadrature (QUADGK) technique

Experimentally, the time-dependent stress and strain variables are represented as vectors wherein each element corresponds to a discrete time value. Numerically, the current discrete stress value within this vector is obtained through integration of the defined relaxation modulus multiplied by the entire (differentiated) strain history. In MATLAB, this integration can be performed by use of the *quadgk* function (which utilizes adaptive Gauss-Konrod quadrature) and defining: (1) the integration variable τ using a MATLAB function handle, and (2) the strain history $\varepsilon(\tau)$ as a cubic spline (using MATLAB's *spline* command) that is evaluated at τ. At the individual 4% and 25% strain magnitudes, the original integral [equation (65)] and its equivalent IBP formulation were evaluated using the *quadgk* function as outlined above. The nonlinear viscoelastic formulation [equation (66)] was not investigated in the current appendix because strain-dependence is not considered during the CVC fitting procedure (i.e., nonlinear viscoelastic behavior is determined after the CVC method is performed). However, strain dependence can be included in the integrand [e.g., for cyclic predictions] by defining the strain as a spline that is evaluated at τ.

F.2.2. Convolution matrix technique

The convolution integral [equation (65)] can be represented as the limit of a sum[94]:

$$\sigma(t) = \lim_{\Delta t \to 0} (\Delta t) \sum_{m=0}^{k} E(k-m) \cdot \frac{d\varepsilon(m)}{dm} + \sigma_0 \tag{67}$$

where Δt is the time increment, m is the discrete history variable (analogous to the continuous history variable τ), $\varepsilon(m)$ is the discrete strain history, $E(k-m)$ is the relaxation modulus, and k is the total number of time increments. For small (but finite) time increments, equation (67) can be closely approximated by the matrix equation:

$$\begin{Bmatrix} \sigma(t_0) \\ \sigma(t_1) \\ \vdots \\ \sigma(t_i) \end{Bmatrix} \cong \Delta t \cdot \begin{bmatrix} E(t_0) & 0 & \cdots & 0 \\ E(t_1) & E(t_0) & \cdots & 0 \\ \vdots & \vdots & \ddots & \vdots \\ E(t_i) & E(t_i - t_1) & \cdots & E(t_0) \end{bmatrix} \begin{Bmatrix} f(t_0) \\ f(t_1) \\ \vdots \\ f(t_i) \end{Bmatrix} + \begin{Bmatrix} \sigma_0 \\ \sigma_0 \\ \vdots \\ \sigma_0 \end{Bmatrix} \tag{68}$$

where $t = t_0, t_1, \ldots, t_i$ are the discrete experimental time values, i is the number of discrete time values for the experiment, and $f(t) = d\varepsilon(t)/dt$. An equivalent matrix representation can be obtained via IBP:

$$\begin{Bmatrix} \sigma(t_0) \\ \sigma(t_1) \\ \vdots \\ \sigma(t_i) \end{Bmatrix} \cong -\Delta t \cdot \begin{bmatrix} \left.\frac{dE(\tau)}{d\tau}\right|_{t_0} & 0 & \cdots & 0 \\ \left.\frac{dE(\tau)}{d\tau}\right|_{t_1} & \left.\frac{dE(\tau)}{d\tau}\right|_{t_0} & \cdots & 0 \\ \vdots & \vdots & \ddots & \vdots \\ \left.\frac{dE(\tau)}{d\tau}\right|_{t_i} & \left.\frac{dE(\tau)}{d\tau}\right|_{t_i - t_1} & \cdots & \left.\frac{dE(\tau)}{d\tau}\right|_{t_0} \end{bmatrix} \begin{Bmatrix} \varepsilon(t_0) \\ \varepsilon(t_1) \\ \vdots \\ \varepsilon(t_i) \end{Bmatrix} + E(0) \cdot \begin{Bmatrix} \varepsilon(t_0) \\ \varepsilon(t_1) \\ \vdots \\ \varepsilon(t_i) \end{Bmatrix} + \begin{Bmatrix} \sigma_0 \\ \sigma_0 \\ \vdots \\ \sigma_0 \end{Bmatrix} \tag{69}$$

For computational efficiency, the square (i x i) matrices in equations (68) and (69) were developed from the experimental data by use of MATLAB's built-in *toeplitz* and *tril* functions.

F.2.3. Computational efficiency

In order to compare the computational efficiencies of the proposed integration techniques, the time required for each technique to integrate a single, representative stress relaxation curve (consisting of 6,025 datum points) was recorded.

F.3. Results

Statistical analyses indicated that there were no significant differences between the fitted coefficients (4% strain magnitude data shown in Figure 35, 25% strain magnitude shown in Figure 36) of either integration technique or their equivalent IBP counterparts ($p>0.98$ for all comparisons). Furthermore, the convolution matrix technique was observed to be significantly more computationally efficient (runtime: 5.2 s) than the QUADGK technique (runtime: 66.6 s).

F.4. Discussion

Direct integration of the constitutive formulation given by equation (66) is requisite in order to describe the viscoelastic behavior of a material subjected to a general strain history. All four integration techniques investigated in this appendix (QUADGK with and without IBP, convolution matrix with and without IBP) were observed to yield equivalent fitted coefficients when used with the CVC algorithm. These findings indicate that any of the above integration techniques can be utilized to create the integral predictions in the CVC algorithm [step (b), page 30].

F.5. Conclusion

Based on the results of this appendix, it is suggested that the computationally efficient convolution matrix technique [equations (68) and (69)] be used to calculate the predicted curve in the CVC method.

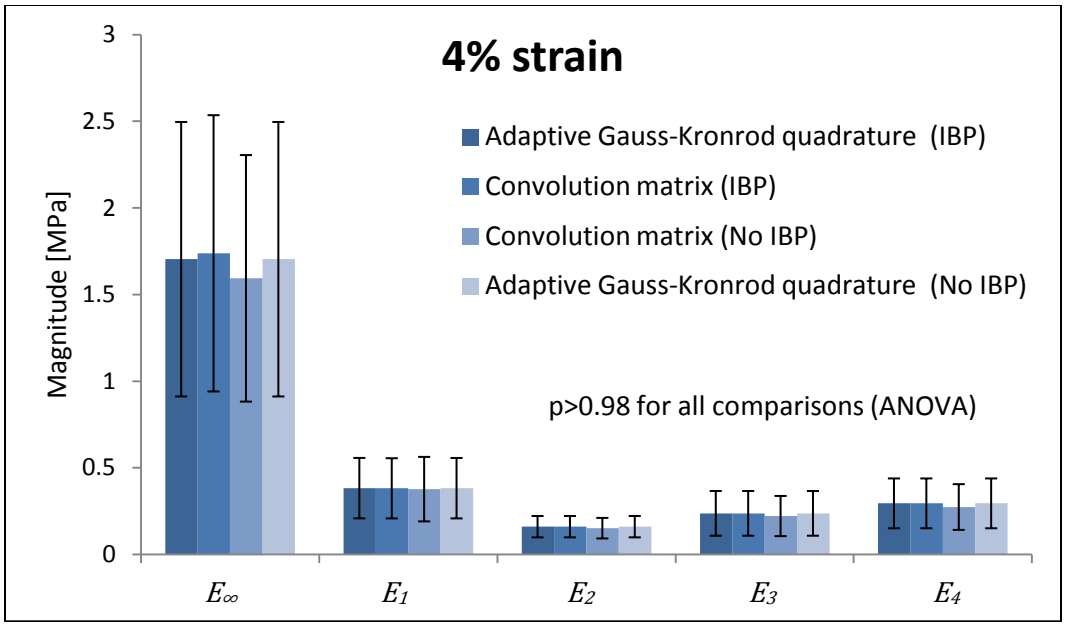

Figure 35: Fitted parameters at the 4% strain magnitude determined from each of the integration techniques. There was no statistical difference between the fitted coefficients obtained using either fitting technique (No IBP) or the equivalent integration by parts (IBP) formulation (p>0.98 for all comparisons). Error bars represent one standard deviation.

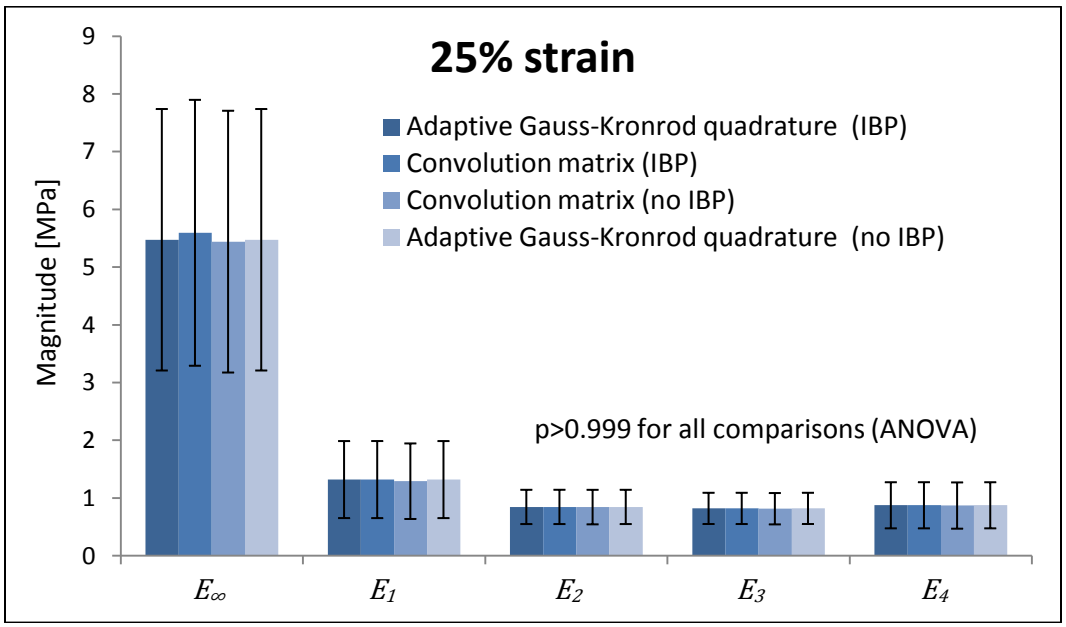

Figure 36: Fitted parameters at the 25% strain magnitude determined from each of the integration techniques. There was no statistical difference between the fitted coefficients obtained using either fitting technique (No IBP) or the equivalent integration by parts (IBP) formulation (p>0.98 for all comparisons). Error bars represent one standard deviation.